# Enhancing Geotechnical Properties of High-Water Content Clay Using Finely Shredded Paper

**2024**

**KEBEDE Teshome Birhanu**

## Abstract

Utilization of waste materials and creating innovative methods to reduce the adverse effects of soft soils minimizes the cost of over design building foundations and also reduces their influence on the ecosystem. The low shear strength of soft soil causes uneven settlement of structures like road pavements and embankments built on such kind of soils. This study describes how a combination of cement and finely shredded paper is used to stabilize soft soils especially with high water content. As the number of research that evaluate the effect of finely shredded paper on soft soil improvement was limited, a comprehensive attempt has been made on soft soils reinforcement using finely shredded paper to enhance their engineering properties and minimize the consumption of stabilizers like cement and lime. A series of tests were conducted to quantify the improved consistency characteristics, shear strength of treated soils and hydraulic conductivity of reinforced soft soil.

Finely shredded paper has been preferred as a new ground-improvement material for high water-content clay. This material is effective for reducing fluidity and for enhancing the shear strength of treated clay. In this study, not only the changes in the physical, mechanical, and hydraulic properties of clay treated with different amounts of FSP, but also the basic properties of the FSP itself, are experimentally examined. FSP shows an intertwisted structure caused by the fibers having various lengths and thicknesses. FSP also shows low bulk density, a rich water-absorption capacity, and shear resistance even under wet conditions. Due to these characteristics of FSP, clay treated with larger amounts of FSP exhibits a more aggregated structure, resulting in the maintenance of a solidly built structure even under low bulk-density and high water-content conditions. In addition to the low bulk density of the treated clay, the creation of concentrated seepage paths, related to the rich water-absorption capacity of FSP, leads to the higher hydraulic conductivity of the treated clay. Clay treated with FSP exhibits a greater amount of consolidation than pure clay, whereas the void ratio converges to a similar value between the treated clay and the pure clay as the normal stress is increased. The shear resistance of clay treated with FSP is enhanced because FSP retains its shear resistance even at high water contents.

However, when the water content of the clay soil is extremely high, it is difficult to reuse the dredged soil as a geomaterial only by treating it with FSP. Therefore, this study aims to investigate the applicability of treated dredged clay soil with FSP and cement as a geomaterial. The mechanical properties of the treated soil were investigated by uniaxial compression tests and cone penetration tests. The results showed that the combination of FSP and cement not only increased the uniaxial compressive strength and the cone index of the treated mud, but also improved its brittleness. This is thought to be due to the reinforcement effect of the FSP fibers in addition to the reduction of apparent free water in the mud which is affected by its high-water absorbing capacity. The free water also facilitates the dissociation of hydration process during chemical reaction with cement which form binding gel that binds clay particles and clay

particles with FSP fibers. So, reducing the cement amount and adding more FSP is a good method to improve ground with low impact on the environment as reduction of cement content due to the inclusion of natural fibers can lead to a lower carbon footprint associated with cement production.

The numerical modelling of a soft ground modification technique utilizing combined finely shredded paper and cement to reinforce embankment constructed on top of multilayer soil that consists soft soil was simulated. To investigate the influences of the treatment thickness on the embankment characteristics, a series of finite element analyses (FEA) was conducted on the full geometry of a finely shredded paper, and cement treated embankment. The treated soil section thickness varied in a range of 0.25 m to 1.0 m which is that integrated into the embankment and modelled into 1.0m width (i.e., longitudinal) road cross section. The numerical results reveal that an increase in the treated soil thickness significantly improved the vertical deformation of the subgrade soil, which clearly improved the stability of the embankment system.

This research gives a promising technique of utilizing as an environmentally friendly additive for treating soft soils, specifically in combination with cement for treatment of low shear strength and problematic soft ground sub surface of road structure.

## Acknowledgements

My PhD journey could not have been possible without the support provided by numerous people. Particularly, I would like to express my sincere appreciation and gratitude to my supervisors at Department of Civil and Earth Resources Engineering at Kyoto University, family members and research colleagues.

Firstly, I would like to take this opportunity to express my deepest gratitude to my principal supervisor, Professor Emeritus Makoto Kimura for giving me the chance to study in his laboratory, and my co-supervisor, Professor Yosuke Higo, Professor Hideaki Yasuhara, Associate Professor Yasuo Sawamura, Associate Professor Ryota Hashimoto, Assistant Professor Ryunosuke Kido in addition Assistant Professor Yusuke Miyazaki for their continuous support associated with my research project, my daily life, their guidance, time, patience, commitment and leadership. Since the begin of my study, I've gained valuable knowledge and skills from them, including interpersonal and technical abilities, critical thinking, presentation skills, and their knowledge and motivation have empowered me to overcome numerous challenges in life and research in reaching this significant milestone.

I'd also like to express my deep appreciation to all the geotechnical research colleagues who have played a direct or indirect role in my PhD journey. Specifically, I extend my gratitude to the supportive staff at Kyoto University Geomechanics laboratories, such as Mr. Yasuichiro Asai former Geomechanics laboratory master course student, Dr. Takao Yano former Geomechanics laboratory specialist, and my research fellow in MNGD project from both Japanese and Ethiopian side, for their assistance in either conducting the experimental program or providing valuable advice.

Furthermore, I want to sincerely recognize the Japan international cooperation agency (JICA), as well as SATREPS MNGD project, for their unwavering support and scholarships that made it possible for me to successfully complete my PhD research.

Last but certainly not least, my immeasurable gratitude goes to my parents for their constant support and unconditional love in the time of hardship. I'm also appreciative of my brother, sister and friends, who consistently bring joy and motivation, encouraging me to work hard and achieve my goals.

February 2024
KEBEDE Teshome Birhanu

## Table of Contents

## List of Figures and Tables

# Chapter 1

# Introduction

## 1.1 Background

Soft soil poses a significant challenge to infrastructure development and maintenance. Infrastructure, including buildings, roads, bridges, railways and other essential facilities, is the backbone of modern society. However, when these structures are built on or near soft soils, several problems can occur. One of the most critical issues is the potential for uneven settlement and subsidence of the structure. Soft soils have a low shear strength and high compressibility, meaning that they are more likely to undergo significant vertical deformation and failure under the weight of a given infrastructure (Liu et al., 2023).This uneven settlement can result in structural damage, tilting, and misalignment, compromising the safety and functionality of the structure and built environment (Zaini et al., 2021).

Soft soils also exert lateral earth pressure on retaining walls and foundations, increasing the risk of structural instability and failure. The challenges extend to environmental concerns as well, as construction on soft soils can disrupt sensitive ecosystems like wetlands and marshes, necessitating careful environmental assessments and mitigation measures. In addition, the poor drainage characteristics of soft soils can lead to waterlogging and increased pore water pressure, further weakening the soil and affecting the stability of infrastructure where appropriate stabilization measures are essential to counterbalance these advert effect.

Soft soil stabilization with cement and fibers is a widely studied topic in the current geotechnical engineering research outlets. The use of binders, such as cement, in soft soil stabilization is a common method to increase the interfacial bonds between soil particles (Ghadir & Ranjbar, 2018) However, the addition of fibers to cement-stabilized soil has been found to further enhance its mechanical properties. Research has shown that the inclusion of fibers in cement-stabilized clay soil can increase the engineering properties like unconfined compressive strength and axial strain at failure, transforming the brittle behavior of the soil to a more ductile one (Estabragh et al., 2012).

Different types of fibers, such as nylon and polypropylene, have been investigated for their effectiveness in improving the strength of fiber-reinforced and cement-stabilized soft clay (Mu et al., 2015). The interfacial shear strength between the fibers and the soil matrix has been found to play a crucial role in the overall performance of the stabilized soil (Tang et al., 2010). In addition to improving the mechanical properties of cement-stabilized soil, the addition of fibers can also affect the microstructure of the soil. Studies have shown that the inclusion of basalt fibers in cement-stabilized soil can lead to the formation of a stable space structure inside the soil, resulting in a remarkable improvement in unconfined compressive strength (Cao et al., 2019). The combination of cement and fibers has also been investigated for its effectiveness in stabilizing other types of soils. For example, the use of cement and fibers in stabilizing sand has been proposed as a method to increase the bearing capacity of spread foundations when placed on a layer of fiber-reinforced cemented sand built over a weak residual soil stratum (Consoli et al., 2009). Utilization of natural fibers like rice straw, corn silk, rice husk on cemented sludge by carrying out strength, hydraulic conductivity and durability test shows that fiber inclusion significantly improves the cemented sludge soil (T. N. Duong et al., 2019). The field application of fiber treated soft soil in some projects in Japan are shown in Figure 1.1 (Phan Thanh Chien, 2019a) . In Kyoto University the treatment of soft soil with finely shredded (FSP) natural fiber started back in 2016 (Sawamura et al., 2017) discovered that, the high-water absorption capacity of this additive desaturates the muddy soil with excess free water between clay particles which increased the transportability of muddy soil.

Construction of Sewerage Pipe in Obanazawa City in Yamagata Prefecture

Construction of River Bank in Hamao Area in Fukushima Prefecture

Construction of Public Utility Conduit in Sendai City in Miyagi Prefecture

**Figure 1.1: Projects which applying Fiber-cement-stabilized soil method (Phan Thanh Chien, 2019)**

In Overall, the research on the stabilization of soft soil with cement and natural fibers has demonstrated the potential to significantly improve the mechanical properties of the soil. The inclusion of natural fibers in cement-stabilized soil can enhance a promising technique for geotechnical applications. Moreover, as the waste papers is a huge burden on the environment and safe disposal is mandatory to protect the ecosystem from pollution, finely shredded paper is a helpful fiber for treatment. Very useful characteristics of finely shredded paper like treatment mechanism and applicability at soft ground as an additive with and without cement is not clearly investigated.

## 1.2 Objectives

As the high-water content clay soil from construction sites in metropolitan area is a major challenge, our research team conducts and evaluate the influence of finely shredded paper (FSP) on transportability and the shear strength properties of high-water content clay soil constitutes another pivotal aspect of this research. Through a systematic investigation involving varying proportions of FSP (ranging from 0% to 20%), the study aims to properly show impact of FSP inclusion on the clay soil's shear strength characteristics. In addition, these parameters are clearly evaluated when FSP combined with cement at different water cement ratio. This investigation holds paramount significance in advancing our understanding of sustainable high water content clay soil stabilization techniques and facilitating the development of environmentally friendly and makes the waste reusable.

One of the study’s aims is intricately unraveling the mechanism underpinning the effect of water content and density on fine shredded paper (FSP) constitutes a critical understanding of this study. Employing direct shear box tests that span a spectrum of void ratios and moisture contents of (ranging from 3.3 and 5.1) and (ranging from 0% to 200%) respectively, the research endeavors to decipher the intricate interaction between FSP specimen’s void ratios, normal stress, and moisture levels. The result of this investigation clarifies the potential mechanism of FSP treatment during the stabilization process.

Soft soils, challenging for their problematic behavior, undergo a comprehensive analysis through a multifaceted approach involving treatment with both finely shredded paper (FSP) and cement. This study makes a detailed examination of both physical and mechanical properties of the treated soft soils. By determining parameters like linear consistency, hydraulic conductivity and unconfined compressive strength characteristics aims to unlock the potential of FSP and cement as stabilizing agents for these kind soils. The outcomes of this investigation are ready to clarify the viability of these treatments and gives methods for sustainable and effective soil stabilization strategies, thus mitigating the challenges posed by extensive soft soils in different infrastructure construction projects.

In this study after determination of the properties of treated soil on laboratory scale a practical application of the findings, the study shifts its focus to the performance evaluation of soil treated with finely shredded paper (FSP) and cement as subgrade soil for road construction. By utilization of finite element method within the PLAXIS 3D program, the research simulates field conditions by taking a case study of roads connecting small villages near Addis Ababa, Ethiopia. This phase of the research holds the promise of translating theoretical insights into tangible benefits for infrastructure development. By assessing the deformation and settlement characteristics of the untreated and treated soil, by considering the effect of thickness of the stabilized subgrade soil with incorporating FSP and hydrated cement treatments into actual road construction projects. Overall, the specific objectives of this study are shown as follows:

- . To evaluate the effects of water cement ratio, additive amount and water content of specimen on the strength properties of soil treated with cement and finely shredded paper (FSP).
- To investigate the effect of finely shredded paper (FSP) on the shear strength properties of high-water content soil water with varying amount of FSP (0%,5%,10% and 20% FSP).
- To evaluate the mechanism of FSP treatment for high water content specimens. Where using direct shear box tests at varying void ratio and moisture content of 0, 50, 100 and 200%.
- To study the behaviors of soft soils treated with FSP and cement which includes physical and mechanical property analysis.
- To evaluate the performance of soil treated with FSP and cement as subgrade soil using finite element method of PLAXIS 3D program. The case study which focuses roads on the vicinity of Addis Ababa city in Ethiopia.

### 1.3 Outline of thesis

This research consists of 6 chapters. The outline of the thesis is described as follows:

- **Chapter 1** is the introduction, which consists of the background of this study which is the problematic soil sources, definitions, problems associated with these soils and techniques to treat such type soils. In addition, it illustrates the objective of the study and research organizations.
- **Chapter 2** is a literature review, which provides a comprehensive literature survey on the problematic soil effect on the infrastructure, properties of treated and untreated problematic soil with cement, lime with combination of natural fibers. Where physical and mechanical properties are extensively evaluated. It also reflects the research gap in the previous studies.
- **Chapter 3** is treatment of high-water content soil; explain the experimental result used to evaluate the influence of fine shredded paper on clay slurry. The soil specimen prepared at varying fine shredded paper and series of experiments conducted to evaluate the physical (i, e, liquid limit, plasticity index, water absorption capacity) and mechanical properties like shear strength, one dimensional consolidation and hydraulic conductivity.
- **Chapter 4** is the mechanical properties of high-water clay soil treated with finely shredded paper and cement. The specimen is prepared by mixing high water content clay with different amounts of standard finely shredded paper and different water cement ratios. Cone index and uniaxial compressive strength test were conducted

to evaluate the performance of the treatment method and strength achieved.

- **Chapter 5** is the evaluation of the performance of treated subgrade soil layer; mainly to numerically analyze for predicting the settlement and deformation of road embankment constructed on different thickness untreated and treated soft soils using PLAXIS 3D finite element program. Parameters obtained in the previous chapter are used for PLAXIS 3D program simulation.
- **Chapter 6** is conclusion and recommendations. Presents the summary of results in previous chapters and conclusions with certain recommendations for future study.

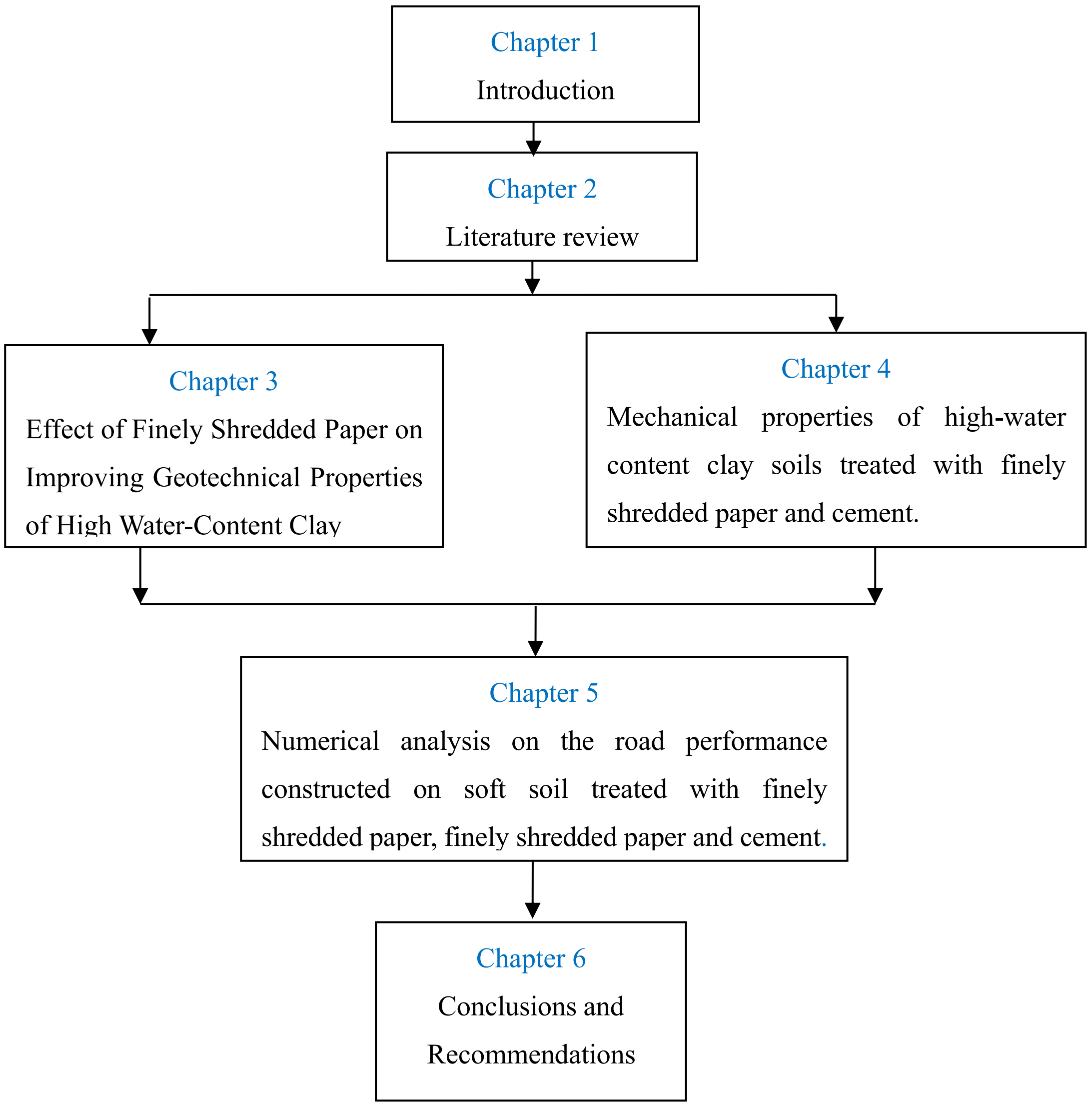


**Figure 1.2: Structure of thesis and corresponding subjects.**

**References for Chapter 1**


Cao, Z., Ma, Q., & Wang, H. (2019). Effect of Basalt Fiber Addition on Static-Dynamic Mechanical Behaviors and Microstructure of Stabilized Soil Compositing Cement and Fly Ash. *Advances in Civil Engineering*. https://doi.org/10.1155/2019/8214534

Consoli, N. C., Vendruscolo, M. A., Fonini, A., & Rosa, F. D. (2009). Fiber Reinforcement Effects on Sand Considering a Wide Cementation Range. *Geotextiles and Geomembranes*. https://doi.org/10.1016/j.geotexmem.2008.11.005

Duong, T. N., Satomi, T., & Takahashi, H. (2019). *Mechanical Behavior Comparison of Cemented Sludge Reinforced by Waste Material and Several Crop Residues*.

Estabragh, A. R., Namdar, P., & Javadi, A. A. (2012). Behavior of Cement-Stabilized Clay Reinforced With Nylon Fiber. *Geosynthetics International*. https://doi.org/10.1680/gein.2012.19.1.85

Ghadir, P., & Ranjbar, N. (2018). Clayey Soil Stabilization Using Geopolymer and Portland Cement. *Construction and Building Materials*. https://doi.org/10.1016/j.conbuildmat.2018.07.207

Liu, H., Lin, P., & Wang, J. (2023). Machine Learning Approaches to Estimation of the Compressibility of Soft Soils. *Frontiers in Earth Science*. https://doi.org/10.3389/feart.2023.1147825

Mu, C., Shen, S., Arulrajah, A., Wu, H.-N., & Hou, D. (2015). Laboratory Evaluation on the Effectiveness of Polypropylene Fibers on the Strength of Fiber-Reinforced and Cement-Stabilized Shanghai Soft Clay. *Geotextiles and Geomembranes*. https://doi.org/10.1016/j.geotexmem.2015.05.004

Phan Thanh Chien, B. (2019). *Study on Mechanical Properties of Rice by-Products-Cement-Reinforced Sludge as Banking Materials.*

Sawamura, Y., Yano, T., & Kimura, M. (2017). Property variation of high moisture sludge by fine powder mainly composed of Cellulose. *Environmental Geotechnical Engineering Symposium*, *12*(September), 505–510.

Tang, C., Shi, B., & Zhao, L. (2010). Interfacial Shear Strength of Fiber Reinforced Soil. *Geotextiles and Geomembranes*. https://doi.org/10.1016/j.geotexmem.2009.10.001

Zaini, M. S. I., Hasan, M., Yie, L. S., Masri, K. A., Jaya, R. P., Hyodo, M., & Winter, M. J. (2021). The Effect of Utilizing Silica Fume and Eggshell Ash on the Geotechnical Properties of Soft Kaolin Clay. *Jurnal Teknologi*. https://doi.org/10.11113/jurnalteknologi.v84.17115

## Chapter 2

## Literature Review

### 2.1 High water content clay

In metropolitan cities, coastal areas and port cities, high water content (dredged clay soils) are a consequence of maintaining and expanding maritime transportation networks and additional reclaimed land, dam, tunnels and other substructures constructions (Shi et al., 2017).The accumulation of fine-grained sediments in navigation channels necessitates regular dredging operations and adjusting the subsoil profile for reclaimed land subsoil profile, leading to the creation of large amounts of dredged clay soil usually ended up as waste (Lang, Chen, & Chen, 2021; Y. Zhang et al., 2022).

The management, disposal and reuse of these materials are critical concerns, prompting researchers and practitioners to explore sustainable methods for their beneficial use. Similarly, inland water bodies, such as rivers and lakes, are subject to sedimentation, leading to the formation of dredged clay soils. Addressing the adverse effect of these soils is essential for maintaining waterway infrastructure, flood control, landfills problem and sustainable urban development.

**Figure 2.1: Dredging operation high water clay soil from seabed (Rinkai Nissan construction, 2023).**

The geotechnical properties of dredged clay soils pose obstacles to construction and development projects. The high-water content and plasticity, swelling, shrinkage, low strength, high compressibility and excessive settlement of these soils can lead to instability, high compressibility, excessive settlement, and low load-bearing capacity, making them unsuitable for direct use as construction materials (Lang, Chen, & Duan, 2021; Onyekwena et al., 2023).

However, the application of innovative geotechnical techniques, such as cement soil stabilization and other soil improvement methods, offers promising solutions to transform these problematic soils into suitable construction geomaterials. By introducing cementitious binders and reinforcing fibers, the physical and mechanical properties of dredged clay soils can be significantly enhanced, rendering them suitable for foundation support, embankment construction, and other infrastructure applications that reduce burden on the scarcity of landfills in major cities due to population growth (Chan & Abdul Jalil, 2014; Wu et al., 2022).

## 2.1 Reutilization of high-water content clay

When the population increases in major metro polytan cities nowadays damping sites are scarce (Çevikbilen et al., 2020) Where the reutilization of dredged soils presents a significant opportunity for sustainable land management and environmental stewardship in such kinds of cities. Dredging activities often yield large volumes of sediment and soil, which can be repurposed for different useful applications. By treating and reusing these materials, we can reduce the need for conventional disposal methods, such as landfilling or open water disposal, which can have negative ecological impacts on the environment. Reutilization options encompass a wide range of possibilities, including habitat restoration, shoreline stabilization, wetland creation, land reclamation as shown in **Figure 2.2** and even agricultural or landscaping uses. As (Sugimura et al., 2022) reported that among the 159,500,00m$^3$ dredged soils produced in Japan in 2019 majority of this waste reused for land reclamation as shown in **Table 2.1**. In addition, 5.9% used for backfilling of borrow pits and 12.9% goes to seagrass meadows, macroalgal beds and tidal flats.

Careful assessment of the sediment's composition, contamination levels, and potential applications is essential to ensure that reutilization efforts are carried out in an environmentally friendly manner (MLIT, 2017). Embracing the reutilization of dredged soils not only minimizes waste and conserves valuable resources but also contributes to the enhancement of ecosystems and the promotion of sustainable development practices.

**Table 2.1: Amount of dredged soil and its utilization in Japan (Sugimura et al., 2022)**

| **Parameters** | **Value** |
|---|---|
| Annual amount of dredged soil | 159,500,000 m$^3$ |
| Utilization rate for backfilling borrow pits | 5.9% |
| Utilization rate for seagrass meadows, macroalgal beds, and tidal flats | 12.9% |
| Utilization rate for land development | 53.2% |

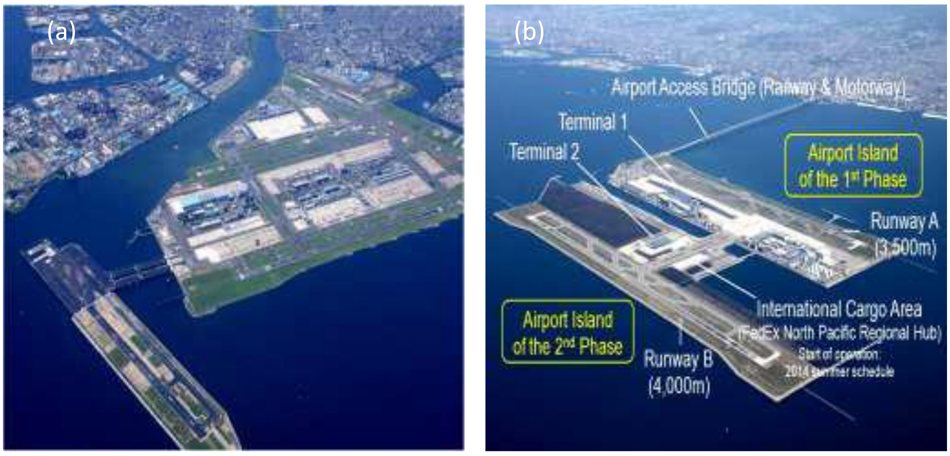


**(a)** Aerial photo of Tokyo Haneda airport (**b**) Aerial photo of Kansai airport

**Figure 2.2: Man made Island by stabilizing dredged soils for airport in Japan (Watabe & Sassa, 2015).**

## 2.2 Mechanism of treatment of dredged marine clay

### 2.2.1. Cement treated dredged soil

The Many solidification techniques for mixing dredged soil with cement have been developed in order to successfully utilize the dredged soil (Shinsha & Kumagai, 2018). When cement is combined with clay, a series of intricate chemical reactions unfold, playing a pivotal role in changing the properties of the resulting mixture. These reactions, explained in equations (2.1) to (2.3), can be categorized into two major significant processes. Initially, cement experiences a primary hydration reaction (John & Lothenbach, 2023) at an early stage. During this early phase, the cement reacts with water to initiate the formation of primary cementitious compounds. This reaction leads to an initial increase in strength and is accompanied by the drying out of the soil-cement amalgamation processes. Consequently, the mixture begins to solidify as primary cementitious products form, contributing to the overall robustness of the resulting matrix.

Subsequently, a secondary pozzolanic reaction takes place, also named solidification (Phan Thanh Chien, 2019b).This intricate chemical transformation transpires between the cement and the clay minerals, fostering a more intricate bond in the composite as shown in equation (2.1) to (2.6). This reaction is particularly essential between the cement and the silica and alumina components present in the clay. The outcome of this reaction is the generation of cementitious materials hydrate compounds in the form of calcium-silicate-hydrates and calcium-aluminate-hydrates (Rachman et al., 2021). These newly formed compounds further enhance the binding properties of the mixture, contributing to its overall strength and durability of the soil matrix in general.

❖ Hydration of Portland cement is given in the following equation (Rachman et al., 2021).

$$2(3CaO.SiO_2) + 6H_2O \rightarrow 3CaO._2SiO_2.3H_2O + 3Ca(OH)_2 \quad (2.1)$$

$$2(2CaO.SiO_2) + 4H_2O \rightarrow 3CaO._2SiO_2.3H_2O + Ca(OH)_2 \quad (2.2)$$

$$3CaO.Al_2O_3 + 12H_2O + Ca(OH)_2 \rightarrow 3CaO.Al_2O_3.Ca(OH)_2.12H_2O \quad (2.3)$$

Where, 2(3 CaO.SiO2) is tricalcium silicate, H2O is water,

3CaO.2SiO2.3H2O is calcium silicate hydrate (CSH),

3Ca (OH)2 is calcium hydroxide and

3CaO.Al2O3.Ca(OH)2.12H2O is. Calcium aluminate hydrate (CAH).

❖ Pozzolanic reaction of Portland cement and clay minerals (Chian & Bi, 2021; Jing et al., 2022; Kitazume, 2013; Xiaoyuan et al., 2019; Zhu et al., 2009)

$$Ca(OH)_2 \rightarrow Ca^{2+} + 2OH^- \quad (2.4)$$

$$Ca^{2+} + 2OH^- + SiO_2(\text{clay silica}) \rightarrow CSH \quad (2.5)$$

$$Ca^{2+} + 2OH^- + Al_2O_3(\text{clay almunia}) \rightarrow CAH \quad (2.6)$$

The main act however, of hydration and pozzolanic reaction process contributes solidification of the dredged clay soils, however the stabilization process affected by different factors like the properties of soils mixed with cement, cement content, water-cement ratio, curing conditions, and environmental conditions (Chian & Bi, 2021; Hoang et al., 2020; Kitazume, 2013). One of the most fundamental factors influencing the strength of cement-stabilized soil is the amount and type of cement used in the mixture (Ho et al., 2020; Vinoth et al., 2018). Higher cement content generally results in greater strength, as it provides more binding agents for solid soil particles. The type of pozzolanic materials chosen also matters; Portland cement and other different cementitious materials like hydrated lime can impact the rate of hydration and the resulting strength. Properly selecting and evaluating the right type and amount of cement is essential for achieving the desired strength and durability.

The water-cement ratio plays a critical role in cement hydration and strength development during hydration and solidification process. Previously water content used for mixing cement-treated soils and the water/cement ratio in cement-treated soils studied by (Y. Liu et al., 2019). Too much water can lead to excessive dilution of the cement paste, weakening the binding effect and has unsuitable workability. Conversely, too little water can hinder proper hydration process. Finding the optimal water-cement ratio is essential to ensure complete cement particle activation and efficient bonding between cement and solid soil particles. Adequate curing is indispensable for developing optimal compressive strength in cement-stabilized soil. Proper curing involves maintaining controlled moisture and temperature levels over a specified time period (Chaiyaput et al., 2022; Kampala et al., 2021) that insufficient curing may result in incomplete hydration and reduced pozzolanic effect. Adequate curing enables the cement particles to form strong bonds and crystalline structures, enhancing the matrix composite's overall strength and durability.

The inherent properties of the soil greatly influence the strength of cement-stabilized mixtures soils (Chian et al., 2017; Chian & Bi, 2021; Kitazume, 2013; Nadeem et al., 2023; N. B. Vu et al., 2022). Clay-rich soils tend to respond well to cement stabilization due to their fine particle size, which offers increased surface area to volume ratio for bonding. In contrast, sandy soils might require adjustments, such as modifying particle size distribution or adding pozzolanic additive materials, to achieve comparable strength enhancements. Similarly adequate compaction is essential for optimizing the density and strength of cement-stabilized soil. This ensures that cement particles are evenly distributed throughout the soil matrix, increases strong interlocking tendencies and reduces voids.

T. B. Vu et al. (2023) evaluated the curing condition, soils under sealed conditions, drying conditions greatly increased the UCS of soils treated with cement, regardless of the cement type, cement content, soil type, or age. Generally speaking, the UCS of specimens dried under different conditions was 1.3–2.5 times more than it was under sealed curing conditions. Considering the amount cement content, an increase in cement content shows the unconfined compressive strength and elastic modulus of the soil specimens treated with cement were clearly increased. In his study the three different cement Vissai Cement, Chinfon Cement, and Nghi Son Cement all performed differently when it came to enhancing soft soils. Vissai Cement outperforms others as shown in figure 7. When the sealed setting considered for failure mode, the cement-treated soil samples displayed a ductile failure mode, whereas when dried, they displayed a brittle failure mode. Regardless of cement amount and curing circumstances, the cement-treated black sandy clay specimens had lower unconfined compressive strength and elasticity than the cement-treated yellow clay specimens due to its fine clay particles as shown in **Figure 2.3**. The Dredged soils which are treated with cement are commonly used across the world, especially in offshore areas. Back in 2000 In Japan 8.6 million m3 of construction fill material to build Chubu International airport as report by (Yamashita et al., 2020).

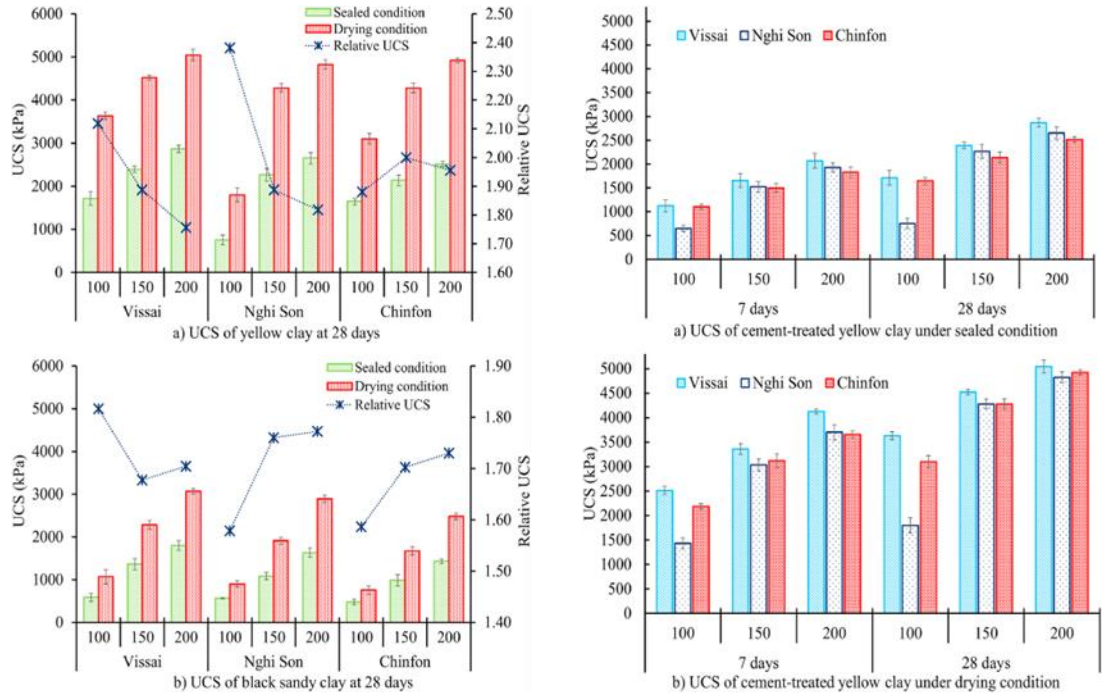


**Figure 2.3: Effect of curing condition on UCS of cemented soils at 28 days (T. B. Vu et al., 2023).**

### 2.2.2. Natural fiber stabilized dredged soils

The utilization of a high amount of pure cement for soil improvement, while offering increased strength and stiffness due to cementing caused by pozzolanic reactions, presents certain drawbacks. The manufacture of cement emits greenhouse gases, especially carbon dioxide, which increases the rise of environmental pollution concerns (Flatt et al., 2012; D. Wang et al., 2019) resulting from high cement usage. Furthermore, the high energy consumption and depletion of resources are associated with cement production. In addition, the cost implications of using high amounts of cement, especially in the context of escalating prices of cement and other binders, have contributed to increased construction, restoration, and maintenance costs for infrastructure development. As a result, it is important to investigate ecologically sound alternative green binders that can substitute for cement in the context of soil solidification (Feng et al., 2023). This pursuit is crucial for advancing a low-carbon economy and fostering sustainable societal progress. Treating dredged clay soils by addition of fibers has gained significant attention in recent years.

However, soil improvement by incorporating random inclusions of fiber, such as straw and hay, into mud blocks to create reinforced building blocks was started during ancient civilization. For instance, the Great Wall of China, where branches of trees were used as tensile elements, and the ziggurats of Babylon also showcased the use of woven mats made from reeds to strengthen the soil stands as one of the earliest examples of reinforced earth.

These ancient constructions demonstrate the recognition of the concept of fiber reinforcement over 5000 years ago (Hejazi et al., 2012). However, the idea and principles of soil reinforcement were initially established by (Vidal, 1969), who demonstrated that incorporating reinforcing elements into a soil mass enhances its shearing strength. Subsequently, the use of fibrous materials for enhancing the engineering properties of soils has seen an uptick, imitating past practices (Hejazi et al., 2012). These fibers can be synthetic fibers, such as nylon, polypropylene, polyester, and glass fibers (Gao & Zhao, 2013) or natural fibers, such as coir, jute, sisal, and wheat straw fibers, have been proven to be effective for soil reinforcement used for soil stabilization (Arifin, 2022). Natural fibers are organic materials derived from various plant sources and possess inherent mechanical, physical, and chemical properties that make them suitable options for soil stabilization applications for construction projects. Some of the natural fibers utilized previously are coconut fibers, jute fibers, straw, hemp fiber, sisal fibers, kenaf fiber, bamboo, and others. While modern alternatives like concrete, glass-fiber/resin composites, steel, and plastics are available, there continues to be a significant demand for naturally occurring materials in various applications because of their affordability along with desirable attributes such as durability, strength, heat resistance capabilities, and fire-resistance characteristics (Nazir et al., 2023). Natural fibers can be categorized into three main groups based on their origin: (i) plant-based fibers like bamboo, jute, coir, hemp, etc., (ii) animal-derived fibers containing protein such as silk, hair, wool, etc., and (iii) mineral-based fibers. Among these categories, there is a growing interest in utilizing plant-based fibers for geotechnical purposes due to their availability and suitability for large-scale applications (Gowthaman et al., 2018).

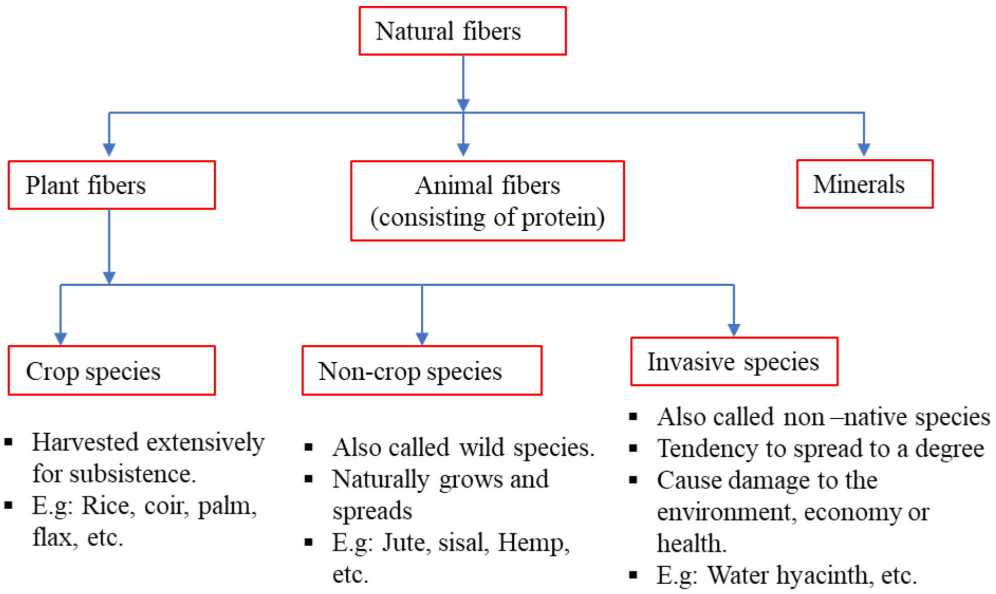


**Figure 2.4: Natural fiber incorporated in soil reinforcement (Gowthaman et al., 2018)**

**Table 2.2: Amount Summery of plant additive effect for soil improvement**

| Fiber type | Amount used (%) | Advantage | References |
|---|---|---|---|
| Bamboo | 0-5 | Enhance thermal stability, weather resistance prevention of water ingress, Prevention of microbial degradation. | (Fard et al., 2022; Javadian et al., 2016; X. Wang et al., 2020) |
| Jute fiber | 5-20 | Increase surface roughness of fiber.<br>Increase strength, decrease water absorption.<br>Prevention of water ingress, prevention of microbial degradation. | (Lee et al., 2017; J. Zhang et al., 2021) |
| Sisal fiber | 10-40 | Modification of fiber cell wall as hydrophobic, increase rigidity and roughness of fiber.<br>Reduce hydrophilic tendency. | (Asim et al., 2018; Ibrahim et al., 2016; Y. Wu et al., 2014) |
| Waste coffee beans | 1-20 | Increased tensile strength and young’s modulus<br>Improved compressive strength.<br>Increased porosity, water absorption capacity & firing temperature. | (Sarasini et al., 2018; Sena Da Fonseca et al., 2014) |

### 2.2.2.1. Bamboo fibers

Bamboo fibers have emerged as a sustainable and innovative solution for soil stabilization, especially in areas prone to erosion, slope failures, and other forms of land degradation. The use of bamboo fibers in soil stabilization processes presents exceptional advantages, primarily rooted in their exceptional mechanical properties and environmentally friendly nature. When mixed with soil, bamboo fibers create a reinforced matrix that enhances the soil's cohesion, shear strength, and load-bearing capacity by interlocking the fine clay soil particles (Koga et al., 2016) reported that addition of bamboo fibers for high water content clay soils increases the cone index properties of the mix by adding 5% to 90% fiber amount as shown in **Figure 2.5**.

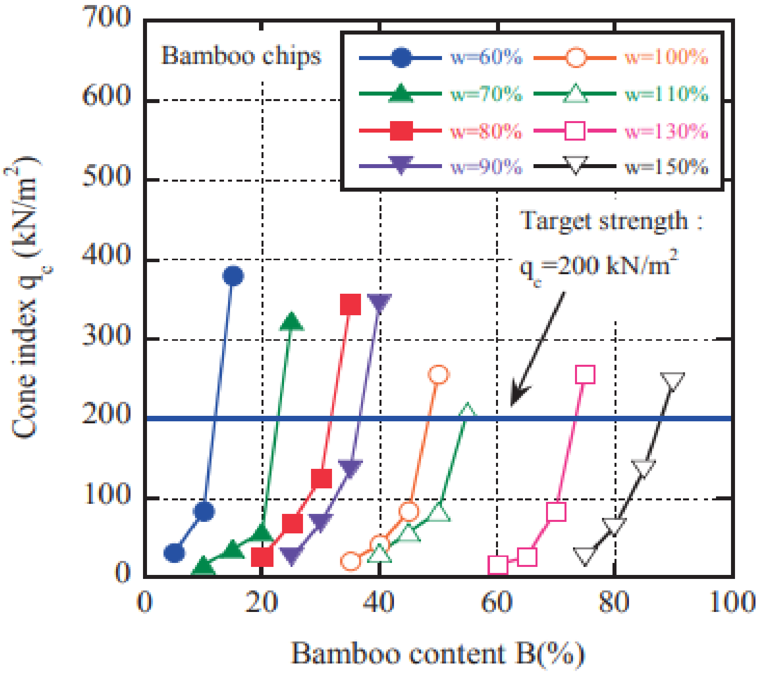


**Figure 2.5: Relationships between bamboo content and cone index qc of treated soil (Koga et al., 2016)**

Utilization of bamboo fibers for stabilization is their remarkable tensile strength and it also possesses impressive strength-to-weight ratios, which allows them to effectively distribute and resist imposed loads within the treated soil matrix. This reinforcement significantly reduces soil erosion and helps to prevent slope instability, making bamboo fiber-treated soils particularly suitable for road embankments, retaining walls backfills, and other construction infrastructure projects. This is shown from the study of (Kanayama & Kawamura, 2019) results of the unconfined compression test showed that the compressive stresses in all samples tended to rise as the proportion of bamboo fiber increased. Where the highest compressive stresses recorded for varying bamboo fiber contents (0%, 1%, 3%, and 5%) were 115, 108, 130, and 152 kN/m$^2$, respectively in his report. It also shows that in arid conditions, the soil containing fibers exhibited reduced rigidity, but greater durability compared to the fiber less soil. This indicates that the addition of fiber enhanced the soil's ability to undergo deformation.

Additionally, the water absorption characteristics of bamboo fibers contribute to their ability to form a stable bond with the clay particles. The fine powder fiber particles absorb water at a very high rate of 742.8% to 775.4% which shown in Table 2.2 by evaluating at different initial water content and absorption time using 1g of dry bamboo fiber using equation 2.7 (Kanayama & Kawamura, 2019). As the fibers absorb moisture from the surrounding soil, the swell characteristics are reduced and make intimate contact with the clay particles. This bonding effect helps to create a reinforced network within the soil matrix, contributing to enhancing its mechanical properties and overall stability. When the soil dries out, the bamboo fibers release the absorbed water, but they still maintain a degree of interlocking with the clay particles, contributing to a stiffer, resilient and cohesive soil structure of treated clay soil. In general, the addition of bamboo fibers increases the ultimate load bearing capacity of soft soils up to sixfold compared to conventional soil (Nazir et al., 2023).

$$CA_r = \frac{m_w}{m_b} * 100 \tag{2.7}$$

Where $A_r$ is the water absorption rate, $m_w$ is the mass of absorbed water in the bamboo fiber, $m_b$ is the dry mass of the bamboo fiber used in the experiment in this study which is 1g.

**Table 2.3: Water absorption test of bamboo fiber (Kanayama & Kawamura, 2019)**

| Initial Water Content in Bamboo Fiber (%) | Absorption Time (min) | Water Absorption Rate, Ar (%) |
|---|---|---|
| 0 | 1 | 775.4 |
| | 1440 | 772.3 |
| 10 | 1 | 751.5 |
| | 1440 | 742.8 |

### 2.2.2.2. Jute fibers

Jute fibers are another promising material that can be utilized as dredged soil reinforcing materials by researchers and engineers which is widely grown, cost-effective, commercially available. In the research conducted by (Ghosh et al., 2017), jute fibers were found to offer several advantages. For instance, the weft yarns of jute create successive obstacles along the sheet flow's route down the slope, leading to a decrease in flow velocity at each crossing point. Additionally, the fabric's pores facilitate improved water absorption, by its temporary pooling of water within these pore spaces which mainly desaturate the high-water content clay soils during treatment process.

In addition, as (Nazir et al., 2023) reported the exceptional surface texture and impressive tensile strength have found practical employment in diverse scenarios. For instance, they have been employed in tasks such as enhancing the solidity of loose soil, crafting roads in less-developed regions, safeguarding riverbanks, strengthening embankments, controlling erosion, and slope stability management. It also shows incorporating jute fibers leads to enhancements in the structural and fracture characteristics of clay modified starch composites. Moreover, the introduction of 15% optimum jute fibers content results in a notable 20% increase in tensile strength and a remarkable 37% boost in modulus for composites composed of polyethylene and nano-clay additives (Hossen et al., 2015).

## 2.3. Cement and natural fibers stabilized dredged soils

Separately both cement and natural fibers can reinforce the dredged clay soils significantly as discussed, the above sections. But the effect of the combined utilization of cement and natural fibers makes the balance for efficient treatment, cost effective and environmentally friendly. (J. S. Li et al., 2023a) studied the usage of straw fiber (SF) as natural reinforcements for cement-stabilized DS (CDS) in their research. They performed a range of unconfined compressive strength (UCS) experiments to investigate how factors such as cement amount, fiber quantity, fiber size, water content, and curing time influence the enhancement of strength and the stress-strain behavior in the context of fiber-reinforced cement-stabilized dredged soils (CSFDS) which explained as follows:

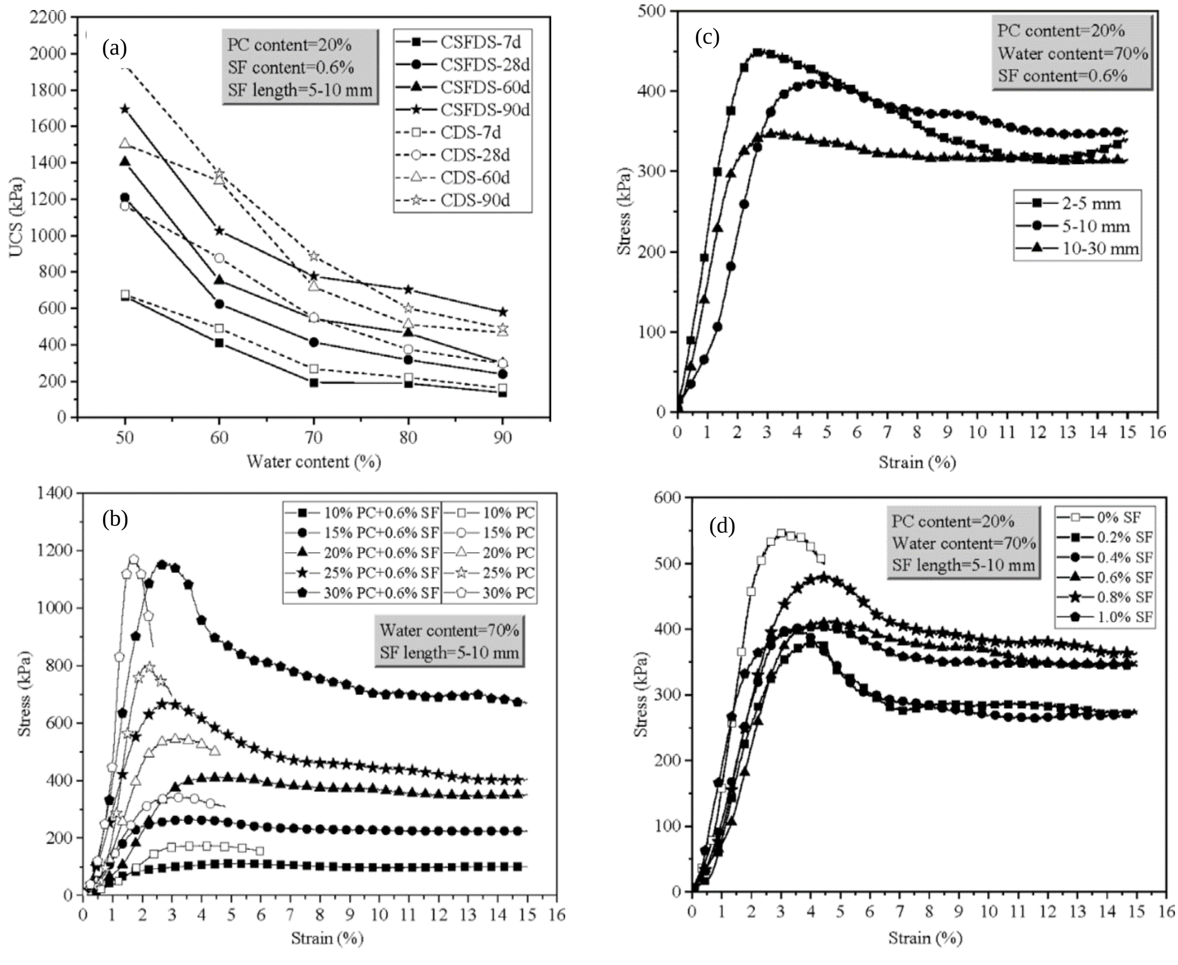


**Figure 2.6: The effect of (a) water content (b) PC cement amount (c) fiber length (d) fiber amount on cement (CDS) and fiber (CSFDS) treated dredged soil (J. S. Li et al., 2023).**

The first is the effect of water content, that the impact of varying water levels on the unconfined compressive strength (UCS) of CSFDS is shown in **Figure 2.5** (a), while the UCS of CDS is provided for comparison. It is observed that the UCS values for both CSFDS and CDS declined as the water content increased. If we considered the 28-day UCS, when the water content increased from 50% to 90%, the UCS of CSFDS and CDS decreased by 80.2% and 74.4% respectively where UCS of CDS was generally higher than that of CSFDS. Three main reasons were responsible for the strength decrease with increasing water content. The reduction in strength with elevated water content was attributed to three primary factors. As (J. S. Li et al., 2023a; Yang & Du, 2021) studied the first one is the augmentation in water content weakened the capacity of cementitious materials to create and solidify, thereby leading to a reduction in the adhesive strength among cemented soil particles. The other is the gap between soil particles widened as water content increased, reducing the compactness of cementation within the specimen (L. Liu et al., 2019; Yin et al., 2019) The third reason which is studied by (J. Li et al., 2014), water acted as a lubricant, causing a decrease in matric suction between soil particles as water content increases, consequently weakening the inter-particle cohesion. The other is the cement PC content as shown in **Figure 2.6** (b) as strain continued to increase, the stress of CSFDS rose until reaching a peak value, then declined to residual stress levels. In contrast, following the attainment of its peak value, the stress of CDS reduced as strain increased, without residual stress levels being present. These observations show that when subjected to compressive forces, CSFDS demonstrated greater ductility and higher residual stress in comparison to CDS, affirming the role of fiber reinforcement in enhancing ductility properties. Additionally, as the PC content increased, the stress-strain behavior at the peak became progressively sharper, indicating an increasingly brittle characteristic of the treated soil. As shown **Figure 2.6** (c) the effect of fiber length on the stress strain curves of CSFDS shows that the stress increased firstly until reaching the peak stress and then decreased to a residual stress level with the continuous reduction of strain. With the increase of fiber length, the steep drop after peak stress tended to be flat, indicating that long fiber was conducive to improving the ductile behavior of CSFDS soil matrix. Furthermore, residual stress of CSFDS increased firstly and then decreased with increasing fiber length, which is slightly different from the corresponding UCS evolutions with natural fiber length. By utilizing the SF length range of 2–5 mm, 5–10 mm and 10–30 mm, the $\varepsilon_f$ of CSFDS is 2.76%, 4.62% and 3.15% respectively and the corresponding $\sigma_{max}$ is 452.65 kPa, 414.16 kPa. Another crucial aspect of fiber is the amount of fiber included in the mixture. As shown in **Figure 2.6** (d), the stress of CSFDS climbed as strain increased, reaching a peak stress before re to residual stress levels (J. S. Li et al., 2023a). In contrast, the stress-strain pattern of CDS did not imply residual stress levels, showing that the addition of fiber contributed to the development of a continuous load-bearing capacity after failure. As fiber content increased, the stress-strain behavior at the peak transitioned towards a more gradual pattern, suggesting that a greater amount of added fiber led to a more pronounced ductile characteristic. Moreover, the residual stress of CSFDS exhibited minimal change as the SF content increased in the treated soil matrix.

As Phan Thanh et al., (2018) studied the effect of incorporating rice husk and cement on unconfined strength of modified sludge with different cement and water content. As shown in **Figure 2.7** with same rice husk fiber content the failure strength increased with increasing the cement content and making the modified sludge more brittle. Regarding the combined rice husk fiber and cement inclusion were added more than the upper limit, the failure strength will decrease. In the comprehensive study conducted by (Phan Thanh et al., 2018), a profound exploration was undertaken to elucidate the impact of integrating rice husk and cement into the composition of modified sludge, considering variations in cement, rice husk fiber and water content. As shown in **Figure 2.7**, a noteworthy trend emerged where, under the same rice husk fiber content, the failure strength of the modified sludge exhibited a significant increament with the progressive increment of cement content. This intriguing finding suggested that the heightened cement presence rendered the modified sludge more susceptible to brittleness, potentially altering its mechanical properties.

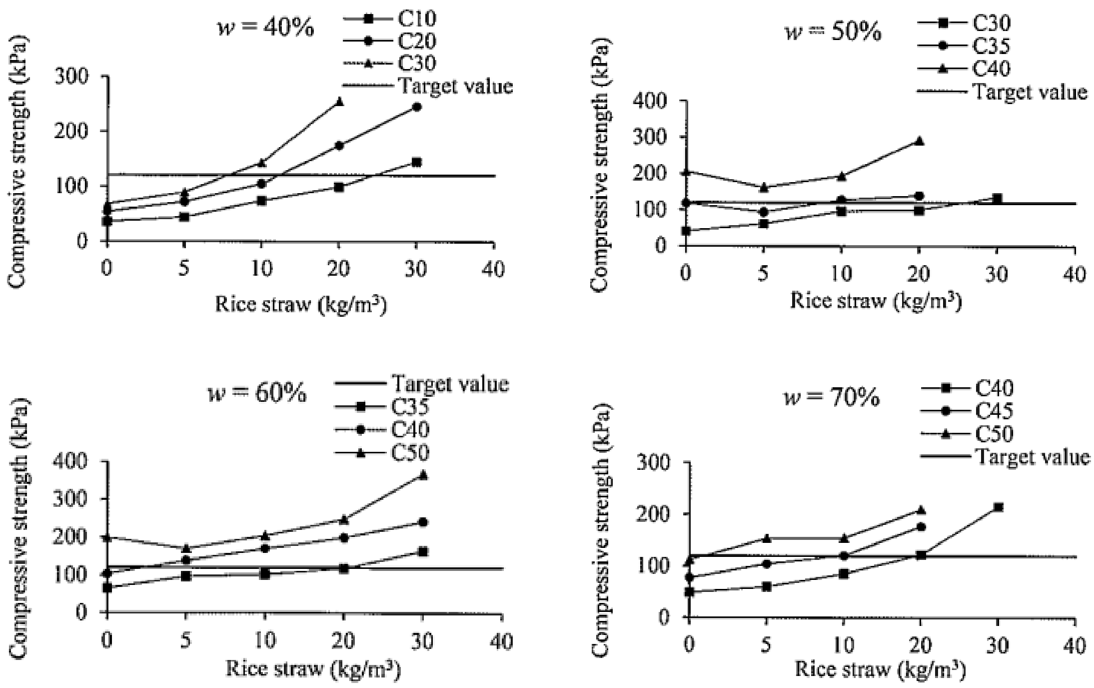


**Figure 2.7: Failure strength and strain of rice husk and cement treated soft soil (Phan Thanh et al., 2018).**

Remarkably, the investigation also digs into the combined effect of both rice husk fiber and cement combined incorporation. It was ascertained that while the initial addition of these components led to an enhancement in the failure strength, surpassing a certain threshold of inclusion for either rice husk fiber or cement resulted in a counterintuitive decrease in the failure strength of in most of test cases. This phenomenon emphasized the critical importance of meticulous optimization when designing composite materials, emphasizing that an excessive concentration of reinforcing agents could compromise the overall structural integrity of the modified sludge which is found for each water content. Thus, the study not only shed light on the intricate interplay between rice husk, cement, and water content but also highlighted the significance of balance and precision in tailoring composite formulations to achieve desired mechanical characteristics.

Sawamura et al. (2017) discovered variations in water absorption characteristics based on the proportion of paper fiber-derived FSP to shredder shavings-derived FSP. Additionally, they observed that the shear strength of clay treated with FSP was greater than that of pure clay. Kida et al. (2018) determined, through flow tests and cone index tests, that the transportation of FSP-treated clay remained viable as long as the flowability had decreased to a measurable extent, even if the strength fell below the typical 200 kN/m$^2$ during the interparticle reinforcement process.

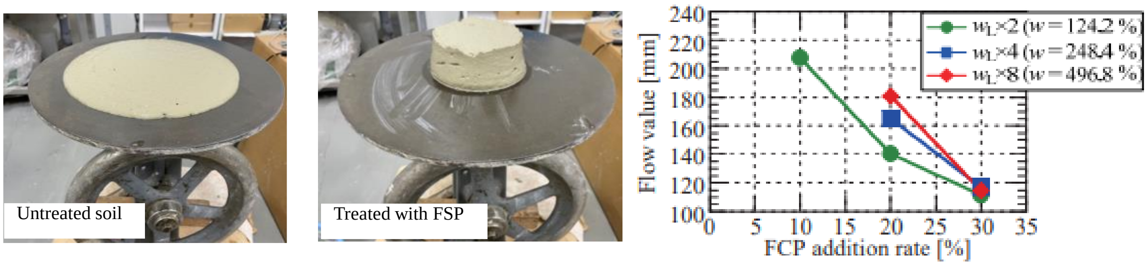


**Figure 2.8: Effect of FSP additive on flowability of highwater content clay soil (Kida et al., 2018).**

However, based on the above comprehensive review, the effect of the finely shredded paper treatment on the different engineering properties of soft soil is not sufficiently studied. Moreover, the advantage of utilization of combined finely shredded paper and cement for the treatment of soft soil needs more detailed study. Therefore, further investigations on the behavior of soft soil treated with finely shredded paper or finely shredded paper with cement combination are carried out and presented the following chapters which aims to search for a practical possible solution of utilizing this ecofriendly waste in the field of infrastructure construction for sustainable development.

**References for Chapter 2**


Abedi, M., Hassanshahi, O., Rashiddel, A., Ashtari, H., Seddik Meddah, M., Dias, D., Arjomand, M. A., & Keong Choong, K. (2023). A sustainable cementitious composite reinforced with natural fibers: An experimental and numerical study. *Construction and Building Materials*, *378*. https://doi.org/10.1016/j.conbuildmat.2023.131093

Abo El-Naga, I., Elsiragy, M. N., & Ragab, M. (2020). Utilization of synthetic reinforcement for enhancement of oil-contaminated subgrade soil in highway pavement. *Innovative Infrastructure Solutions*, *5*(2). https://doi.org/10.1007/s41062-020-00289-9

ACI Committee 230, S. Cement., & American Concrete Institute. (2009). *Report on soil cement (ACI 230.1R-09)*. American Concrete Institute.

Ahmad, F., Bateni, F., & Azmi, M. (2010). Performance evaluation of silty sand reinforced with fibres. *Geotextiles and Geomembranes*, *28*(1), 93–99. https://doi.org/10.1016/j.geotexmem.2009.09.017

Akbari, H. R., Sharafi, H., & Goodarzi, A. R. (2021). Effect of polypropylene fiber and nano-zeolite on stabilized soft soil under wet-dry cycles. *Geotextiles and Geomembranes*, *49*(6), 1470–1482. https://doi.org/10.1016/j.geotexmem.2021.06.001

Amar, M., Benzerzour, M., Kleib, J., & Abriak, N. E. (2021). From dredged sediment to supplementary cementitious material: characterization, treatment, and reuse. In *International Journal of Sediment Research* (Vol. 36, Issue 1, pp. 92–109). Elsevier B.V. https://doi.org/10.1016/j.ijsrc.2020.06.002

Arifin, Y. F. (2022). Tensile Strength and Durability of Oil Palm Empty Fruit Bunch Fiber in Soft Soil. *International Journal of Geomate*. https://doi.org/10.21660/2022.99.3610

Asai, Y., Ryunosuke, K., Sawamura, Y., & Makoto, K. (2021). Mechanical properties of clayey soil with fine shredded paper by the addition of cement. *Environmental Geotechnical Engineering Symposium*, *14*(September), 415–422.

Asim, M., Jawaid, M., Abdan, K., Ishak, M. R., & Alothman, O. Y. (2018). Effect of Hybridization on the Mechanical Properties of Pineapple Leaf Fiber/Kenaf Phenolic Hybrid Composites. *Journal of Renewable Materials*, *6*(1), 38–46. https://doi.org/10.7569/JRM.2017.634148

Babu, G. L. S., Srivastava, A., & Sivapulliah, P. V. (2011). Reliability analysis of strength of cement treated soils. *Georisk: Assessment and Management of Risk for Engineered Systems and Geohazards*, *5*(3–4), 157–162. https://doi.org/10.1080/17499518.2010.490116

Bo, M. W., Arulrajah, A., & Nikraz, H. (2007). Preloading and prefabricated vertical drains design for foreshore land reclamation projects: a case study. *Ground Improvement*, *11*, 67–76. https://api.semanticscholar.org/CorpusID:55080359

Cao, Z., Ma, Q., & Wang, H. (2019). Effect of Basalt Fiber Addition on Static-Dynamic Mechanical Behaviors and Microstructure of Stabilized Soil Compositing Cement and Fly Ash. *Advances in Civil Engineering*. https://doi.org/10.1155/2019/8214534

Çevikbilen, G., Merve Başar, H., Karadoğan, Ü., Teymur, B., Dağlı, S., & Tolun, L. (2020). *Assessment of the use of marine dredged materials in the sanitary landfills: A case study from the Marmara Sea Assessment of the use of dredged marine materials in sanitary landfills: a 1 case study from the Marmara Sea 2*.

Chaiyaput, S., Arwaedo, N., Kingnoi, N., Nghia-Nguyen, T., & Ayawanna, J. (2022). Effect of curing conditions on the strength of soil cement. *Case Studies in Construction Materials*, *16*. https://doi.org/10.1016/j.cscm.2022.e01082

Chan, C. M., & Abdul Jalil, A. N. (2014). Some insights to the reuse of dredged marine soils by admixing with activated steel slag. *Advances in Civil Engineering*, *2014*. https://doi.org/10.1155/2014/345134

Chian, S. C., & Bi, J. (2021). Influence of grain size gradation of sand impurities on strength behaviour of cement-treated clay. *Acta Geotechnica*, *16*(4), 1127–1145. https://doi.org/10.1007/s11440-020-01090-9

Chian, S. C., Chim, Y. Q., & Wong, J. W. (2017). Influence of sand impurities in cement-treated clays. *Geotechnique*, *67*(1), 31–41. https://doi.org/10.1680/jgeot.15.P.179

Chu, S. H., & Yao, J. J. (2020). A strength model for concrete made with marine dredged sediment. *Journal of Cleaner Production*, *274*. https://doi.org/10.1016/j.jclepro.2020.122673

Consoli, N. C., Vendruscolo, M. A., Fonini, A., & Rosa, F. D. (2009). Fiber Reinforcement Effects on Sand Considering a Wide Cementation Range. *Geotextiles and Geomembranes*. https://doi.org/10.1016/j.geotexmem.2008.11.005

Duong, N. T., Satomi, T., & Takahashi, H. (2021). Potential of corn husk fiber for reinforcing cemented soil with high water content. *Construction and Building Materials*, *271*. https://doi.org/10.1016/j.conbuildmat.2020.121848

Duong, T. N., Satomi, T., & Takahashi, H. (2019). *Mechanical Behavior Comparison of Cemented Sludge Reinforced by Waste Material and Several Crop Residues*.

Estabragh, A. R., Namdar, P., & Javadi, A. A. (2012). Behavior of Cement-Stabilized Clay Reinforced with Nylon Fiber. *Geosynthetics International*. https://doi.org/10.1680/gein.2012.19.1.85

Fard, H. S., König, D., & Goudarzy, M. (2022). SOIL-WATER CHARACTERISTICS CURVE OF FIBER REINFORCED SOILS. *Journal of Geo Engineering*, *17*(3), 153–163. https://doi.org/10.6310/jog.202209_17(3).4

Feng, D., Liang, B., He, X., Yi, F., Xue, J., Wan, Y., & Xue, Q. (2023). Mechanical properties of dredged soil reinforced by xanthan gum and fibers. *Journal of Rock Mechanics and Geotechnical Engineering*, *15*(8), 2147–2157. https://doi.org/10.1016/j.jrmge.2023.02.010

Flatt, R. J., Roussel, N., & Cheeseman, C. R. (2012). Concrete: An eco material that needs to be improved. *Journal of the European Ceramic Society*, *32*(11), 2787–2798. https://doi.org/10.1016/j.jeurceramsoc.2011.11.012

Fukushima, S., Kitajima, A., Ishiguro, K., Ikeda, Y., Sakamaki, K., & Tani, S. (2000). Applicability of cement-stabilized pond-mud soil as embankment material for irrigation pond dam repairment. *Journal of Japan Society of Civil Engineers, 666*(in Japanese), 99–116.

Gao, Z., & Zhao, J. (2013). Evaluation on Failure of Fiber-Reinforced Sand. *Journal of Geotechnical and Geoenvironmental Engineering*. https://doi.org/10.1061/(asce)gt.1943-5606.0000737

García, G., José, R., Jiménez, A., Iván, V., Manteca, A., Encarnación, M., & Moreno, M. (2022). *Resolution of Geotechnical engineering problems with Plaxis 2D*.

Ghadir, P., & Ranjbar, N. (2018). Clayey Soil Stabilization Using Geopolymer and Portland Cement. *Construction and Building Materials*. https://doi.org/10.1016/j.conbuildmat.2018.07.207

Ghosh, S. K., Bhattacharyya, R., & Mondal, M. M. (2017). Potential Applications of Open Weave Jute Geotextile (Soil Saver) in Meeting Geotechnical Difficulties. *Procedia Engineering*, *200*, 200–205. https://doi.org/10.1016/j.proeng.2017.07.029

Gowthaman, S., Nakashima, K., & Kawasaki, S. (2018). A state-of-the-art review on soil reinforcement technology using natural plant fiber materials: Past findings, present trends and future directions. In *Materials* (Vol. 11, Issue 4). MDPI AG. https://doi.org/10.3390/ma11040553

Guo, Q., Zhan, L., Shen, Y., Wu, L., & Chen, Y. (2022). Classification and quantification of excavated soil and construction sludge: A case study in Wenzhou, China. *Frontiers of Structural and Civil Engineering*, *16*(2), 202–213. https://doi.org/10.1007/s11709-021-0795-8

Gupta, A., & Kumar, M. (2021). Clayey soil stabilization using fly ash and jute fiber. Materials Today: Proceedings, 48, 1205–1210. https://doi.org/10.1016/j.matpr.2021.08.246

Haakeel, M. S. S., Ramzi, M. Z. M., & Nasvi, M. C. M. (2019). Compressibility Behavior of Peat Reinforced with Single and Multiple Deep Soil Mixing (DSM) Columns. *Engineer: Journal of the Institution of Engineers, Sri Lanka*, *52*(3), 1. https://doi.org/10.4038/engineer.v52i3.7360

Hassan, H. J. A., Rasul, J., & Samin, M. (2021). Effects of Plastic Waste Materials on Geotechnical Properties of Clayey Soil. *Transportation Infrastructure Geotechnology*, *8*(3), 390–413. https://doi.org/10.1007/s40515-020-00145-4

He, J., Shi, X. kang, Li, Z. xiang, Zhang, L., Feng, X. ying, & Zhou, L. rong. (2020). Strength properties of dredged soil at high water content treated with soda residue, carbide slag, and ground granulated blast furnace slag. *Construction and Building*

*Materials*, *242*. https://doi.org/10.1016/j.conbuildmat.2020.118126

Hejazi, S. M., Sheikhzadeh, M., Abtahi, S. M., & Zadhoush, A. (2012). A simple review of soil reinforcement by using natural and synthetic fibers. In *Construction and Building Materials* (Vol. 30, pp. 100–116). https://doi.org/10.1016/j.conbuildmat.2011.11.045

Ho, L. S., Nakarai, K., Eguchi, K., & Ogawa, Y. (2020). Difference in strength development between cement-treated sand and mortar with various cement types and curing temperatures. *Materials*, *13*(21), 1–15. https://doi.org/10.3390/ma13214999

Hoang, N. H., Ishigaki, T., Kubota, R., Tong, T. K., Nguyen, T. T., Nguyen, H. G., Yamada, M., & Kawamoto, K. (2020). Waste generation, composition, and handling in building-related construction and demolition in Hanoi, Vietnam. *Waste Management*, *117*, 32–41. https://doi.org/10.1016/j.wasman.2020.08.006

Hossen, Md. F., Hamdan, S., Rahman, Md. R., Rahman, Md. M., Liew, F. K., & Lai, J. C. (2015). Effect of fiber treatment and nanoclay on the tensile properties of jute fiber reinforced polyethylene/clay nanocomposites. *Fibers and Polymers*, *16*(2), 479–485. https://doi.org/10.1007/s12221-015-0479-x

Hu, Q. M., Huang, Y. X., Zhang, W. Y., Shao, G. T., Xu, Y., Zhang, Y. H., Pan, Y., & Mi, J. X. (2023). Industrial-scale extraction of high value-added kaolin from excavation waste: Demonstration from Xiamen, China. *Waste Management*, *163*, 144–153. https://doi.org/10.1016/j.wasman.2023.03.028

Huayang, L., Yinggang, X., Xin, L., Mingjing, J., & Liangzhi, L. (2019). Effect of Polyacrylamide on Improvement of Dredger Fill with Vacuum Preloading Method. *Journal of Materials in Civil Engineering*, *31*(9), 04019193. https://doi.org/10.1061/(ASCE)MT.1943-5533.0002860

Ibrahim, I. D., Jamiru, T., Sadiku, E. R., Kupolati, W. K., & Agwuncha, S. C. (2016). Impact of Surface Modification and Nanoparticle on Sisal Fiber Reinforced Polypropylene Nanocomposites. *Journal of Nanotechnology*, *2016*. https://doi.org/10.1155/2016/4235975

Jan, O. Q., & Mir, B. A. (2018). Strength Behaviour of Cement Stabilised Dredged Soil. *International Journal of Geosynthetics and Ground Engineering*, *4*(2). https://doi.org/10.1007/s40891-018-0133-y

Javadian, A. A., Wielopolski, M. B., Smith, I. F. C., Hebel, D. E., Javadian, A., Wielopolski, M., Smith, I. F. C., & Hebel, D. E. (2016). *Bond-behavior study of newly developed bamboo-composite 4 reinforcement in concrete*.

Jiang, P., Chen, L., Li, N., Qian, J., & Wang, W. (2022). Study on the mechanical properties of fiber-modified iron tailings stabilized by lime and fly ash based on energy analysis. *Case Studies in Construction Materials*, *17*. https://doi.org/10.1016/j.cscm.2022.e01638

Jing, P., Song, X., Zhang, J., & Nowamooz, H. (2022). A review of hydro-mechanical coupling behaviour of cement-treated materials. In *Construction and Building*

*Materials* (Vol. 322). Elsevier Ltd. https://doi.org/10.1016/j.conbuildmat.2022.126446

John, E., & Lothenbach, B. (2023). Cement hydration mechanisms through time – a review. In *Journal of Materials Science* (Vol. 58, Issue 24, pp. 9805–9833). Springer. https://doi.org/10.1007/s10853-023-08651-9

Kamaruddin, F. A., Nahazanan, H., Huat, B. K., & Anggraini, V. (2020). Improvement of marine clay soil using lime and alkaline activation stabilized with inclusion of treated coir fibre. *Applied Sciences (Switzerland)*, *10*(6). https://doi.org/10.3390/app10062129

Kampala, A., Jitsangiam, P., Pimraksa, K., & Chindaprasirt, P. (2021). An investigation of sulfate effects on compaction characteristics and strength development of cement-treated sulfate bearing clay subgrade. *Road Materials and Pavement Design*, *22*(10), 2396–2409. https://doi.org/10.1080/14680629.2020.1753564

Kanayama, M., & Kawamura, S. (2019). Effect of Waste Bamboo Fiber Addition on Mechanical Properties of Soil. *Open Journal of Civil Engineering*, *09*(03), 173–184. https://doi.org/10.4236/ojce.2019.93012

Kasama, K., Zen, K., & Kiyoharu, I. (2007). High-strengthening of cement -treated clay by mechanical dehydration. In *SOILS AND FOUNDATIONS* (Vol. 47, Issue 2).

Khodabandeh, M. A., Nagy, G., & Török, Á. (2023). Stabilization of collapsible soils with nanomaterials, fibers, polymers, industrial waste, and microbes: Current trends. In *Construction and Building Materials* (Vol. 368). Elsevier Ltd. https://doi.org/10.1016/j.conbuildmat.2023.130463

Kida, S., Sawamura, Y., Yano, T., & Kimura, M. (2018). *Changes in strength and transportability of high-water content mud treated by fine powder made from wastepaper*.

Kitazume, M., & T. M. (2013). The Deep Mixing Method (1st ed.). In *The Deep Mixing Method (1st ed.)*. CRC Press.

Kodicherla, S. P. K., & Nandyala, D. K. (2019). Influence of randomly mixed coir fibres and fly ash on stabilization of clayey subgrade. *International Journal of Geo-Engineering*, *10*(1). https://doi.org/10.1186/s40703-019-0099-1

Koga, C., Kenichi, S., & Fujikawa, T. (2016). Examination of the Utilization of Bamboo in the Soft Ground Improvement. *Journal of the Society of Materials Science*, *65*(1), 16–21.

Koike, K., Nakazaki, K., Miyoshi, M., Nishijima, T., Matsumoto, K., Yamaguchi, F., & Todoroki, K. (2004). In-situ test of vacuum consolidation method for the densification of fine-grained dredging material (Vol.1). *Proceedings of 58th Japan National Conference on Geotechnical Engineering*, *478*(In Japanese), 955–956.

Kumar, A., Walia, B. S., & Mohan, J. (2006). The compressive strength of fiber reinforced highly compressible clay. *Construction and Building Materials*, *20*(10), 1063–1068.

https://doi.org/10.1016/j.conbuildmat.2005.02.027
Kutter, B. L. (1992). *Dynamic Centrifuge Modeling of Geotechnical Structures*.
Lang, L., Chen, B., & Chen, B. (2021). Strength evolutions of varying water content-dredged sludge stabilized with alkali-activated ground granulated blast-furnace slag. *Construction and Building Materials*, *275*. https://doi.org/10.1016/j.conbuildmat.2020.122111
Lang, L., Chen, B., & Duan, H. (2021). Modification of nanoparticles for the strength enhancing of cement-stabilized dredged sludge. *Journal of Rock Mechanics and Geotechnical Engineering*, *13*(3), 694–704. https://doi.org/10.1016/j.jrmge.2021.01.006
Lee, J. Y., An, J., & Chua, C. K. (2017). Fundamentals and applications of 3D printing for novel materials. In *Applied Materials Today* (Vol. 7, pp. 120–133). Elsevier Ltd. https://doi.org/10.1016/j.apmt.2017.02.004
Li, J. S., Chen, X., Lang, L., He, X. X., & Xue, Q. (2023a). Evaluation of natural and artificial fiber reinforcements on the mechanical properties of cement-stabilized dredged sediment. *Soils and Foundations*, *63*(3). https://doi.org/10.1016/j.sandf.2023.101319
Li, J. S., Chen, X., Lang, L., He, X. X., & Xue, Q. (2023b). Evaluation of natural and artificial fiber reinforcements on the mechanical properties of cement-stabilized dredged sediment. *Soils and Foundations*, *63*(3). https://doi.org/10.1016/j.sandf.2023.101319
Li, J., Tang, C., Wang, D., Pei, X., & Shi, B. (2014). Effect of discrete fibre reinforcement on soil tensile strength. *Journal of Rock Mechanics and Geotechnical Engineering*, *6*(2), 133–137. https://doi.org/10.1016/j.jrmge.2014.01.003
Lirer, S., Liguori, B., Capasso, I., Flora, A., & Caputo, D. (2017). Mechanical and chemical properties of composite materials made of dredged sediments in a fly-ash based geopolymer. *Journal of Environmental Management*, *191*, 1–7. https://doi.org/10.1016/j.jenvman.2017.01.001
Liu, H., Lin, P., & Wang, J. (2023). Machine Learning Approaches to Estimation of the Compressibility of Soft Soils. *Frontiers in Earth Science*. https://doi.org/10.3389/feart.2023.1147825
Liu, L., Zhou, A., Deng, Y., Cui, Y., Yu, Z., & Yu, C. (2019). Strength performance of cement/slag-based stabilized soft clays. *Construction and Building Materials*, *211*, 909–918. https://doi.org/10.1016/j.conbuildmat.2019.03.256
Liu, Y., He, L. Q., Jiang, Y. J., Sun, M. M., Chen, E. J., & Lee, F. H. (2019). Effect of in situ water content variation on the spatial variation of strength of deep cement-mixed clay. *Geotechnique*, *69*(5), 391–405. https://doi.org/10.1680/jgeot.17.P.149
Liu, Y., Lu, H., Liu, M., Cai, L., Wei, N., & Liu, Y. (2022). Microanalytical characterizations, mechanical strength and water resistance performance of solidified

dredged sludge with industrial solid waste and architecture residue soil. *Case Studies in Construction Materials*, *17*. https://doi.org/10.1016/j.cscm.2022.e01492

Ma, C., Chen, B., & Chen, L. (2018). Experimental feasibility research on a high-efficiency cement-based clay stabilizer. *KSCE Journal of Civil Engineering*, *22*(1), 62–72. https://doi.org/10.1007/s12205-017-0782-8

Medvey, B., & Dobszay, G. (2020). Durability of Stabilized Earthen Constructions: A Review. In *Geotechnical and Geological Engineering* (Vol. 38, Issue 3, pp. 2403–2425). Springer. https://doi.org/10.1007/s10706-020-01208-6

Ministry of Land, I. T. and T. [MLIT]. (2017). *Part I National Land and Transportation Administration for Dramatically Changing Lifestyles: Aiming for a Society where Everyone Can Shine*.

Miyazaki, Y., Tang, Y. X., Ochiai, H., Yasufuku, N., Omine, K., & Tsuchida, T. (2003). Utilization of cement treated dredged soil with working ship. *Journal of Japan Society of Civil Engineers* , *750*(in Japanese), 193–204.

MLIT. (2020, January). Results of the survey on Construction By-Products in FY 2018 (in Japanese) Ministry of Land, Infrastructure, Transport and Tourism (2020) Results of the Survey On Construction By-Products in FY2018 (in Japanese). *MLIT*. https://www.mlit.go.jp/report/press/sogo03_hh_000233.html

Mu, C., Shen, S., Arulrajah, A., Wu, H.-N., & Hou, D. (2015). Laboratory Evaluation on the Effectiveness of Polypropylene Fibers on the Strength of Fiber-Reinforced and Cement-Stabilized Shanghai Soft Clay. *Geotextiles and Geomembranes*. https://doi.org/10.1016/j.geotexmem.2015.05.004

Nadeem, M., Ullah, S., Chen, S., Alkahtani, M. Q., Khan, M. A., Salih, R., Jian, L., Mursaleen, M., Islam, S., & Ahmad, J. (2023). Evaluation of engineering properties of clayey sand bio-mediated with terrazyme enzyme. *Frontiers in Materials*, *10*. https://doi.org/10.3389/fmats.2023.1195310

Nazir, M. H., Al-Marzouqi, A. H., Ahmed, W., & Zaneldin, E. (2023). The potential of adopting natural fibers reinforcements for fused deposition modeling: Characterization and implications. In *Heliyon* (Vol. 9, Issue 4). Elsevier Ltd. https://doi.org/10.1016/j.heliyon.2023.e15023

Nguyen, B. T. T., Takeyama, T., & Kitazume, M. (2015). Numerical analyses on the failure of deep mixing columns reinforced by a shallow mixing layer. *15th Asian Regional Conference on Soil Mechanics and Geotechnical Engineering, ARC 2015: New Innovations and Sustainability*, 2144–2148. https://doi.org/10.3208/jgssp.VNM-01

Onyekwena, C. C., Xue, Q., Li, Q., Umeobi, H. I., Ghaffar, A., & Fasihnikoutalab, M. H. (2023). Advances in the carbonation of MgO-based binder and CO2 utilization in the construction industry. In *Clean Technologies and Environmental Policy* (Vol. 25, Issue 6, pp. 1763–1782). Springer Science and Business Media Deutschland GmbH. https://doi.org/10.1007/s10098-023-02482-7

Paula Furlan, A., Razakamanantsoa, A., Ranaivomanana, H., Levacher, D., & Katsumi, T. (2018). Shear strength performance of marine sediments stabilized using cement, lime and fly ash. *Construction and Building Materials*, *184*, 454–463. https://doi.org/10.1016/j.conbuildmat.2018.06.231ï

Phan Thanh, C., Tomoaki, S., & Hiroshi TAKAHASHI. (2018). Study on Strength Characteristics of Rice Straw Fiber-Cement-Reinforced Sludge. *Int. J. Soc. Mater. Eng. Resource*, *23*(2), 147–151.

Phan Thanh Chien, B. (2019a). *Study on Mechanical Properties of Rice by-Products-Cement-Reinforced Sludge as Banking Materials.*

Public Works Research Institute. (2008). *Construction Sludge Recycling Manual* .

Puspita, N., & Capri, A. (2020). The effectiveness of vacuum consolidation to soft soil settlement. *International Journal on Advanced Science, Engineering and Information Technology*, *10*(4), 1610–1616. https://doi.org/10.18517/ijaseit.10.4.3943

Rachman, R. M., Ngii, E., & Sriyani, R. (2021). Effect of using portland cement and tras soil to stabilize and solidify mercury-contaminated tailings in small-scale gold mining. *IOP Conference Series: Earth and Environmental Science*, *871*(1). https://doi.org/10.1088/1755-1315/871/1/012026

Sarasini, F., Luzi, F., Dominici, F., Maffei, G., Iannone, A., Zuorro, A., Lavecchia, R., Torre, L., Carbonell-Verdu, A., Balart, R., & Puglia, D. (2018). Effect of different compatibilizers on sustainable composites based on a PHBV/PBAT matrix filled with coffee silverskin. *Polymers*, *10*(11). https://doi.org/10.3390/polym10111256

Sawamura, Y., Yano, T., & Kimura, M. (2017). Property variation of high moisture sludge by fine powder mainly composed of Cellulose. *Environmental Geotechnical Engineering Symposium*, *12*(September), 505–510.

Sena Da Fonseca, B., Vilão, A., Galhano, C., & Simão, J. A. R. (2014). Reusing coffee waste in manufacture of ceramics for construction. *Advances in Applied Ceramics*, *113*(3), 159–166. https://doi.org/10.1179/1743676113Y.0000000131

Shi, W., Chen, Q., Nimbalkar, S., & Liu, W. (2017). A new mixing technique for solidifier and dredged fill in coastal area. *Marine Georesources & Geotechnology*, *35*(1), 52–61. https://doi.org/10.1080/1064119X.2015.1102183

Shinsha, H., & Kumagai, T. (2018). Material properties of solidified soil grains produced from dredged marine clay. *Soils and Foundations*, *58*(3), 678–688. https://doi.org/10.1016/j.sandf.2018.03.003

Sugimura, Y., Okada, T., Kuwae, T., Mito, Y., Naito, R., & Nakagawa, Y. (2022). New possibilities for climate change countermeasures in ports: Organic carbon containment and creation of blue carbon ecosystems through beneficial utilization of dredged soil. *Marine Policy*, *141*. https://doi.org/10.1016/j.marpol.2022.105072

Takahashi, H., Mori, M., Shibata, S., & Sasaki, K. (2006). Urgent countermeasure construction for imogawa river channel blockage by fiber-cement-stabilized method.

Proceedings of 3rd symposium on sediment disasters. *Proceedings of 3rd Symposium on Sediment Disasters*, *in Japanese*, 1–6.

Takeyama, K., Hamatani, S., Kashima, F., Wakuri, N., Yamauchi, H., Iwamoto, H., & Ukai, A. (2017). Environmental improvement technology utilizing modified soil using paper sludge ash and dredged soil. *Journal of Japan Society of Civil Engineers, Ser. B3 (Ocean Engineering)*, *73 (2)*(in Japanese), 947–952.

Tang, C., Shi, B., & Zhao, L. (2010). Interfacial Shear Strength of Fiber Reinforced Soil. *Geotextiles and Geomembranes*. https://doi.org/10.1016/j.geotexmem.2009.10.001

Tiwari, N., Satyam, N., & Patva, J. (2020). Engineering Characteristics and Performance of Polypropylene Fibre and Silica Fume Treated Expansive Soil Subgrade. *International Journal of Geosynthetics and Ground Engineering*, *6*(2). https://doi.org/10.1007/s40891-020-00199-x

Vidal, H. (1969). The principle of reinforced earth.

Vinoth, G., Moon, S. W., Moon, J., & Ku, T. (2018). Early strength development in cement-treated sand using low-carbon rapid-hardening cements. *Soils and Foundations*, *58*(5), 1200–1211. https://doi.org/10.1016/j.sandf.2018.07.001

Vu, N. B., Do, M. N., Thi, N. N., & Ho, L. S. (2022). Effects of additives on the results of improving peat soil: A case study at Mekong delta in Vietnam. *Journal of Applied Science and Engineering (Taiwan)*, *25*(5), 799–807. https://doi.org/10.6180/jase.202210_25(5).0011

Vu, T. B., Dang, V. Q., Ngo, Q. A., & Ho, L. S. (2023). Influence of some factors on the mechanical properties of cement-treated clay for shallow mixing in Vietnam: A comparative study. *Results in Engineering*, *17*. https://doi.org/10.1016/j.rineng.2023.101011

Wang, D., Xiao, J., & Gao, X. (2019). Strength gain and microstructure of carbonated reactive MgO-fly ash solidified sludge from East Lake, China. *Engineering Geology*, *251*, 37–47. https://doi.org/10.1016/j.enggeo.2019.02.012

Wang, J., Cai, Y., Fu, H., Hu, X., Cai, Y., Lin, H., & Zheng, W. (2018). Experimental study on a dredged fill ground improved by a two-stage vacuum preloading method. *Soils and Foundations*, *58*(3), 766–775. https://doi.org/10.1016/j.sandf.2018.02.028

Wang, R., Tang, C. S., Pan, X. H., Wang, D. L., Dong, Z. H., & Shi, B. (2023). Stabilization of dredged sludge using bio-carbonation of reactive magnesia cement method. *Acta Geotechnica*, *18*(3), 1529–1541. https://doi.org/10.1007/s11440-022-01683-6

Wang, X., Cheng, D., Huang, X., Song, L., Gu, W., Liang, X., Li, Y., & Xu, B. (2020). Effect of high-temperature saturated steam treatment on the physical, chemical, and mechanical properties of moso bamboo. *Journal of Wood Science*, *66*(1). https://doi.org/10.1186/s10086-020-01899-8

Wassermann, A., Abdallah, A., & Cuisinier, O. (2022). Impact of wetting and drying cycles on the mechanical behaviour of a cement-treated soil. *Transportation Geotechnics*, *36*.

https://doi.org/10.1016/j.trgeo.2022.100804

Wu, J., Liu, L., Deng, Y., Zhang, G., Zhou, A., & Xiao, H. (2022). Use of recycled gypsum in the cement-based stabilization of very soft clays and its micro-mechanism. *Journal of Rock Mechanics and Geotechnical Engineering*, *14*(3), 909–921. https://doi.org/10.1016/j.jrmge.2021.10.002

Wu, Y., Li, Y., & Niu, B. (2014). Assessment of the mechanical properties of sisal fiber-reinforced silty clay using triaxial shear tests. *The Scientific World Journal*, *2014*. https://doi.org/10.1155/2014/436231

Xiaoyuan, W., Pengju, H., Xiaohong, B., & Xiangyu, L. (2019). Influences of slag on properties of lightweight cement-treated soils subjected to sulfate corrosion. *Construction and Building Materials*, *205*, 511–518. https://doi.org/10.1016/j.conbuildmat.2019.02.043

Xu, G., Han, Q., Geng, W., Yin, J., & Liu, L. (2023). Evaluation of fiber reinforcement on the strength behaviors of dredging slurry cemented at high water content. *Soils and Foundations*, *63*(1). https://doi.org/10.1016/j.sandf.2022.101264

Yamashita, E., Aristo Cikmit, A., Tsuchida, T., & Hashimoto, R. (2020). Strength estimation of cement-treated marine clay with wide ranges of sand and initial water contents. *Soils and Foundations*, *60*(5), 1065–1083. https://doi.org/10.1016/j.sandf.2020.05.002

Yang, Q., & Du, C. (2021). Experimental Study on the Effect of Plant Ash on Soft Clay Stabilized with Cement-Based Composites. *Geotechnical and Geological Engineering*, *39*(1), 105–117. https://doi.org/10.1007/s10706-020-01476-2

Yin, J., Han, W., Xu, G., Hu, M., & Miao, Y. (2019). Effect of Salinity on Strength Behavior of Cement-treated Dredged Clay at High Initial Water Contents. *KSCE Journal of Civil Engineering*, *23*(10), 4288–4296. https://doi.org/10.1007/s12205-019-0695-9

Yohanna, P., Johnson, P., Victor, B. P., Badamasi, A., Mije, F. G., Ako, T., & Bassey Bassey, A. (2022). Evaluation of Geotechnical Properties of Black Cotton Soil Reinforced with Sisal Fibre for Waste Containment Application. *Engineering Science & Technology*, 151–168. https://doi.org/10.37256/est.3220221354

Zaini, M. S. I., Hasan, M., Yie, L. S., Masri, K. A., Jaya, R. P., Hyodo, M., & Winter, M. J. (2021). The Effect of Utilizing Silica Fume and Eggshell Ash on the Geotechnical Properties of Soft Kaolin Clay. *Jurnal Teknologi*. https://doi.org/10.11113/jurnalteknologi.v84.17115

Zeng, L. L., Bian, X., Zhao, L., Wang, Y. J., & Hong, Z. S. (2021). Effect of phosphor gypsum on physiochemical and mechanical behaviour of cement stabilized dredged soil from Fuzhou, China. *Geomechanics for Energy and the Environment*, *25*. https://doi.org/10.1016/j.gete.2020.100195

Zhang, J., Deng, A., & Jaksa, M. (2021). Enhancing mechanical behavior of micaceous soil with jute fibers and lime additives. *Journal of Rock Mechanics and Geotechnical*

*Engineering*, *13*(5), 1093–1100. https://doi.org/10.1016/j.jrmge.2021.04.008

Zhang, M., Na, M., Yang, Z., Shi, Y., Guerrieri, M., & Pan, Z. (2022). Study on mechanical properties and solidification mechanism of stabilized dredged materials with recycled GFRP fiber reinforced geopolymer. *Case Studies in Construction Materials*, *17*. https://doi.org/10.1016/j.cscm.2022.e01187

Zhang, Y., Ong, Y. J., & Yi, Y. (2022). Comparison between CaO- and MgO-activated ground granulated blast-furnace slag (GGBS) for stabilization/solidification of Zn-contaminated clay slurry. *Chemosphere*, *286*. https://doi.org/10.1016/j.chemosphere.2021.131860

Zhu, W., Chiu, C. F., Zhang, C. L., & Zeng, K. L. (2009). Effect of humic acid on the behaviour of solidified dredged material. *Canadian Geotechnical Journal*, *46*(9), 1093–1099. https://doi.org/10.1139/T09-045

## Chapter 3

## Effect of Finely Shredded Paper on Improving Geotechnical Properties of High Water-Content Clay

### 3.1 Introduction

The rapid growth of the economy and population in metropolitan cities has increased the need for advanced infrastructure projects (Zeng et al., 2019b; Losini et al., 2021; Mei et al., 2021; Xie et al., 2021; Silva et al., 2022) (i.e., railways, expressways, viaducts, tunnels, and skyscrapers) which require deep excavations (Pujades et al., 2015; Xu et al., 2018; Lyu et al., 2019; Zeng, et al., 2019a). These construction projects generate large quantities of high water-content clay due to the excavations of foundations and other underground structures (Anagnostopoulos, 2015; Rahgozar et al., 2018; Pongsivasathit et al., 2019; Lv et al., 2020; Ni et al., 2020; Abbey et al., 2021; Mei et al., 2021; Xie et al., 2021). According to the Japanese Ministry of Land, Infrastructure, Transport and Tourism (MLIT, 2020), it was estimated that around 132.63 million cubic meters of these clay soils were produced at construction sites in Japan in 2018. The reclamation of high water-content clay is a worldwide challenge due to the shortage of landfill space (Katsumi et al., 2008; Wong, 2022). Considering the transport and reuse of the high water-content clay generated at construction sites, ground-improvement measures are required.

The traditional methods of ground improvement are dehydration, drying, and cement solidification. Cement solidification has been widely adopted, although a large amount of cement is needed for this method and the value of the pH in the improved soil increases during the solidification process (Japan Cement Association, 2017). In addition to environmental concerns, cement solidification can be costly and time-consuming (Khodabandeh et al., 2023). It has additional disadvantages, including decreased mechanical strength due to water loss, incomplete hydration during the initial stages, and significant plastic shrinkage. These drawbacks are especially crucial in geotechnical engineering applications, particularly in hot regions, as noted by Miraki et al. (2022).

In recent years, there has been growing interest in the use of alternative materials, such as plant additives and agricultural waste, due to their abundance and eco-friendliness, as potential alternatives for soil stabilization (Moayedi et al., 2019; Adeyanju et al., 2020; Bozyigit et al., 2021; Adeboje et al., 2022; Fadmoro et al., 2022; Ojuri et al., 2022; Khandelwal et al., 2023; Khayat and Nasiri, 2023). These materials can modify the properties of soil, such as the strength, stability, and water-adsorption capacity, and enhance the biological activity of soil (Yang et al., 2018). Numerous studies have been conducted on the use of agricultural waste and plant additives for soil stabilization, and their effectiveness has been demonstrated in various applications. In a study conducted by Li et al. (2012), the use of plant-based wheat straw for stabilizing saline soil was investigated. It was found that the addition of plant-based wheat straw improved the corrosion resistance, tensile force, and elongation of the soil. In a study conducted by Nethravathi et al. (2018), the use of sugarcane bagasse ash (SCBA) and sawdust ash (SDA) for stabilizing expansive soil was examined. It was found that the addition of SCBA and SDA improved the strength, stability, and durability of the soil and reduced its shrinkage potential. Similarly, in a study conducted by Yifru et al. (2022), the use of corn straw biochar (CSB) for stabilizing coastal soil was examined. It was found that the addition of CSB improved the strength, stability, and water-adsorption capacity of the soil and reduced its erodibility.

A new ground-improving material for soil, using finely shredded paper (hereinafter, referred to as FSP), has been developed by a Japanese company (Growth Partners, Ltd). FSP can be produced from any kind of wastepaper and shows a high water-absorption capacity due to the cellulose component in the paper. One of the advantages of this technique is the immediate reduction in the fluidity of soft soil just after adding FSP to the soil; this result has been confirmed in some field applications, as shown in **Figure 3.1** (Sawamura et al., 2017). In addition, FSP has a low environmental impact during the process of improving the soft soil, because no chemical reactions occur, and it can improve any kind of soft soil regardless of its chemical composition. Our research group has examined the properties of FSP and its effectiveness in improving clay materials. Sawamura et al. (2017) found that there is a difference in the water-absorption characteristics depending on the ratio of FSP made from paper fiber to that made from shredder shavings. The shear strength of clay treated with FSP was higher than that of pure clay. Kida et al. (2018) found from flow tests and cone index tests that the transport of clay treated with FSP was possible as long as the flowability had decreased to where the flow value could be measured, even if the strength was less than the 200 kN/m$^2$ cone index that is generally used for cementitious solidification treatment. Asai et al. (2022) conducted some uniaxial compressive strength tests, using clay specimens improved with both FSP and cement, in order to examine the possibility of reusing treated clay as construction material.


**Figure 3.1: Treatment of high water-content clayey soil using finely shredded paper. Original photos are shown in (Sawamura et al., 2017).**

As mentioned above, changes in the physical and mechanical properties of high water-content clay, brought about by adding FSP, have been examined. However, the effect of FSP on improving the geotechnical properties of clay and the specific mechanism of the improvement using FSP have not been sufficiently clarified. It is important to investigate not only the changes in the geotechnical engineering properties of clay treated with FSP, but also the fundamental properties of the FSP itself, in order to confirm the specific roles of FSP and the mechanism of the ground improvement using FSP. This paper presents experimental results for FSP itself and those for high water-content clay treated with FSP, respectively. The former results mainly focus on the shear strength of FSP with different values for the water content and void ratio. The latter results focus on the changes in consistency, shear strength, consolidation characteristics, and hydraulic conductivity of clay treated with different amounts of FSP. The role of FSP in changing the geotechnical properties of high water-content clay is analyzed based on the experimental data, and then the possible mechanism of the ground improvement using FSP is discussed.

### 3.2. Materials

The soils used for this study are Fujinomori clay sampled from Kyoto Prefecture and Kasaoka clay sampled from Okayama Prefecture, Japan. These clay soils were air-dried and powdered before the experiment. The physical properties of the soils are shown in **Table 3.1**. It is found from this table and the Unified Soil Classification System that Fujinomori clay is medium plastic and Kasaoka clay is highly plastic. The other material used in this study is finely shredded paper (FSP), which is made from wastepaper milled in a grinding factory.

(a)

(b)

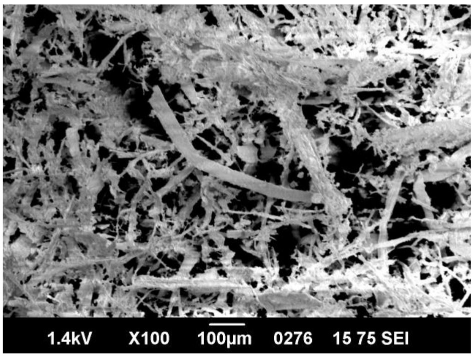


**Figure 3.2: Finely shredded paper (FSP) used in this study: (a) picture and (b) SEM image.**

**Figure 3.2** shows a picture and a SEM image of the FSP used in this study. The SEM image indicates that the FSP has fibers of various lengths and thicknesses, and the non-uniformity of the fibers within the matrix is caused during the manufacturing process. **Figure 3.3** provides particle size distribution curves for the clay materials and the FSP. As FSP is a material that is not typically spherical in shape, a certain method and special equipment are required to measure its size accurately. In this study, the particle size of the FSP was evaluated by the particle size test of JIS A 1204 (Japanese Industrial Standard).

**Table 3.1: Physical properties of clay soils**

| | Fujinomori clay | Kasaoka clay |
|---|---|---|
| Specific gravity of soil particle $G_s$ | 2.68 | 2.70 |
| Liquid limit $w_L$ [%] | 48.5 | 54.6 |
| Plastic limit $w_p$ [%] | 28.0 | 26.8 |
| Plasticity index $I_p = w_L - w_p$ | 20.5 | 27.8 |

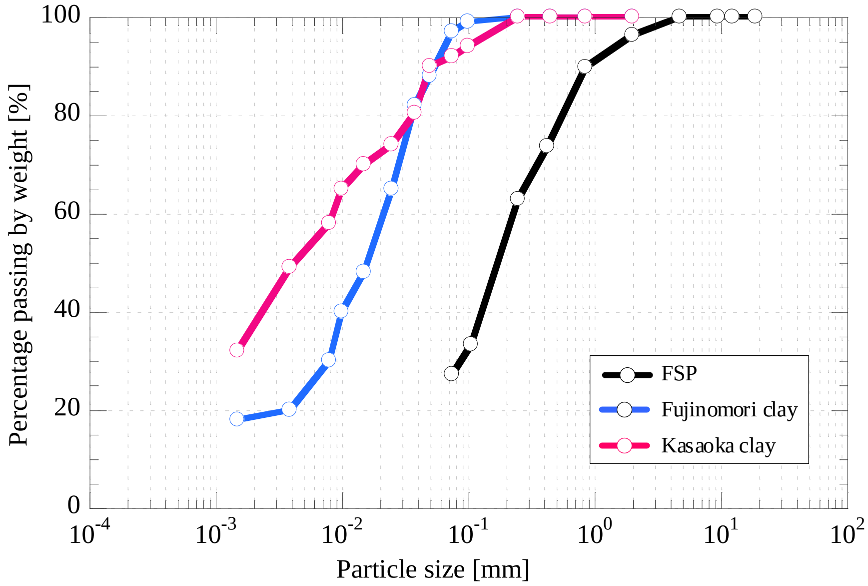


**Figure 3.3: Particle size distribution curves of materials used in this study.**

### 3.3. Experimental conditions

In this study, two stages of experimental work were conducted. In the first one, the properties of FSP, such as the water-absorption capacity and shear stress under different amounts of water, which probably contribute to the treatment's effectiveness, were evaluated. In the second stage, changes in the consistency, shear strength, consolidation characteristics, and hydraulic conductivity of the clay treated with FSP were assessed. It should be noted that, in the second stage, Fujinomori clay was used for the experiments to examine the consistency, shear strength, and consolidation, whereas Kasaoka clay was used for the permeability tests. The experimental procedures and test conditions are presented in this chapter.

The FSP treatment of high water-content clay is based on three fundamental principles. Firstly, it involves the water-absorption capacity of the FSP, which allows it to effectively absorb excess moisture from the clay, thereby reducing its water content. Secondly, FSP provides fiber reinforcement to clay, enhancing its mechanical properties and stability. The fibers interlock within the clay matrix, increasing its strength and preventing excessive deformation. Thirdly, FSP treatment aids in lowering the level of soil saturation in the ground which increases the effective strength of the soil. In the context of these particular experiments, saturated soil was chosen as the testing medium for the clay treated with FSP to simplify the experimental conditions.

### 3.3.1. Water absorption tests on FSP

An evaluation of the water-absorption capacity of the additive materials is important for estimating their application as building materials, particularly for materials with higher water contents, as it helps to improve their quality. Phan et al. (2021) efficiently evaluated the water-absorption capacity of paper sludge ash (PS ash) using a 53-μm sieve (i.e., the smallest sieve for which the effects of surface tension do not prevent extra water from going through the sieve) and a sieve shaker. The specimens were prepared by mixing PS ash and distilled water, using a PS ash/water ratio of 0.25, and curing them in sealed plastic zipper storage bags at room temperature (20±1). Curing periods were from 10 minutes to 72 hours based on the test cases, then transferred to a sieve (three sieves having 53 μm at the top, 4.75 mm in the middle, and a pan at the bottom) and shaken for 10 minutes. This sieve arrangement was used to minimize the excess water sticking to the underside of the sieve and reducing the actual amount of absorbed water. Using a similar methodology, the water-absorption capacity of FSP can be measured. However, the finer powders migrate beyond the sieve and the measurement of the water-absorption capacity is not precise. Therefore, the typical design of a suitable technique for measuring the water-absorption capacity of the FSP is needed.

In this study, water-absorption tests for FSP were conducted using a non-woven polyester fabric bag. **Figure 3.4** shows a schematic illustration and pictures of the water-absorption test conducted by Sawamura et al. (2017). A 500-ml beaker, a 95-mm × 70-mm bag of non-woven polyester fabric, degassed water, and a magnetic stirrer for stirring were used for the water-absorption tests. Firstly, 3 g of FSP was placed in the non-woven fabric bag, and the top of the bag was folded over several times and stapled. The test specimens were then placed in a 500-ml beaker filled with degassed water and stirred at 300 rpm using a 20-mm stirrer to absorb water for 24 hours. After the water absorption was complete, the specimens were removed from the beaker, left out at room temperature for 10 minutes, and then weighed. The water absorption of the FSP was calculated by subtracting the water absorption of the non-woven fabric from the measured value. All the water-absorption tests were conducted in a room with a constant temperature of 20°C, and the temperature of the degassed water was kept constant at 19°C. The gas that dissolved in the tap water probably affected the measurement accuracy of the water absorption of the FSP; and hence, degassed water was used in each test to maintain uniform conditions. The bulk density of the FSP was measured by gently pouring the FSP into a 2000-ml measuring cylinder and weighing it.

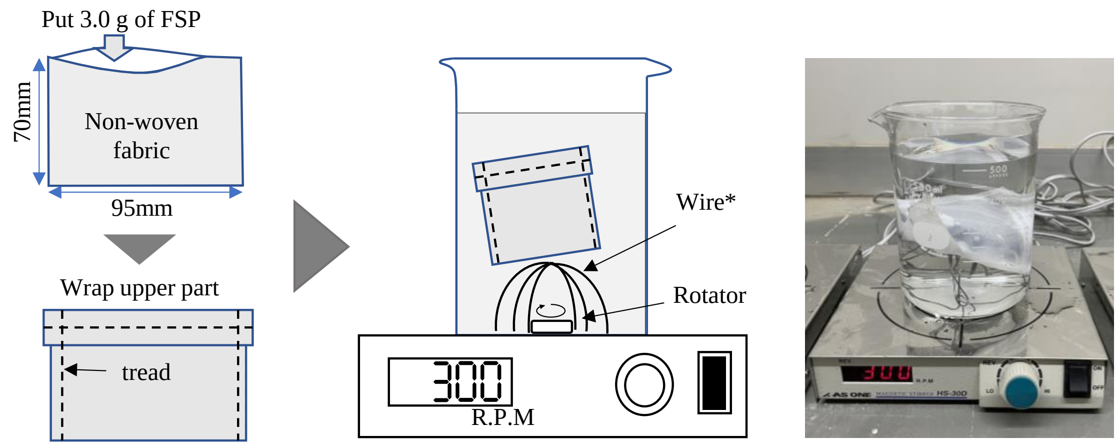


*Wire that prevents contact between the bag holding the specimen and the rotator

During water absorption test

**Figure 3.4: Schematic illustration and pictures of water-absorption test.**

### 3.3.2. Direct shear box test on FSP

To evaluate the shear stress properties of FSP at different water contents and void ratios, direct shear box tests were conducted. The procedure for the specimen preparation and the situation after shearing are shown in **Figure 3.5**. The air-dried FSP was mixed with degassed water to attain the target water content. The wet FSP was placed in a shear box, layer by layer, and proper compaction was applied to each layer to obtain the target density of the specimen. The consolidation process was conducted by applying normal stress. Shearing load was applied to the specimen at a constant shear rate of 1 mm per minute. The shear stress and dilatancy were measured during each test. **Table 3.2** lists the cases of the FSP specimens prepared in this study.

The specimens were prepared with four values for the initial void ratio and four values for the target water content, of either 0%, 50%, 100% or 200%, after the consolidation process. Since the only way to measure the amount of water drainage from the FSP was to remove each specimen from the direct shear box, it was not only difficult to measure the water content of each specimen after consolidation, but also difficult to then perform the shear tests. In this study, two specimens, made to have the same weight as the dry FSP and water, were prepared for every case. One specimen was used as a reference specimen, namely, to estimate the exact water content after consolidation of the specimen that was adjusted to a target water content. The other specimen was used as a tested specimen for the direct shear box tests, assuming that the water content after consolidation would be identical between the reference specimen and the tested specimen.

**Table 3.2: Cases of FSP specimens used for direct shear box tests**

| Cases | Normal stress [kPa] | $e$ for tested specimen | w [%] after consolidation for reference specimen | w [%] after shearing for tested specimen |
|---|---|---|---|---|
| 1 | 39.2 | 5.10 | 0, 48, 97, 198 | 0, 47, 94, 196 |
| 2 | 39.2 | 3.40 | 0, 48, 97, 198 | 0, 47, 96, 191 |
| 3 | 78.5 | 4.50 | 0, 47, 94 | 0, 45, 91 |
| 4 | 78.5 | 3.90 | 0, 46, 95 | 0, 44, 93 |

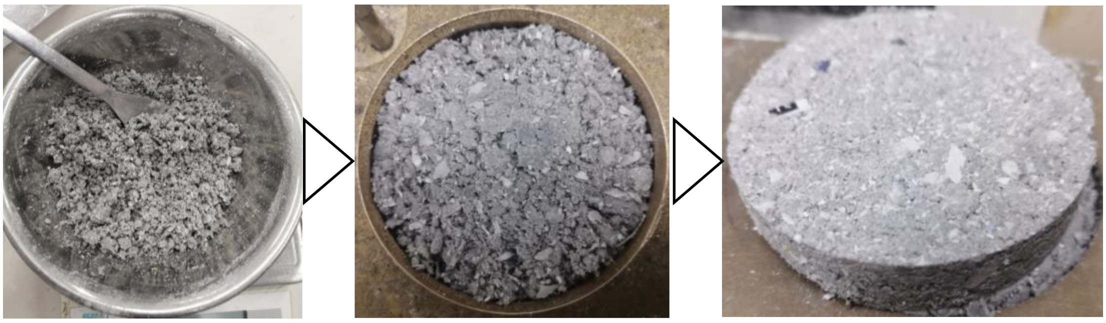

Mixing FSP and water　Placing FSP in a shear box　Specimen after shearing

**Figure 3.5: Specimen preparation and shearing process.**

### 3.3.3. Vane shear tests on clay treated with FSP

In this study, vane shear tests were conducted on Fujimori clay, in a saturated over consolidated state, and on Fujimori clay with FSP, under conditions in which the water content (void ratio) was varied in many ways. One specimen of pure Fujimori clay and four specimens of Fujimori clay mixed with degassed FSP were prepared. For the latter, the weight of the FSP was 5%, 10%, 20%, and 30% of that of the dry weight of Fujimori clay. In order to prepare specimens at various values of water content (void ratio) for saturated clay, it is necessary to consolidate each specimen by applying a load to it. However, the preparation of specimens with a low water content ratio requires a long period of consolidation under a very large load, which means a great amount of time for the specimen preparation. In this study, a geotechnical centrifuge device, installed at the Disaster Prevention Research Institute (DPRI), Kyoto University, was used to prepare specimens with different water contents by consolidation under different centrifugal force fields. **Table 3.3** shows the scaling law at the centrifugal field (Kutter, 1992). In a model experiment using the centrifugal device, a centrifugal force of $N$ times gravity is applied to a model, $1/N$ in size, which can reproduce the stress condition of the ground due to its self-weight. As the consolidation of soil is dominated by the flow of porewater, the consolidation time is reduced to $1/N^2$ of the actual field. In this study, therefore, the specimen can be consolidated using the centrifugal device with large stress and over a short time.

The standard specifies that the diameter of the sample or the internal mold must be large enough to provide a gap having twice the blade diameter of the vane between the shearing surface circumference and the external perimeter of the sample. The test procedure for the pure Fujinomori clay is described below. **Figure 3.6** shows the specimen preparation procedure.

**Table 3.3: Scaling law at centrifugal field (after Kutter, 1992)**

| Quantity | Symbol | Unit | Scale factor |
|---|---|---|---|
| Length | L | L | $N^{-1}$ |
| Volume | v | $L^3$ | $N^{-3}$ |
| Mass | M | M | $N^{-3}$ |
| Gravity | g | $LT^{-2}$ | N |
| Force | F | $MLT^{-2}$ | $N^{-2}$ |
| Stress | s | $ML^{-1}T^{-2}$ | 1 |
| Modulus | E | $ML^{-1}T^{-2}$ | 1 |
| Strength | s | $ML^{-1}T^{-2}$ | 1 |
| Acceleration | a | $LT^{-2}$ | N |
| Time (dynamic) | tdyn | T | $N^{-1}$ |
| Frequency | f | $T^{-1}$ | N |
| Time (diffusion)* | tdif | T | $N^{-1}$ or $N^{-2}$ |

*The diffusion time scale factor depends on whether the diffusion coefficient (e.g., coefficient of consolidation) is scaled. If the same soil is used in model and prototype, tdif* = $N^{-2}$

1) Add water to dry Fujimori clay to produce a clay slurry with a water content of 1.5 times the liquid limit (Figure 3. 6a).
2) Fully saturate the clay slurry over a period of 2 hours using a suction pump and mixer (Figure 3. 6b and 6c).
3) Gently pour the saturated slurry into a PVC pipe with an inner diameter of 195.4 mm and a height of 300 mm (Figure 3. 6d).

4) Subject five specimens to centrifugal forces of 10 G, 20 G, 30 G, 40 G, and 50 G, respectively. In this way, the self-weight consolidation progresses (**Figure 3.7**).
5) Prepare specimens with different values for the void ratio by consolidation in each centrifugal force field.
6) Place the specimens in a room at a constant temperature of 20℃ for at least 24 hours, and then conduct vane shear tests (Figure 3. 7). The temperature of the specimen at the time of the experiment was 19℃.
7) Measure the water content of each specimen after every test.

On the other hand, the test procedure for treating the clay with FSP is described below.

a) Add FSP of 5%, 10%, 20%, and 30% by weight to the dry Fujimori clay and mix it well in the dry state.
b) Add water to the mixture of Fujimori clay and FSP to make a clay slurry containing FSP. The amount of water to be added and the initial water content of the clay slurry vary depending on the amount of FSP added due to the torque of the agitator used when degassing and stirring the clay slurry. Therefore, the amounts of water added were 92.4%, 110.1%, 147.7%, and 188.4% for the initial water content in order of the smaller additive amounts of the FSP.
c) After step b), make each specimen according to steps 2) to 7).


**Figure 3.6: Specimen preparation and testing procedure of vane shear test: (a) mixing materials, (b) making slurry, (c) degassing slurry, (d) pouring slurry into PVC pipe.**

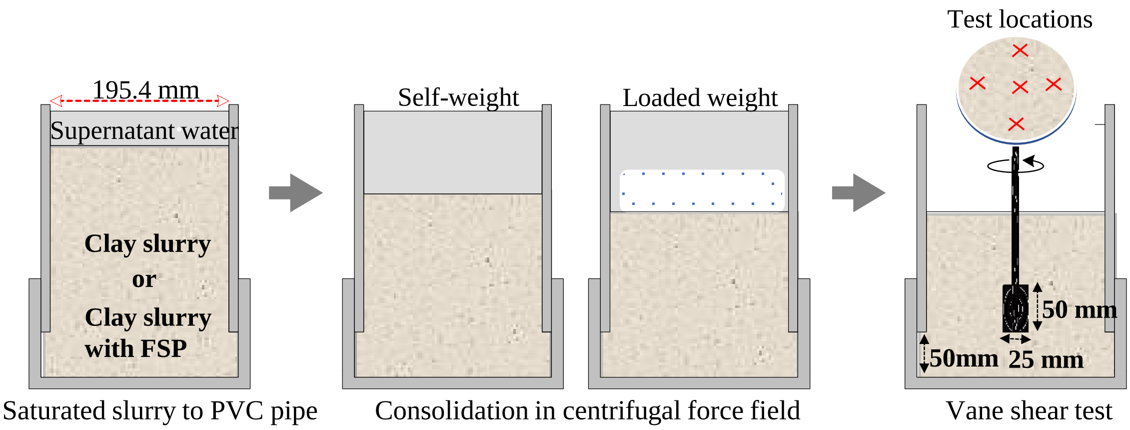


**Figure 3.7: consolidating specimen and test locations.**

### 3.3.4. Consolidation tests on clay treated with FSP

Consolidation tests were conducted on Fujimori clay with different amounts of FSP additive to investigate the changes in the consolidation properties when FSP was added to the clay. The experimental cases were pure Fujimori clay (no FSP) and a total of 10% and 30% FSP in an air-dried state added to the dry weight of the Fujimori clay.

..Three different cases were examined and, as in the previous section 3.3, the test specimens were prepared by consolidating clay slurry that had been thoroughly degassed and stirred in a centrifuge field. However, the consolidation was carried out at a centrifugal force of 35 G, based on the results of section 3.3, with the goal of achieving the minimum strength that would allow the sampling of specimens from the consolidated clay using a thin wall sampler, as shown in **Figure 3.8**. The procedures for setting the initial water content and preparing the specimens are the same as those in section 3.3. Consolidation tests were conducted in accordance with "JIS A 1217 Consolidation test by loading in stage", and the consolidation time for one stage was 24 hours. One cycle of consolidation and one cycle of swelling were conducted to investigate the swelling characteristics.

**Figure 3.8: Sampling saturated specimen using thin wall sampler.**

### 3.3.5. Permeability tests on clay treated with FSP

To assess the hydraulic conductivity of the clay specimens, falling head permeability tests were carried out following ASTM D 5084, which is a standard test method for measuring the hydraulic conductivity of saturated porous materials using a flexible wall permeameter. **Figure 3.9** provides views of the procedure for the specimen preparation and the permeability tests. **Figure 3.10** shows an overview of the setup of the permeability test apparatus.

Regarding the specimen preparation, the air-dried Kasaoka clay and air-dried FSP were blended thoroughly. Subsequently, the blended material and degassed water were mixed together for 30 minutes under suction to achieve a fully water-saturated slurry. This study investigates three cases: Case-1, involving pure Kasaoka clay without any FSP additive; Case-2, with 10% FSP added to the treated clay; and Case-3, with 20% FSP added to the treated clay. The amount of water added to the blended material corresponded to 1.5 times the liquid limit of each case, specifically 81.3% for Case-1, 97.1% for Case-2, and 124.7% for Case-3.

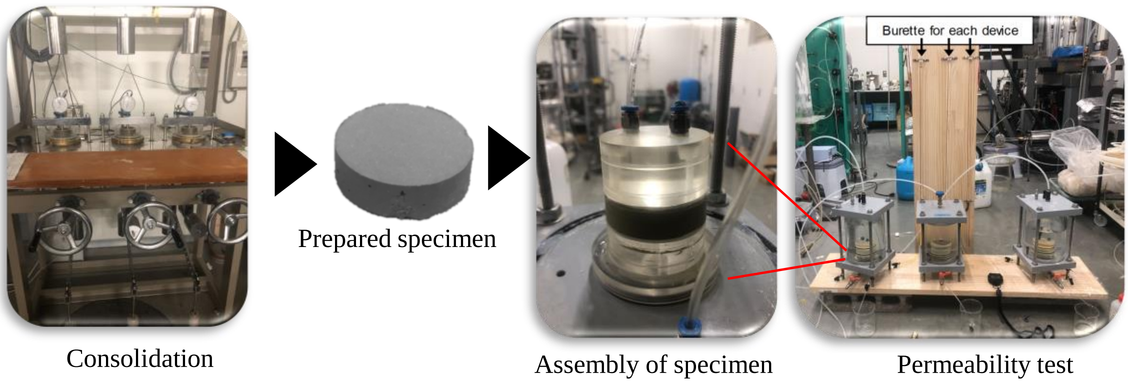


**Figure 3. 9: Procedure for specimen preparation of falling head permeability test.**

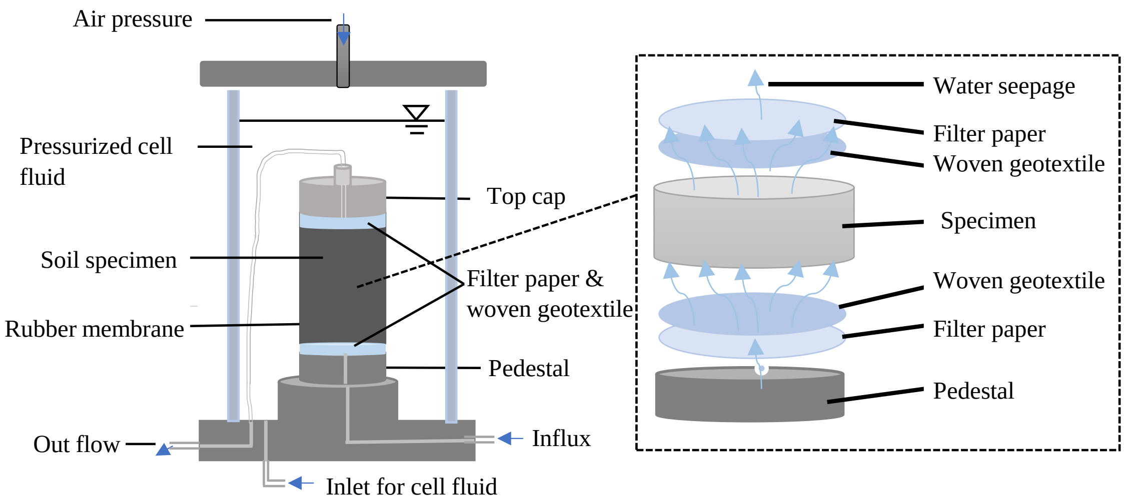


**Figure 3.10: Overview of setup of permeability test apparatus.**

The slurry was then placed in an odometer consolidation device with a diameter of 60.0 mm and a height of 20.0 mm. One stage of consolidation was conducted under a normal stress of 60 kPa. Once the specimen was consolidated, it was positioned on the permeability test apparatus for the hydraulic conductivity tests. To ensure water distribution over the specimen, a woven geotextile was equipped at both the top and bottom surfaces of the specimen. Additionally, filter paper was placed on each woven geotextile. The specimen was covered with a rubber membrane and an acrylic cell was installed. Water was poured into the cell, and 30 kPa of air pressure was applied, resulting in the exertion of confining pressure on the specimen immersed in water. The confining pressure of 30 kPa, which corresponds to an over consolidation ratio (OCR) of 2, enabled the measurement of the water flow related solely to the water percolation inside the specimen, excluding any drainage due to consolidation. All tests were conducted at room temperature, specifically 24±1°C.

## 3.4 Result and discussion

### 3.4.1 Water absorption characteristics of FSP

**Figure 3.11** shows the test results for the water absorption of the FSP fiber with various minimum bulk densities for which the lower bulk densities retain higher amounts of water, as obtained by Sawamura et al. (2017). The FSP used in this study shows 5.5 g of water absorption per 1 g of dry finely shredded paper. It is found from this figure that the lower bulk densities of the FSP provide a higher water-absorption capacity. This linear relation indicates that the water-absorption capacity can be approximately evaluated by measuring the bulk density of the FSP at the time of its production.

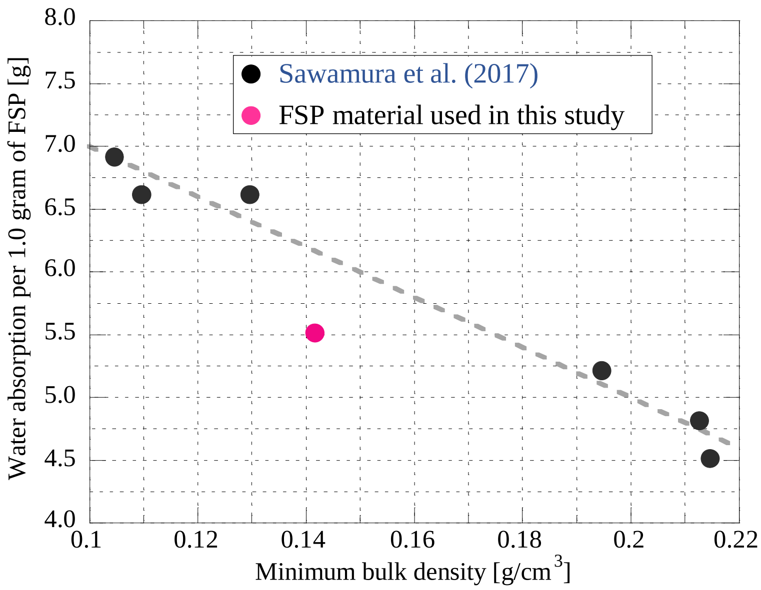


**Figure 3.11: Water-absorption test results for FSP Sawamura et al. (2017).**

One of the possible reasons why FSP shows such a high water-absorption capacity is that the large surface area of the fibers has various lengths and widths. Paper shredded into smaller pieces has a large total surface area with fibers having various thicknesses and lengths, as shown in **Figure 3.2**. It is thought that the larger the specific surface area, the smaller the bulk density, and the more opportunities there are for water molecules to come into contact with the paper fibers that are made from cellulose. The increased contact area between the water and the paper allows for more efficient absorption. The capillary effect probably also plays a role in such high-water absorption of the FSP. The FSP shows a high hydrophilic property because of the cellulose molecules, and the fibers with various lengths and thicknesses lead to the creation of small bulk spaces. Hence, water can easily be retained in the bulk spaces due to the capillary effect. The combination of the increased surface area and the capillary effect leads to a larger amount of water absorption for FSP. The water-retention characteristics of FSP will be studied in the future from a microscopic viewpoint to confirm the above discussion.

### 3.4.2 Shear stress characteristics of FSP

**Figure 3.12** shows the shear stress-shear displacement relationship under different levels of normal stress. It is found from this figure that the shear stress of the FSP specimen made with a 50% water content is larger than that of the dry FSP specimen, and that the shear stress decreases when the water content of the specimen is increased from 50% to 100%.

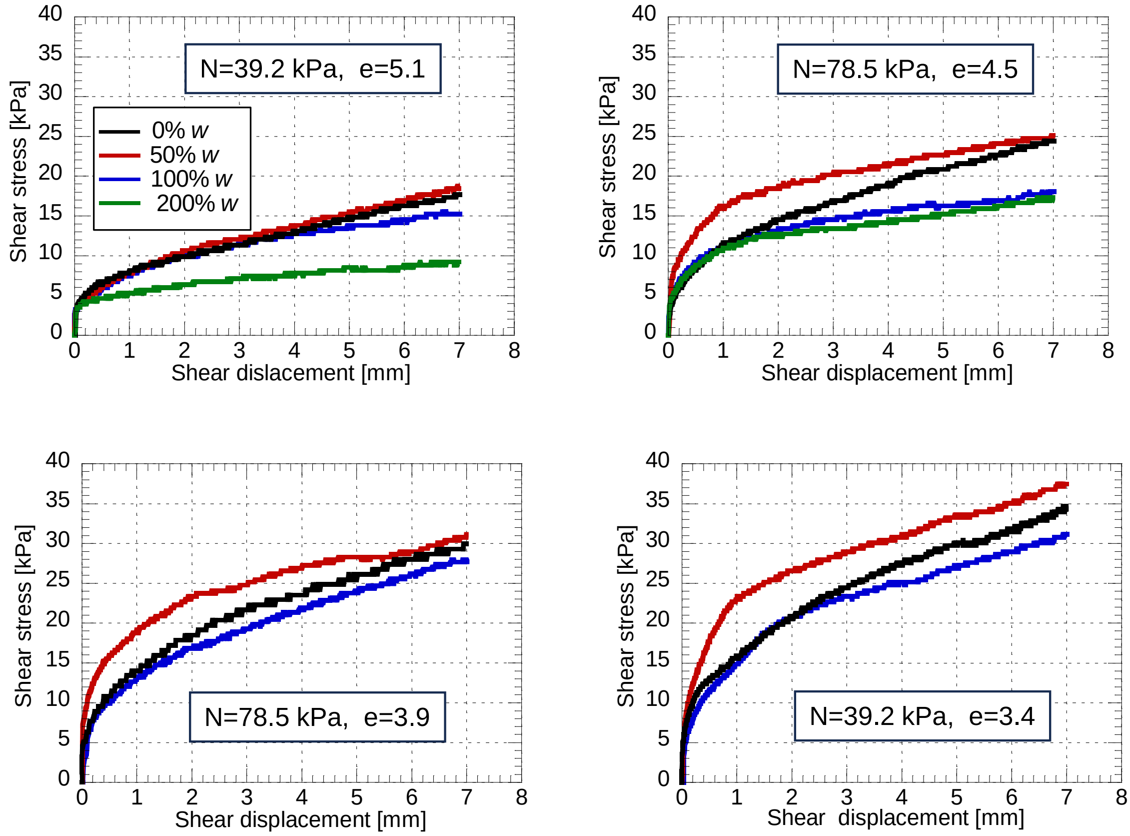


**Figure 3.12: Shear stress-shear displacement relationship of FSP for a) Case-1, b) Case-2, c) Case-3, and d) Case-4.**

These tendencies can be observed in all cases. At a normal stress of 39.2 kPa, as shown in **Figure 3.12a**, the shear stress is the lowest at 200% water content. Case-2, for which the normal stress is the same as Case-1 and the void ratio is lower than Case-1, shows larger shear stress than Case-1 at each value of water content, except for the 100% water content. As a comparison between **Figure 3.12c** and **12d**, the dependency of the void ratio on the shear resistance is clearly observed. These results indicate that the void ratio plays a crucial role in the shear resistance under a similar water content and normal stress. It is also clear from comparisons between **Figure 3.12a** and **12c** and between **Figure 3.12b** and **12d**, that the shear stress increases when the normal stress is larger under a similar void ratio and water content. Therefore, FSP shows a clear density dependence and a confining stress dependence on the shear stress, which are consistent with the shear characteristics of soil materials. For the 200% water content in **Figure 3.12a** and **12b**, the shear stress curves become gentle slopes. This indicates that the stiffness of the specimen matrix decreases during the shearing process. Although the shear stress of FSP decreases above a certain level of water content, it is certain that the FSP can resist shear deformation even at the high-water content of 200%. It is clear from **Figure 3.12** that the shear stress tends to keep increasing as the shear displacement increases. This tendency suggests that the FSP specimens used in this study are in relatively loose conditions, which may change if higher density specimens are examined. It is also possible that the FSP specimens used in the present study are in dense conditions, whereas the FSP fibers are more easily deformed compared to the soil particles; and hence, the behavior of dense FSP may be different from that of typical dense soils that exhibit a peak strength followed by a reduction in strength. An evaluation of relative density Dr would be important for discussing the shear strength properties of FSP in more detail. Currently, there is no suitable method for obtaining the maximum and minimum densities of FSP itself since FSP fibers are intertwisted with each other. The density dependence of FSP will be investigated in further detail in future works.

One of the possible reasons why the shear strength of FSP changes with the different amounts of water content is the suction effect. The FSP with a 50% water content is in an unsaturated condition and still has more capacity to absorb water, so that a certain level of suction contributes to bonding and confining among the FSP fibers with various lengths and thicknesses. The dry FSP can resist shear deformation due to its intertwisted structure, while such a suction effect probably enhances the shear resistance of the FSP. Similar to the soil compaction characteristic, there is most likely an optimum water content at which the highest shear strength of the FSP is obtained. This point will be studied in detail in the future.

### 3.4.3 Consistency of clay treated with FSP

The consistency characteristics of the treated specimens play a crucial role in predicting and understanding the fundamental behavior of the soil and the additive. Therefore, consistency tests were conducted on the untreated and treated clays based on the ASTM D

4318 (2018) standard. The storage of the materials and the experiments were done at a constant temperature of 20°C.

**Figure 3.13** presents a plasticity chart for both the pure clay and the treated clay with different amounts of FSP. It should be noted that, as shown in Figure 3.13a, the water content for the treated clay is defined as the ratio of the mass of the water to the total mass of the FSP and the clay. It is observed from **Figure 3.13b** that both the plasticity index and the liquid limit increase as the amount of added FSP increases. The tendency for an increment not only in the liquid limit, but also in the plastic limit for the treated clay, is consistent with the results reported by several researchers. (e.g., Taha and Taha, 2012).The results for the specimens with FSP are located below the A-line, and the distance between the plot and the A-line becomes larger as the amount of FSP increases. In addition, the results for the specimens with FSP move from low liquid limit clay (CL) to high liquid limit silt (MH) as the amount of FSP increases. These results indicate that the tendency for aggregation and compressibility is more significant for the treated clay with FSP than for the pure clay. Such a change in consistency as that obtained in this study was also reported in Locat al. (1996), where it was explained that the water trapped in the inter-particle spaces increases the apparent water content without affecting the original particle size.

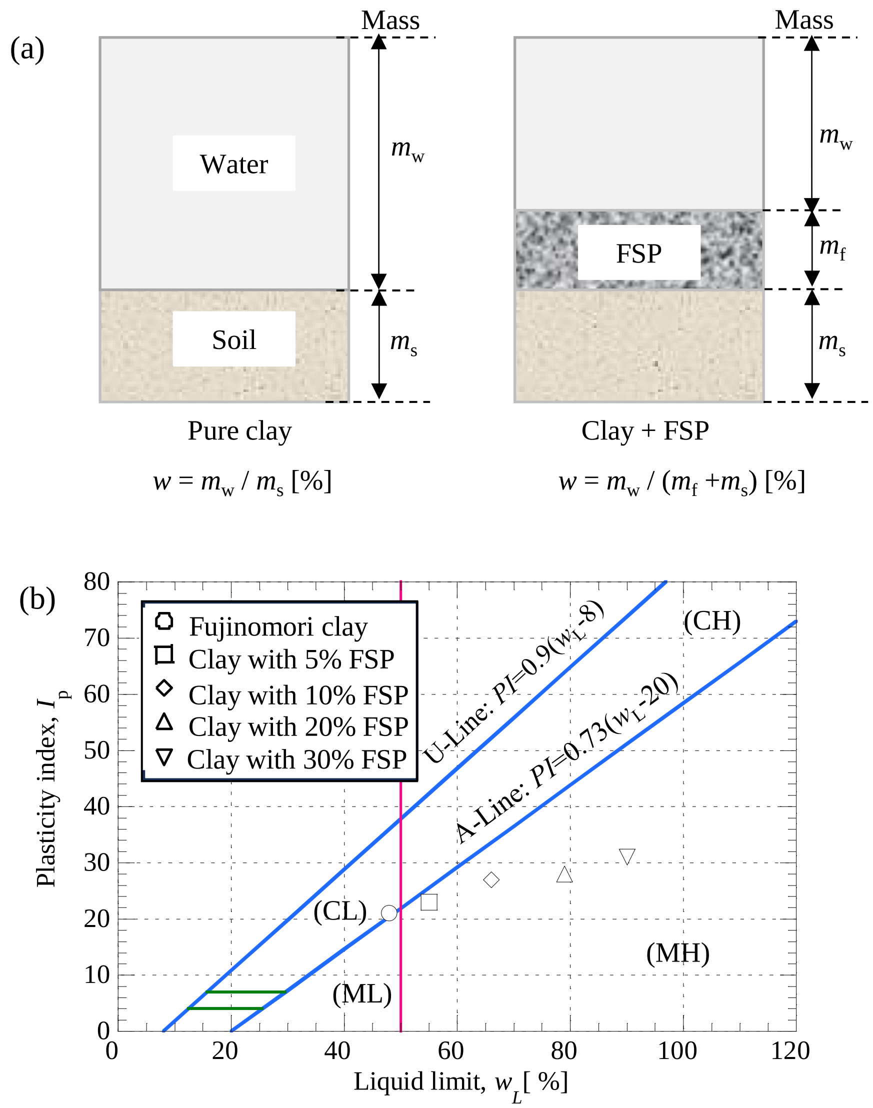


**Figure 3.13: Plasticity chart for both pure and FSP treated clay (a) definition of water content in this study and (b) test results.**

### 3.4.4 Vane shear tests on clay treated with FSP

**Figure 3. 14** shows the results of the vane shear tests. The figure shows that there is a good correlation between the water content ratio and the shear strength in all cases; namely, the shear strength tends to decrease as the water content increases in all cases. At the same shear strength, the water content increases as the amount of FSP increases. This indicates that the shear strength of the clay treated with FSP is enhanced even at high water contents. On the other hand, the specimens with FSP show higher shear strength at the same water content, confirming the reinforcing effect due to the fibrous additive material. In the evaluation of the shear properties by the vane shear tests, the reinforcement effect of the fibers was remarkable. This situation was also reported by Kwon et al. (2019), whereby the

undrained strength increases with the addition of Xanthan gum (0% to 2%) and the water content decreases in the range of 80% to 30%.

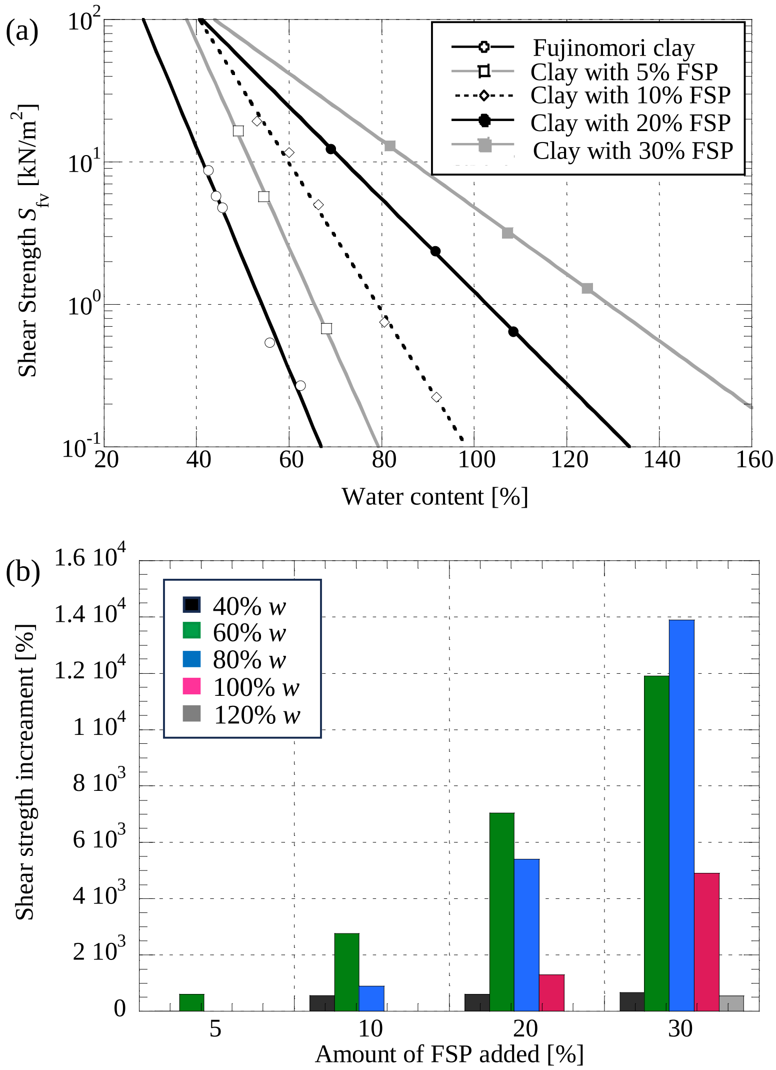


**Figure 3. 14: Vane shear strength test (a) shear strength value (b) shear strength increament**

### 3.4.5 Consolidation of clay treated with FSP

**Figure 3.15** shows the e-logP curves obtained from the consolidation tests. The void ratio for each sample containing FSP is defined as the volume of pore spaces to the volume of soil particles and FSP, as was the case for the water content ratio. For the treated clay, the density of the soil particles, Gs, was calculated based on the densities of Fujimori clay and FSP (Fujimori clay: 2.68 and FSP: 1.75), depending on the mixing ratio of the two materials.

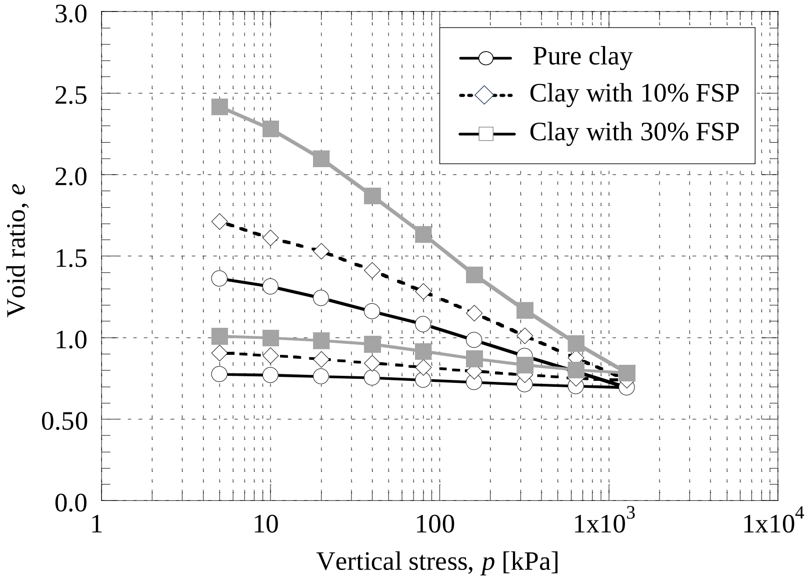


**Figure 3.15: e-log P curves obtained from consolidation tests.**

It can be confirmed from **Figure 3.15** that the void ratio of the specimens containing FSP is large in the initial stage, and that the change in void ratio is more significant with subsequent loading. However, as the load is increased, the void ratio converges to a similar value regardless of the amount of FSP additive, indicating that the volume of treated clay can be reduced by pressurization, and that the increase in volume of the treated clay due to FSP addition is slight.

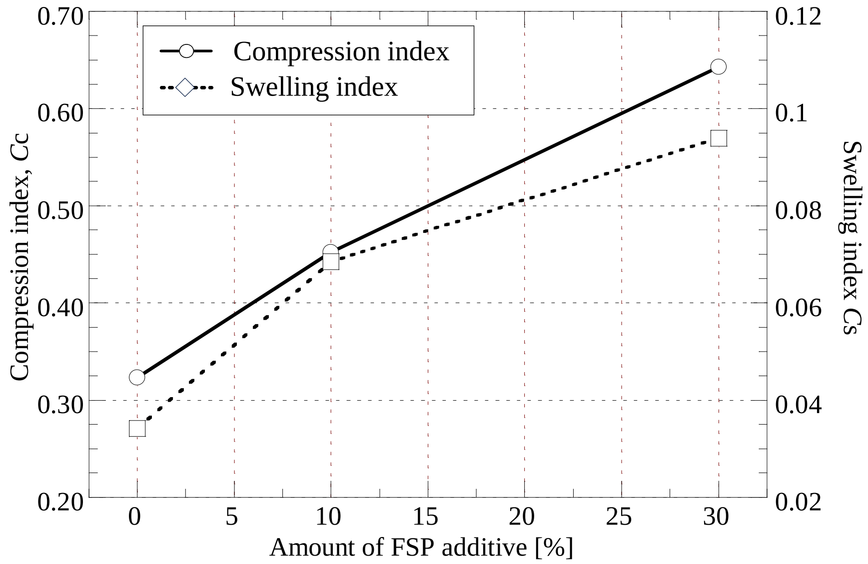


**Figure 3.16: Relationship between compression index and swelling index.**

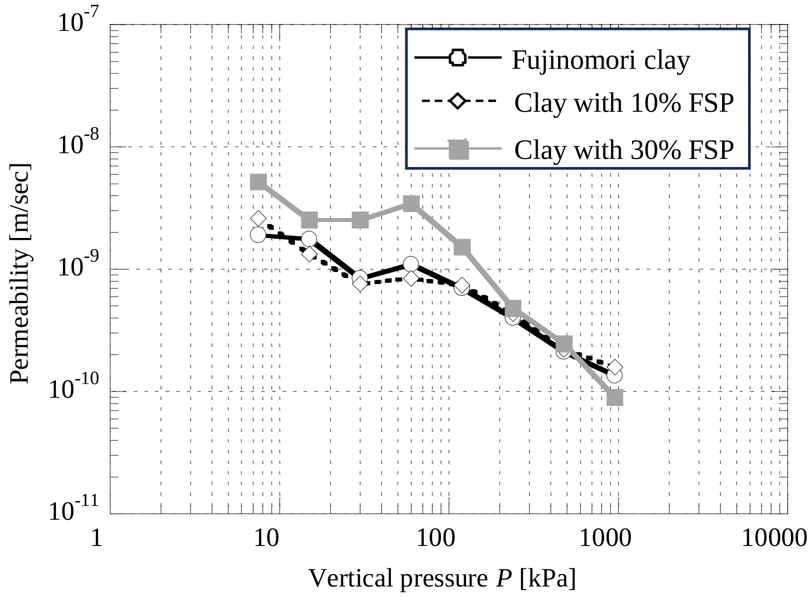


**Figure 3.17: k-log P curves obtained from consolidation tests.**

To reuse FSP-treated clay, it is important to reduce the compressibility of the treated clay by prior application of compaction on the specimen. **Figure 3.16** shows the compression index and swelling index for specimens with different amounts of FSP, calculated from the slopes of the consolidation curves during the compressive and swelling processes, as shown in **Figure 3.15**, respectively. It is clear from this figure that both the compressive index and the swelling index increase with an increase in the amount of FSP, and that there is a nearly linear relationship between each index and the amount of FSP. It is possible, therefore, to estimate the e-logP curve for clay treated with any amount of FSP, if the base clay is the same. This estimation will be useful for developing measures to reduce the volume of treated clay.

At the end of each loading sequence, the hydraulic conductivity was calculated using Terzaghi's consolidation theory (Keramatikerman et al., 2017). **Figure 3.17** shows the *k*-log*P* relationship obtained from the consolidation tests. The hydraulic conductivity calculated indirectly for all the samples is seen to decrease with an increase in vertical stress. The hydraulic conductivity of the clay treated with 30% FSP is the highest for low vertical loading up to 80 kPa. However, the hydraulic conductivity of the clay treated with 10% FSP is almost identical to that of the pure clay, and the hydraulic conductivity in all cases becomes similar with vertical stress levels higher than 200 kPa. These results confirm that the FSP treatment enhances the permeability of clay, while its magnitude is limited, and that such an improvement may be effective under lower confining stress conditions.

### 3.4.6 Hydraulic conductivity of clay treated with FSP

**Figure 3.18** shows the change in specimen height during the consolidation process before the permeability tests for each case. **Table 3-4** provides the values of the void ratio for each case before and after consolidation. **Figure 3.19** indicates that the amount of consolidation is larger when adding a larger amount of FSP, which is a similar tendency to that seen in the consolidation test results given in the previous section. The FSP is composed of tiny fibers of various lengths and thicknesses that are more flexible than clay particles, so that the structure of the FSP can be bulky and largely compressed under a certain level of normal stress compared to pure clay. FSP fibers, especially short fibers, can act as filler materials within the soil structure, occupying the spaces between the clay particles. This may result in an increase in the void ratio of the overall mixture, as shown in **Table 3.4**, and in a decrease in the effective stress of the soil. Therefore, the compressibility of the clay treated with FSP is increased, leading to a larger amount of consolidation. It is also found from **Figure 3.19** that the specimen height tends to change more rapidly when clay soil is mixed with FSP. This is probably because the drainage of water occurs, not only from the FSP that contains some amount of water, but also from the pore spaces of the treated clay. Hence, a larger amount of water can be drained at the same time.

**Table 3.4: Void ratio before and after consolidation**

| | Before consolidation | After consolidation |
|---|---|---|
| Case-1 (pure clay) | 1.42 | 0.83 |
| Case-2 (clay with 10% FSP) | 1.85 | 1.39 |
| Case-3 (clay with 20% FSP) | 2.40 | 1.87 |

**Figure 3.19** presents a time profile of the hydraulic conductivity of the treated clay specimens measured during the falling head permeability tests. At the beginning of the permeability tests, the distribution of water flow in each specimen may be inhomogeneous, so a large fluctuation in hydraulic conductivity is observed. After that, for Case-2 and Case-3, the hydraulic conductivity tends to increase over the first 50 hours and then decrease, while for Case-1, the hydraulic conductivity tends to decrease at the same stage. This difference in tendencies may be due to the presence of FSP. The water flowing through the section of the specimen occupied by FSP fibers percolates faster than that flowing through the section fully occupied by clay particles, leading to the temporal increase in hydraulic conductivity. On the other hand, the clay particles may get clogged in the matrix of the FSP and the soil during the water percolation, leading to a decrease in hydraulic conductivity with time. The change in hydraulic conductivity over time tends to be small for each case, showing an almost stable value. Finally, larger hydraulic conductivity is observed when a

larger amount of FSP is added to the clay. This is probably because the FSP fibers create concentrated seepage paths.

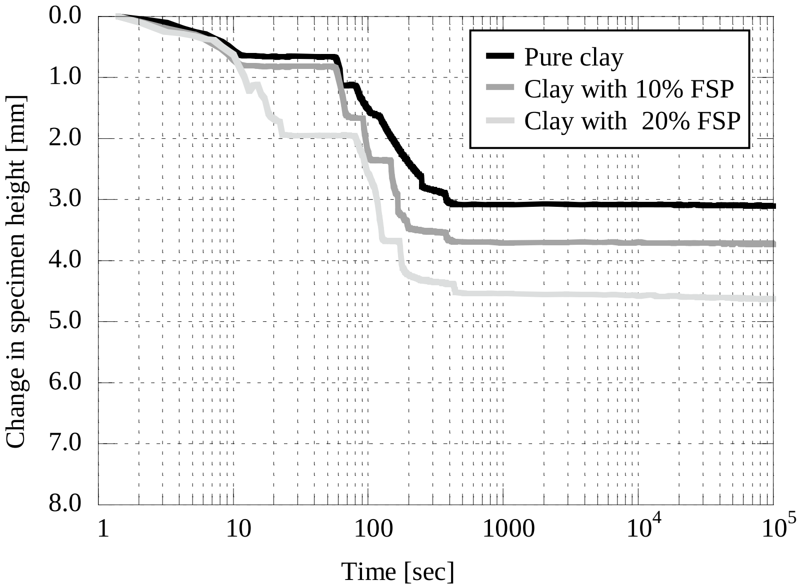


**Figure 3.18: Consolidation of specimen before Permeability test.**

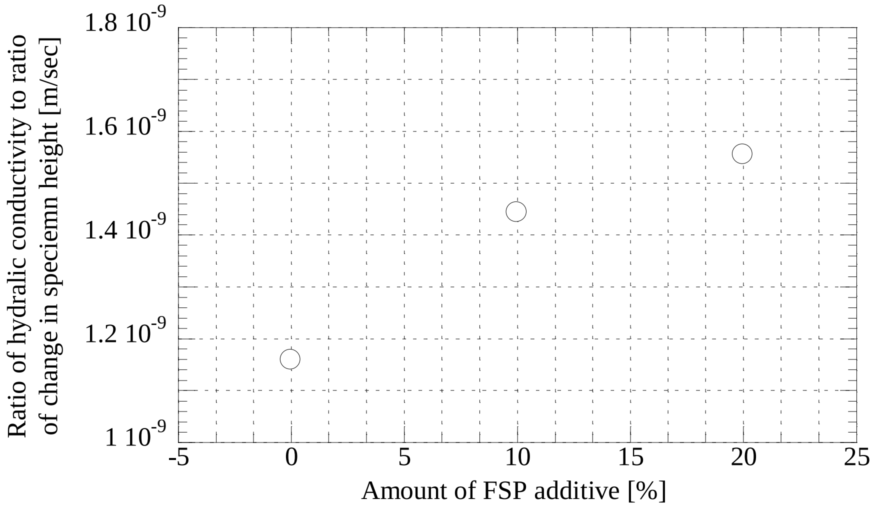


**Figure 3.19: Hydraulic conductivity of FSP-treated soil.**

### 3.4.7 Mechanism of improving clay with FSP

The mechanism of the changes in the physical and strength properties of the clay treated with FSP is mainly discussed based on the results shown in the previous sections 4.1 to 4.4. Firstly, the mechanism of the changes in the physical properties of the clay treated with FSP is discussed. It was found from the changes in consistency, mentioned in section 4.2 and shown in **Figure 3.13**, that the treated clay tends to have a more aggregated and compressible structure than the pure clay when a larger amount of FSP is added. **Figure 3.20** shows the changes in the state of the Kasaoka clay with a water content twice its liquid limit by adding different amounts of FSP, which clearly indicates the aggregation of the clay by adding larger amounts of FSP. The reason is considered to be as follows: FSP shows an intertwined structure due to fibers with various lengths and thicknesses (**Figure 3.2**), shear resistance (**Figure 3.12**), low bulk density, and a rich water-absorption capacity (**Figure 3.11**). Clay particles are easily caught in the intertwined structure of the FSP fibers, even in the high water-content clay. With an increase in the FSP in the clay, the clay particles are more easily caught in the FSP and a larger amount of water in the treated clay is absorbed by the FSP due to the rich water-absorption capacity of the FSP. In this case, the fluidity of the treated clay is significantly reduced and the FSP still maintains a certain level of shear resistance. Therefore, the treated clay can retain its solidly built structure even under both low bulk density and high water-content conditions. It is certain that the higher hydraulic conductivity of the clay treated with larger amounts of FSP, discussed in section 4.4, is attributed not only to the creation of concentrated seepage paths, but also to the lower bulk density of the FSP fibers. It is also possible that the larger amount of water absorption by the FSP leads to an unsaturated condition of the treated clay. In this case, a certain level of suction enhances the bonding and confining effects among the clay particles and the FSP; and hence, the tendency of the aggregation and compressibility may become more significant. There are no data to support this idea, so it will be important to study how the water distributes around FSP in treated clays in the future.

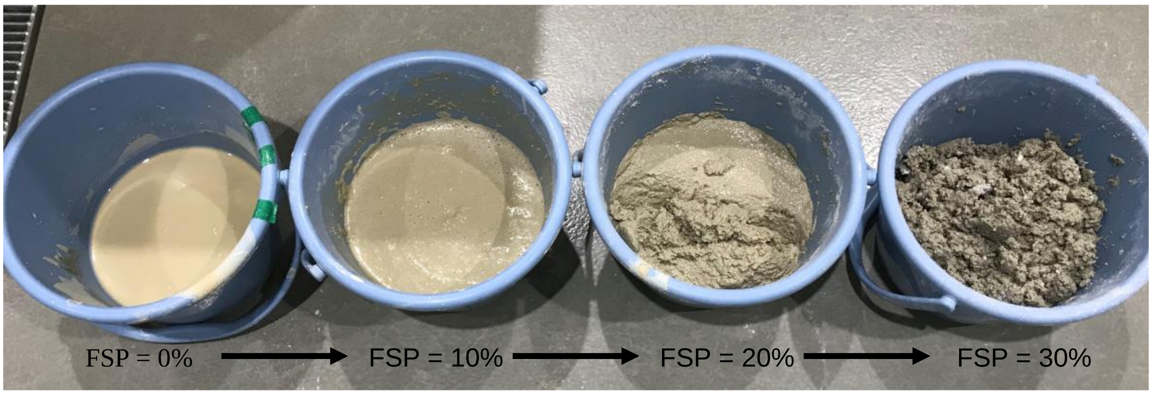


**Figure 3.20: Changes in state of high water-content clay by adding FSP. The initial content of the clay is twice the liquid limit.**

Secondly, the mechanism of the changes in the strength properties of the clay treated with FSP is discussed. As shown in **Figure 3.14**, a larger amount of FSP leads to higher shear strength of the treated clay compared at any values of water content. The FSP can resist the shear deformation, and the shear strength of the FSP itself tends to keep increasing as the shear displacement increases, independent of all levels of water content, as confirmed by **Figure 3.12**. These results support the idea that the shear resistance of fully cohesive clay, at any levels of water content, is significantly improved by increasing the shear resistance for the fiber reinforcement by FSP. According to the discussion on the consistency and changes in the state of the clay by adding FSP, shown in **Figures 3.13** and **20**, a larger amount of FSP in clay leads to more significant aggregation of the treated clay. This probably means that, in treated clay, a larger amount of FSP fibers with various lengths and thicknesses extends the reinforcing structures where the shear resistance is higher than when there are only clay particles. It is also probable that the suction generated by the water absorption of FSP enhances the bonding and confining effects on the soil-FSP mixture. Therefore, the reinforcing effect on the shear property and the desaturation effect on the increase in suction, produced by the addition of the FSP, allows the treated clay to be more resistant to shear deformation than pure clay.

### 3.5 Conclusions

In this study, high water-content soft clay was treated by finely shredded paper (FSP), and the changes in the geotechnical properties, such as the consistency, shear strength, consolidation property, and hydraulic conductivity property, were experimentally investigated. The water-absorption capacity and shear strength characteristics of the FSP itself were also examined. Based on the test results, the mechanism for improving the geotechnical properties of the clay treated with FSP was discussed. The main findings of this study are as follows:

1) FSP has a high water-absorption capacity, and its capacity tends to be higher when the bulk density of the FSP is lower. Accordingly, the water-absorption capacity of FSP can be approximately evaluated by measuring the bulk density of the FSP at the time of its production.
2) There is certainly an optimum water content at which FSP exhibits the highest shear stress. Although the shear stress of FSP decreases above the optimum water content, FSP can resist shear deformation until the water content is 200%. Similar to the shear characteristics of soil materials, FSP shows a clear density dependence and a confining stress dependence on the shear stress.
3) Both the plasticity index and liquid limit increase when the amount of FSP added to the mixture is increased, leading to a change in the consistency characteristics of the treated soil. The test results confirm that the tendency for aggregation and compressibility is more significant for the clay treated with FSP than for the pure clay. This is because of the FSP characteristics, such as the intertwisted structure, shear resistance, low bulk density, and rich water-absorption capacity. Clay particles are more easily caught in the FSP fibers, even at high levels of water content, as the FSP in the clay is increased. In this case, the fluidity of the treated clay is significantly reduced, and the FSP fibers still maintain a certain level of shear resistance. Therefore, the treated clay is stable even under both lower bulk-density and high water-content conditions.

4) The hydraulic conductivity of the clay is increased by adding a larger amount of FSP. This is probably attributed not only to the creation of concentrated seepage paths, related to the rich water-absorption capacity of FSP, but also to the lower bulk density of the treated clay.
5) The treated clay exhibits a larger amount of consolidation than the pure clay at a given normal stress, whereas the void ratio converges to a similar value between the pure clay and the clay treated with different amounts of FSP, as the normal stress is increased. These results confirm that the volume of treated clay can be reduced by pressurization, and that the increase in the volume of the treated clay, due to the addition of FSP, is slight.
6) The shear resistance of pure clay, at any levels of water content, is significantly improved when different amounts of FSP fiber reinforcement are utilized.

## References for Chapter 3


Abbey, S. J., Eyo, E. U., Okeke, C. A. U., Ngambi, S., 2021. Experimental study on the use of RoadCem blended with by-product cementitious materials for stabilisation of clay soils. *Construction and Building Materials* 280. doi: 10.1016/J.CONBUILDMAT.2021.122476.

Adeboje, A. O., Bankole, S. O., Apata, A. C., Olawuyi, O. A., Busari, A. A., 2022. Modification of Lateritic Soil with Selected Agricultural Waste Materials for Sustainable Road Pavement Construction. *International Journal of Pavement Research and Technology*, 1327–1339. doi: 10.1007/s42947-021-00091-5.

Adeyanju, E., Okeke, C. A., Akinwumi, I., Busari, A., 2020. Subgrade Stabilization using Rice Husk Ash-based Geopolymer (GRHA) and Cement Kiln Dust (CKD). *Case Studies in Construction Materials* 13, doi: 10.1016/J.CSCM.2020.E00388.

Anagnostopoulos, C. A., 2015. Strength properties of an epoxy resin and cement-stabilized silty clay soil. *Applied Clay Science* 114, 517–529. doi: 10.1016/J.CLAY.2015.07.007.

Asai, Y., Sawamura, Y., Miyazaki, Y., Kimura, M., 2022. Reuse-aimed treatment of high water-content clay with fine shredded paper: Mechanical characteristics in cement addition. *Japanese Geotechnical Journal* 17(4), 497–509. (in Japanese)

ASTM D 4318, 2018. Standard Test Methods for Liquid Limit, Plastic Limit, and Plasticity Index of Soils 1, *ASTM D4318* (3). doi: 10.1520/D4318-17.

Bozyigit, I., Javadi, A., Altun, S., 2021. Strength properties of xanthan gum and guar gum treated kaolin at different water contents. *Journal of Rock Mechanics and Geotechnical Engineering* 13(5), 1160–1172. doi: 10.1016/J.JRMGE.2021.06.007.

Fadmoro, O. F., Kar, S. S., Tiwari, D., Singh, A., 2022. Environmental and Economic Impact of Mixed Cow Dung and Husk Ashes in Subgrade Soil Stabilization. *International Journal of Pavement Research and Technology* 15(4), 835–846. doi: 10.1007/s42947-021-00056-8.

Japan Cement Association, 2017. Manual of ground improvement using cement-based solidifying material. *Gihodo Shuppan Co., Ltd*, 4th edition.

Katsumi, T., Ishimori, H., Ogawa, A., 2008, Effects of water content distribution on hydraulic conductivity of prehydrated GCLS against calcium chloride solutions. *Soil and Foundations* 48(3), 407–417. doi.org/10.3208/sandf.48.407

Keramatikerman, M., Chegenizadeh, A., Nikraz, H., 2017. An investigation into effect of sawdust treatment on permeability and compressibility of soil-bentonite slurry cut-off wall. *Journal of Cleaner Production* 162, 1–6. doi: 10.1016/j.jclepro.2017.05.160.

Khandelwal, A., Kishor, R., Singh, V. P., 2023. Sustainable utilization of sugarcane bagasse ash in highway subgrade- a critical review. *Materials Today: Proceedings*

78, 114–119. doi: 10.1016/J.MATPR.2022.11.310.

Khayat, N., Nasiri, H., 2023. Study of Strength Characteristics and Micro-structure Analysis of Soil Stabilized with Wastewater and Polymer. *International Journal of Pavement Research and Technology*. doi: 10.1007/s42947-023-00296-w.

Khodabandeh, M. A., Nagy, G., Török, Á., 2023. Stabilization of collapsible soils with nanomaterials, fibers, polymers, industrial waste, and microbes: Current trends. *Construction and Building Materials*. doi: 10.1016/j.conbuildmat.2023.130463.

Kida, S., Sawamura, Y., Yano, T., Kimura, M., 2018. Changes in strength and transportability of high water content mud treated by fine powder made from waste paper. *Proc of 13th National Symposium on Ground Improvement*, 443–450. (in Japanese)

Kutter, B. L. (1992). Dynamic Centrifuge Modeling of Geotechnical Structures

Kwon, Y. M., Chang, I., Lee, M., Cho, G. C., 2019. Geotechnical engineering behavior of biopolymer-treated soft marine soil. *Geomechanics and Engineering* 17(5), 453–464. doi: 10.12989/gae.2019.17.5.453.

Li, M., Chai, S. X., Zhang, H. Y., Du, H. P., Wei, L., 2012. Feasibility of saline soil reinforced with treated wheat straw and lime. *Soils and Foundations* 52(2), 228–238. doi: 10.1016/j.sandf.2012.02.003.

Locat, J., Tremblay, H., Leroueil, S., 1996. *Mechanical and hydraulic behaviour of a soft inorganic clay treated with lime*. Sainte-Foy.

Losini, A. E., Grillet, A. C., Bellotto, M., Woloszyn, M., Dotelli, G., 2021. Natural additives and biopolymers for raw earth construction stabilization – a review. *Construction and Building Materials*. doi: 10.1016/j.conbuildmat.2021.124507.

Lv, Y., Jiang, Y., Hu, W., Cao, M., Mao, Y., 2020. A review of the effects of tunnel excavation on the hydrology, ecology, and environment in karst areas: Current status, challenges, and perspectives. *Journal of Hydrology* 586. doi: 10.1016/J.JHYDROL.2020.124891.

Lyu, H. M., Shen, S., L., Zhou, A., Yang, J., 2019. Perspectives for flood risk assessment and management for mega-city metro system. *Tunnelling and Underground Space Technology* 84, 31–44. doi: 10.1016/J.TUST.2018.10.019.

Mei, Y., Zhang, X., Nong, X., Fu, L., 2021. Experimental study of the comprehensive technology of grouting and suspension under an operating railway in the cobble stratum. *Transportation Geotechnics* 30. doi: 10.1016/J.TRGEO.2021.100612.

Miraki, H., Shariatmadari, N., Ghadir, P., Jahandari, S., Tao, Z., Siddique, R., 2022. Clayey soil stabilization using alkali-activated volcanic ash and slag. *Journal of Rock Mechanics and Geotechnical Engineering* 14(2), 576–591. doi: 10.1016/j.jrmge.2021.08.012.

Ministry of Land, Insfastructure, Transport and Tourism (MLIT), 2020. Results of the survey on Construction By-Products in FY 2018 (in Japanese) Ministry of Land, Infrastructure, Transport and Tourism (2020) Results of the Survey On Construction By-Products in FY2018 (in Japanese)', *MLIT*, January. Available at: https://www.mlit.go.jp/report/press/sogo03_hh_000233.html (Accessed: 2 July 2023).

Moayedi, H., Aghel, B., Abdullahi, M. M., Nguyen, H., Rashid, A. S. A., 2019. Applications of rice husk ash as green and sustainable biomass. *Journal of Cleaner Production* 237. doi: 10.1016/J.JCLEPRO.2019.117851.

Nethravathi. S, Ramesh, H. N., Udayashankar, B. C., Vittal, M., 2018. Improvement of Strength of Expansive Black Cotton Soil Using Sugarcane Bagasse Ash-Lime as Stabilizer, Geo Edmonton 2018.

Ni, J., Li, S. S., Ma, L., Geng, Z. Y., 2020. Performance of soils enhanced with eco-friendly biopolymers in unconfined compression strength tests and fatigue loading tests. *Construction and Building Materials* 263. doi: 10.1016/j.conbuildmat.2020.120039.

Ojuri, O. O., Ramdas, V., Aderibigbe, E. A., Williams, C. G., Ramchuran, S., Al-Nageim, H., 2022. Improving strength and hydraulic characteristics of regional clayey soils using biopolymers. *Case Studies in Construction Materials* 17. doi: 10.1016/J.CSCM.2022.E01319.

Phan, N. B., Hayano, K., Mochizuki, Y., Yamauchi, H., 2021. Mixture design concept and mechanical characteristics of PS ash–cement-treated clay based on the water absorption and retention performance of PS ash. *Soils and Foundations* 61(3), 692–707. doi: 10.1016/j.sandf.2021.02.006.

Pongsivasathit, S., Horpibulsuk, S., Piyaphipat, S., 2019. Assessment of mechanical properties of cement stabilized soils. *Case Studies in Construction Materials* 11. doi: 10.1016/J.CSCM.2019.E00301.

Pujades, E., Vazquez-Sune, E., Culi, L., Carrera, J., ledesma, A., Jurado, A., 2015. Hydrogeological impact assessment by tunnelling at sites of high sensitivity. *Engineering Geology* 193, 421–434. doi: 10.1016/J.ENGGEO.2015.05.018.

Rahgozar, M. A., Saberian, M., Li, J., 2018. Soil stabilization with non-conventional eco-friendly agricultural waste materials: An experimental study. *Transportation Geotechnics* 14, 52–60. doi: 10.1016/j.trgeo.2017.09.004.

Sawamura, Y., Yano, T., Aihara, K., Nishiura, M., Kimura, M., 2017. Property variation of high moisture sludge by fine powder mainly composed of Cellulose. *Proc of 12th Environmental Geotechnical Engineering Symposium*, 12(September), 505–510. (in Japanese)

Silva, G., Nanez, R., Zavaleta, D., Burgos, V., Kim, S., Ruiz, G., Pando, M. A., Aguilar, R., Nakamatsu, J., 2022. Eco-friendly additive construction: Analysis of the printability of earthen-based matrices stabilized with potato starch gel and sisal fibers. *Construction and Building Materials* 347. doi: 10.1016/j.conbuildmat.2022.128556.

Taha, M. R., Taha, O. M. E., 2012. Influence of nano-material on the expansive and shrinkage soil behavior. *Journal of Nanoparticle Research* 14(10). doi: 10.1007/s11051-012-1190-0.

Wong, M. H., 2022. Integrated sustainable waste management in densely populated cities: The case of Hong Kong. *Sustainable Horizons* 2. doi: 10.1016/j.horiz.2022.100014.

Xie, H., Yanhui, Z., Yiyan, C., Qi, P., Zhiyi, L., Jianbo, Z., 2021. A case study of development and utilization of urban underground space in Shenzhen and the Guangdong-Hong Kong-Macao Greater Bay Area. *Tunnelling and Underground Space Technology* 107. doi: 10.1016/J.TUST.2020.103651.

Xu, Y. S., Shen, S. L., Lai, Y., Zhou, A. N., 2018. Design of sponge city: Lessons learnt from an ancient drainage system in Ganzhou, China. *Journal of Hydrology* 563, 900–908. doi: 10.1016/J.JHYDROL.2018.06.075.

Yang, B., Zhang, Y., Ceylan, H., Kim, S., Gopalakrishnan, K., 2018. Assessment of soils stabilized with lignin-based byproducts. *Transportation Geotechnics* 17, 122–132. doi: 10.1016/j.trgeo.2018.10.005.

Yifru, W., Getu, N., Kifile, D., Mesfin, A., Sewunet, A., Tamene, M., 2022. Effects of Corn Cob Ash as Partial Replacement of Cement for Stabilization of an Expansive Clay. *Advances in Civil Engineering*. doi: 10.1155/2022/6788120.

Zeng, C. F., Zheng, G., Xue, X. L., 2019a. Combined recharge: A method to prevent ground settlement induced by redevelopment of recharge wells. *Journal of Hydrology* 568, 1–11. doi: 10.1016/J.JHYDROL.2018.10.051.

Zeng, C. F., Zheng, G., Zhou, X. F., 2019b. Behaviours of wall and soil during pre-excavation dewatering under different foundation pit widths. *Computers and Geotechnics* 115. doi: 10.1016/J.COMPGEO.2019.103169.

## Chapter 4

## Mechanical properties of high-water content clay soils treated with finely shredded paper and cement

### 4.1 Introduction

Due to increase in population and rapid urbanization rapid development of complex infrastructure with large underground structures excavation of these mega cities generates large amounts of dredged soils (Guo et al., 2022; Hu et al., 2023; M. Zhang et al., 2022) that is usually associated with poor engineering properties like high water content, low strength, high compressibility (He et al., 2020). The Japanese Ministry of Land, Infrastructure, Transport and Tourism (MLIT, 2020) estimated that approximately 132.63 million cubic meters of these soils were generated from construction sites in Japan in 2018 where several hundred million tons are annually produced worldwide (Amar et al., 2021; Chu & Yao, 2020; Lirer et al., 2017; Y. Liu et al., 2022; Zeng et al., 2021) that accounts more than 20% of all industrial waste. Disposal and reuse of these soils often poses challenges due to their high-water content, low strength, and potential environmental risks. Soil exhibiting these properties is incapable of sustaining construction machinery, to transport to landfill, serving as a subsoil of foundation for erecting superstructures (Huayang et al., 2019; Wang et al., 2018) .In recent years, researchers have explored various treatment techniques to mitigate these challenges and utilize dredged soils effectively. One of the stabilization methods was traditional stabilizer like cement (R. Wang et al., 2023). Jan & Mir (2018) studied that the addition of cement to the dredged soil changes the structural arrangement of the clay particles where developed cementitious products which increases inter particle bonding that form flocculated specimen matrix.

When cement stabilizes the marine sediments, the presence of soil particles causes the restrained shrinkage of cement hydration products, leading to the formation of substantial new macropores because of the cracking phenomenon (Paula Furlan et al., 2018). In spite of stiffer soil matrix and higher strength, cement treated soil will increase brittleness, reduce sorption capacity and at some point, ductility of construction during static and cyclic loading (Kasama et al., 2007; Ma et al., 2018; Medvey & Dobszay, 2020; Wassermann et al., 2022).Due to excessive amount of cement, shrinkage cracks tend to flourish as (American Concrete Institute (ACI), 2009) reported on expansive soil.

To mitigate this adverse effect fibers were introduced for reinforcement in combination with cement. Recently several research has been studied to evaluate the mechanical properties of soils treated by the utilization of combined fiber and cement additive (Xu et al., 2023). To reinforce and improve the soil engineering properties numerous fibers including. synthetic fibers (i.e., polyester fiber, polyethylene fiber, polypropylene fiber, nylon fiber, etc.) (Abo El-Naga et al., 2020; Hassan et al., 2021; Kumar et al., 2006; Tiwari et al., 2020). The polypropylene fiber addition to the stabilized soft soil matrix significantly increased the ductility and energy absorption of the specimens, and durability significantly improved.

Akbari et al. (2021) in other hand fiber bridge exhibited that prevent evolution of tensile cracks and deformation by utilization of polypropylene fiber with cement to treated dredged sediment (J. S. Li et al., 2023b). However, the natural fibers were preferable for the economical, sustainable, and ecofriendly treatment process that reduce environmental burdens (N. T. Duong et al., 2021). The natural fibers (i.e., coconut fiber, sisal fiber, palm fiber, jute fiber, coir fiber, bamboo fiber, etc.) (Ahmad et al., 2010; Gupta & Kumar, 2021; Kamaruddin et al., 2020; Kodicherla & Nandyala, 2019; Yohanna et al., 2022) have been used in combination with cement. When ordinary Portland cement was combined with kenaf and coconut fibers (Abedi et al., 2023) to sandy soil, the monotonic compression showed 96% and 77% improvement by utilization of 1.5% and 1% fiber amount respectively.in addition the tensile strength increased by 18 to 2.3 times approximately. The corn husk fiber used to reinforce by Duong et al. (2021) cemented soil with high water content that the fiber inclusion improves compressive strength and tensile strength of cemented soil, and the higher amount of fiber content leads to higher the increase in energy absorption. The study shows that with 100% water content, at the same strain, stiffness increases with increasing fiber content for a given strain value. Khodabandeh et al. (2023) studied the effect of different percentages of mixing rice straw fibers on the unconfined compressive strength of collapsible soils treated with different amounts of cement, where. strength is increased by 172.8% and decreases the failure strain by 68.10% just by increasing the percentage of fiber by 1%. The shrinkage and cracking behavior of the expansive soil is controlled due to addition of fiber and cement.

In this study finely shredded paper (here in after called FSP) fibers incorporated into mixture of clay soil and cement at high water content (i, e. slurry) where the treatment method is economical and ecofriendly. The improved soil can be utilized for subsoil of foundation which also reduces the west on the environmental. Sawamura et al. (2017) discovered variations in water absorption characteristics based on the proportion of paper fiber-derived FSP to shredder shavings-derived FSP. Additionally, they observed that the shear strength of clay treated with FSP was greater than that of pure clay. Kida et al. (2018) determined, through flow tests and cone index tests, that the transportation of FSP-treated clay remained viable as long as the flowability had decreased to a measurable extent, even if the strength fell below the typical 200 kN/m$^2$ during the interparticle reinforcement process. Asai et al. (2022) conducted uniaxial compressive strength tests on clay specimens enhanced with both FSP and cement after curing to explore the potential for reusing treated clay as construction material. However, the strength development during cementitious treatment of high-water content clay with different amounts of FSP additive and cement is not clearly understood. A series of unconfined compressive strength (UCS) tests and cone index test were conducted to investigate the effects of cement water ratio, FSP fiber amount and water content of the mix on the strength development and stress–strain evolutions of FSP fiber- cement reinforced high water content muddy soil is investigated in this study. From the experimental results, the cementation and reinforcement mechanisms inside fiber-cement reinforced high water content clay soil were explored and analyzed via the macro failure characteristics and interfacial morphology. The key findings of this study could provide the understanding and reference for improving the mechanical properties of high-water content clay soil by incorporating natural fibers in combination with traditional stabilizers like cement.

## 4.2 Materials

### 4.2.1 Physical properties of Finely shredded paper (FSP) and Kasaoka clay

The raw materials of the FSP made from used papers can be divided into two types: paper powders, which are generated by cutting and grinding in printing companies, and shredder dusts, which are the general cutting dusts generated during the processing of confidential documents in offices and other places. It is known that shredder dust absorbs more amounts of water than paper powders. Therefore, in our research group, the FSP made from the shredder dusts has been used (e.g., Asai et al., 2021; Kida et al., 2018; Sawamura et al., 2017). On the other hand, it is difficult to identify the uniform performance of the FSP because the FSP is made from any kind of used papers such as office papers, magazines and so on, each probably exhibiting different properties. In other words, a usage of the FSP made from only one kind of paper allows us to unify the test conditions, and to evaluate not only the standard performance of water absorption of the FSP itself, but also the standard performance of the FSP for improving characteristics of the treated soil. Therefore, the FSP made from an office paper (hereinafter referred to as standard FSP) is generated and is used in this study. The FSP which has been used in our research group is referred to as the original FSP.

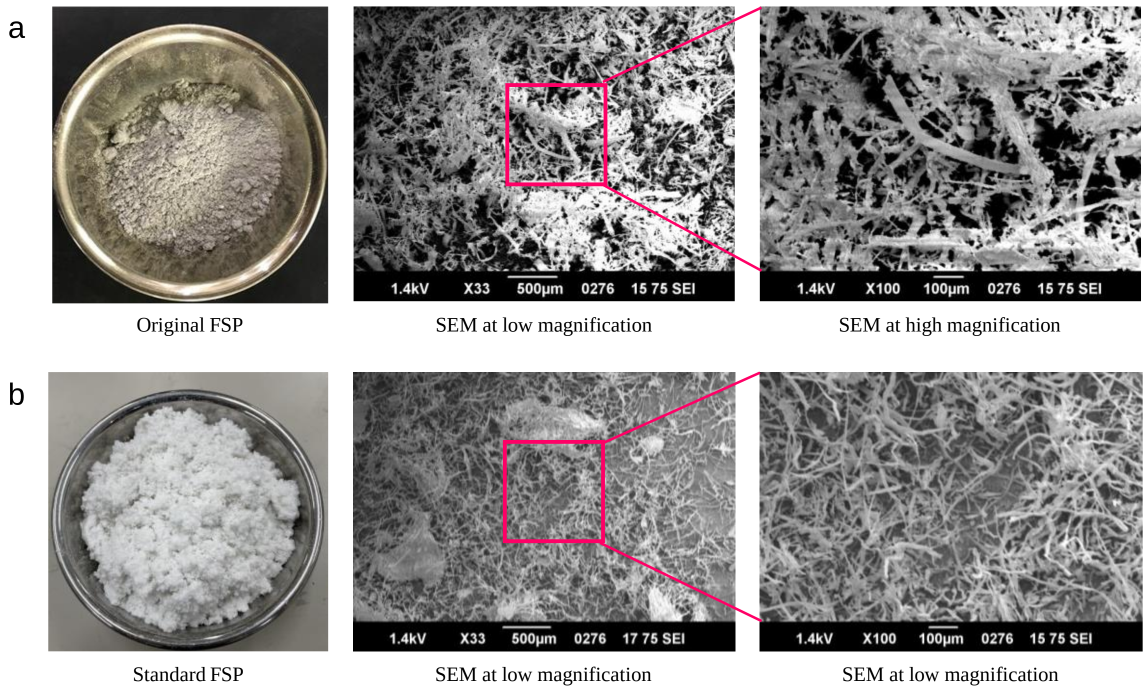


**Figure 4.1: Pictures and SEM images: (a) original FSP and (b) standard FSP used in this study.**

**Figure 4.1** shows pictures and SEM image for original FSP and standard FSP used in this study. The original FSP and standard FSP are made from shredded paper using a special machine. The shredded papers are first shredded into pieces and then pressed into a millstone mill, where they are processed into powder by impact, centrifugal force, and shear force generated when they pass through the gap between the two grinding stones. The SEM images show that both types of the FSP have complex fiber entangled structures, and the standard FSP shows more fine fiber entanglements.

The density of the FSP was measured by the density tests of soil particles (JIS A 1202). A pycnometer with a capacity of 100 mL was used in the test. When a 100 mL pycnometer is used in the density test of soil particles, a sample with a dry mass of 10.0 g or more is used. On the other hand, the volume of FSP is much larger than that of soil particles at a given mass, and it was difficult to put 10.0 g of FSP into the pycnometer. Therefore, a sample of 2.0 g was used for the test. The density of the original FSP was 1.74 g/cm$^3$ (Asai et al., 2021) and that of the standard FSP was 1.78 g/cm$^3$, respectively. **Figure 4.2** shows the particle size additive curves for FSP and standard FSP, which were obtained by soil particle size tests (JIS A 1204). It is clearly seen from **Figure 4. 2** that the standard FSP shows larger particle size than the original FSP.

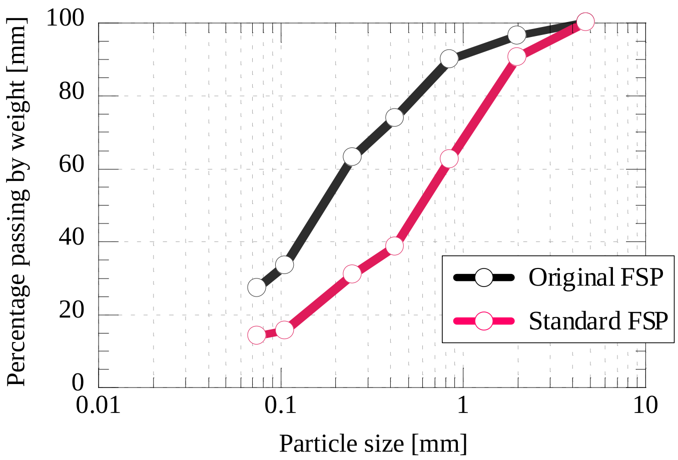


**Figure 4. 2: Particle size distribution curves.**

The other material used in this study is Kasaoka clay, sampled in Okayama prefecture, Japan. This clay is air dried and powdered before the experiment. The physical properties of this soil include specific gravity ($G_s$) 2.70, liquid limit of 54.6% and plasticity index of 27.8% which indicate that the soil categorized as high plastic clay soil using Unified Soil Classification System.

### 4.2.2. Water absorption characteristics for FSP

The water absorption characteristic for the FSP is characterized by a bulk density test and a water absorption test. The bulk density test method is described below as a similar method studied by (Sawamura et al., 2017).

(1) Gently place the standard FSP into a 2000-mL graduated cylinder, avoiding vibrations as much as possible.

(2) Weigh the sample after the top surface has reached the 2000-mL mark.

The water absorption test method is described below where Figure 4.3 shows a schematic diagram of the test.

(1) Place 3.0 g of the sample onto a 100 mm × 100 mm nylon mesh. Fold over the top of the mesh and stitch it closed with a sewing machine.

(2) Lace the sample in a 500-mL beaker filled with degassed water, stir at 300 rpm using a 20 mm stirrer, and allow it to absorb water for 24 hours in a room with a constant temperature of 20°C.

(3) After the water absorption is complete, air dry the sample for 10 minutes, weigh it, and subtract the amount of water absorbed by the nylon mesh to determine the water absorption of the sample.

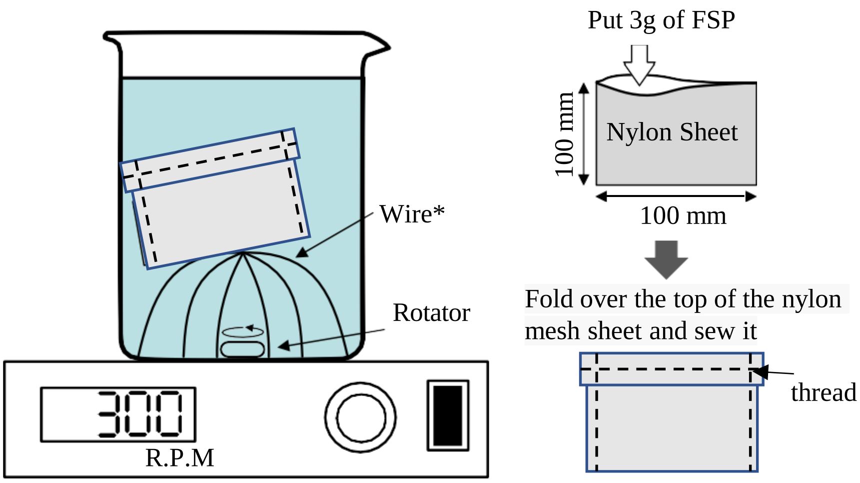


*Wire prevents contact between specimen and rotator

**Figure 4. 3: Schematic diagram of water absorption test.**

**Figure 4.4** shows the relationship between bulk density and water absorption, in which test results for the original FSP obtained in Sawamura et al. (2017) and the test result for the standard FSP obtained in this study are displayed. There is a correlation between water absorption and bulk density, that is, lower bulk densities give a higher amount of water absorption. The results for the standard FSP show a good agreement with the correlation. It is obvious from **Figure 4.4** that the standard FSP has a higher water absorption than the original FSP. **Figure 4.1** confirms that the standard FSP has a more porous structure due to the entanglement of fine fibers than the original FSP. It is considered that the pores between the fibers result in a small bulk density and that the capillary action caused by this porous structure results in a large amount of water absorption.

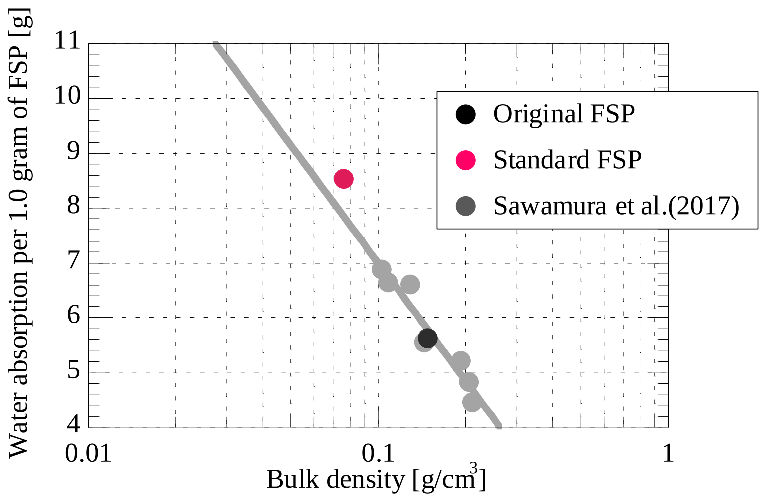


**Figure 4. 4: Bulk density – water absorption relationship**

The water absorption characteristic of the FSP is probably determined by microstructure of fibers and fiber lengths. Therefore, the water-absorption capability of the standard FSP of different particle sizes was investigated. The standard FSP was sieved according to JIS A 1204, and water-absorption tests were conducted using the standard FSP particles that remained in each sieve. The test method is the same as that described above, and a 100 mm × 100 mm bag made of a nylon mesh sheet, with a mesh size of 50.8 μm, was used to prevent the outflow of fine particles from the bag. **Figure. 5** shows the water absorption of the standard FSP with different particle sizes. The particle size of the standard FSP was determined as the average size of the opening of the sieve on which the standard FSP particles remained and the sieve into which the sample had been placed. The standard FSP with a particle size of 178 μm, which remained at 106 μm, had the highest water absorption. The water-absorption capacity tends to increase with the decreasing particle size up to 178 μm, while the water-absorption capacity of samples smaller than 178 μm decreases with the decreasing particle size. **Figure. 6** shows SEM images and photographs of the original FSP and the standard FSP with each particle size. The shapes of the FSP can be roughly classified into two types: fibrous fragments and paper fragments. The paper fragments decrease as the particle size increases. The standard FSP with a particle size of 178 μm that remained at 106 μm, with the highest water absorption, and the standard FSP with a particle size of 90.5 μm that remained at 75 μm, with the second highest water absorption, were sieved through the 75 μm sieve. They both showed large proportions of long and thin fiber entanglements. This indicates that the entanglement of the fibers contributed greatly to the water-absorption capacity of the standard FSP.

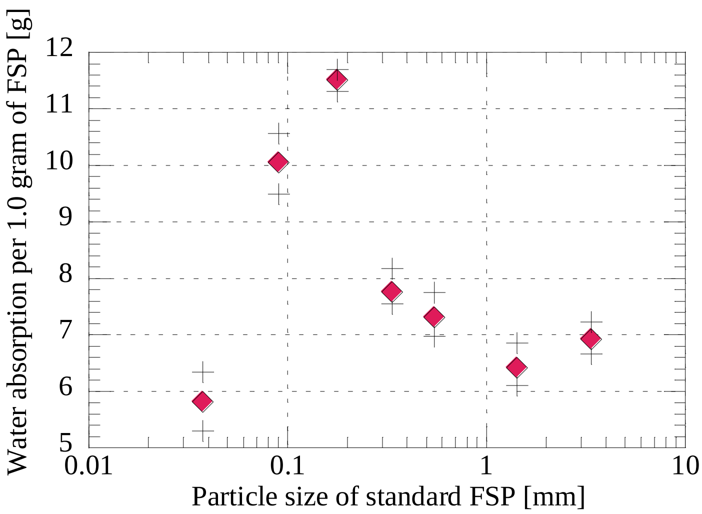


**Figure 4. 5: Effect of particle size and water absorption of standard FSP**

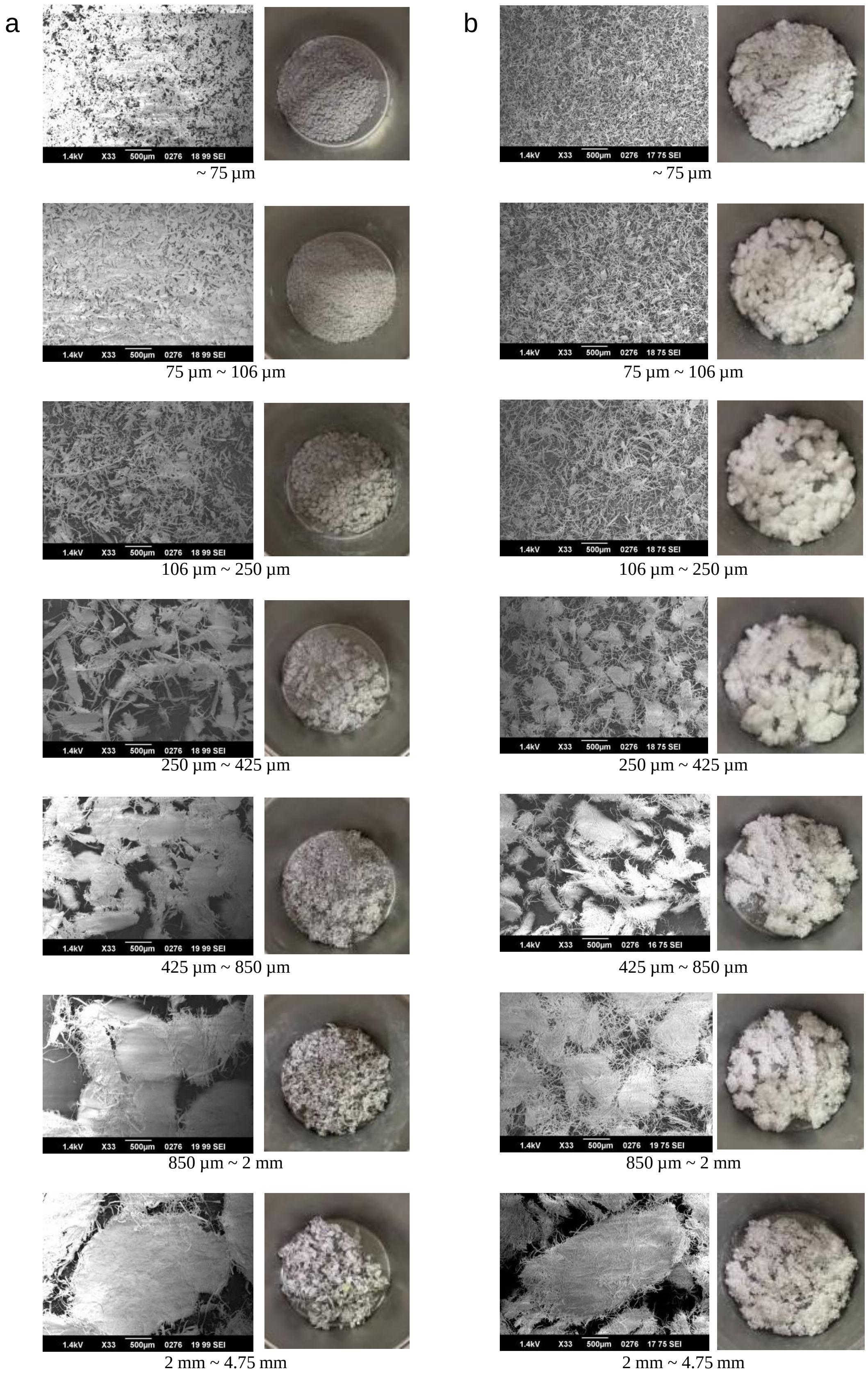


**Figure 4. 6: SEM images and photographs of (a) original FSP and (b) standard FSP with various particle sizes.**

## 4.3 Experiment methods

In this study experiments are conducted for treated soil with only FSP and treated soils with FSP and cement. The preparation methods and test conditions are described below.

### 4.3.1 Preparation method of specimens of clay treated with FSP

To investigate the possibility of reusing treated clays with FSP as a geomaterial, cone index tests and uniaxial compression tests were conducted using clays with different initial water contents and the standard FSP with different amounts of addition rate. **Table 4.1** shows the experimental cases. This study focuses on treating high water content mud, such as dredged soils, using FSP. According to data of construction sites obtained in previous studies (Fukushima et al., 2000; Koike et al., 2004; Miyazaki et al., 2003; Takahashi et al., 2006; Takeyama et al., 2017) , the range of water contents for dredged soils is roughly between 50% and 120%. Considering the data, the target water contents of the clays in this study were determined as 40%, 60%, 80%, and 100%. 100% of water content is almost two times the liquid limit of the Kasaoka clay. The target amounts of the standard FSP were 0%, 10%, 30%, and 50% by weight relative to the dry weight of the clay. The preparation method of the specimens is shown below.

(1) Standard FSP was added to and mixed with the dry clay at the prescribed ratio, and then degassed water was added and mixed to prepare a uniform specimen. In the field, FSP is added to high-water-content clay. This is different from the sample preparation methods used in this study, for the sake of obtaining uniformity of the specimens in the laboratory.

(2) In accordance with the compaction test method A (JIS A 1210:2009), the specimen was placed in a mold with the specified dimensions using a rammer and then compacted in three layers so that the compaction energy was 550 kJ/ $m^3$.

(3) Once the specimen had been compacted, it was weighed.

(4) Specimens that were difficult to compact with a rammer, due to their high fluidity, were placed in a mold while removing air bubbles with a rammer ($\phi$ = 4.0 mm). For samples that were difficult to compact with a rammer and had relatively low fluidity, a pestle ($\phi$ = 50. 7 mm) was used for dense filling.

For the cone index tests, the samples in molds, having a diameter of 100 mm and a height of 127 mm, were tamped with a 2.5 kg rammer 25 times in three layers, each layer starting at a height of 300 mm. In the uniaxial compression tests, molds with a diameter of 50 mm and a height of 100 mm were used along with a 1.5-kg rammer. The 1.5-kg rammer was used to compact the soil into three equal layers with 12 blows per layer in molds having a diameter of 50 mm and a height of 100 mm. For the samples that were difficult to compact with a rammer, due to their high fluidity, the samples were placed in molds, the bubbles were removed using the rammer ($\phi$ = 4.0 mm), and then the molds were filled. The samples that were difficult to compact with a rammer, due to low fluidity, were packed densely with a pestle ($\phi$ = 50.7 mm). The specimens, in their initial condition, were mixed with 0, 10, 30, and 50% FSP and with water contents of 60% and 100% as shown in **Figure 4:11**. Uniaxial compression tests on standard FSP and cemented high-water-content muddy clay soil were also conducted to investigate the mechanical properties of the cement in addition to the FSP. The test conditions and specimen preparation methods are described below.

**Table 4. 1: Test cases for cone index test and uniaxial compression test**

| Case | *w* [%] | Amount of FSP [%] | *w* after FSP additive [%] |
|---|---|---|---|
| *w* 40 - FSP_0 | 40 | 0 | 40.0 |
| *w* 40 - FSP_10 | | 10 | 36.4 |
| *w* 40 - FSP_30 | | 30 | 30.8 |
| *w* 60 - FSP_0* | 60 | 0 | 60.0 |
| *w* 60 - FSP_10* | | 10 | 54.5 |
| *w* 60 - FSP_30* | | 30 | 46.2 |
| *w* 60 - FSP_50* | | 50 | 40.0 |
| *w* 80 - FSP_30 | 80 | 30 | 61.5 |
| *w* 80 - FSP_50 | | 50 | 53.3 |
| *w* 100 - FSP_0* | 100 | 0 | 100.0 |
| *w* 100 - FSP_10* | | 10 | 90.9 |
| *w* 100 - FSP_30* | | 30 | 76.9 |
| *w* 100 - FSP_50* | | 50 | 66.7 |

*Conducted cone index test

### 4.3.2 Method of specimen preparation of clay treated with FSP and cement additive

It is considered that there is a limit in improving the strength of high-water content muds exceeding 100% when treated with FSP alone. Therefore, in this study, cement is used in combination with FSP to further improve the strength of the treated soil, and the uniaxial compressive strength of the treated soil is investigated.

**Table 4.2** shows the test cases considered for the study. The moisture content of the clay was set at 100 %. Standard FSP and ordinary Portland cement were used as samples for the experiments. The amounts of standard FSP added were 0%, 5%, and 10 % by weight relative to the dry weight of the clay. The amount of cement added was 5 %, 8 %, and 10 % by weight relative to the dry weight of the clay.

**Table 4. 2: Uniaxial compression test cases with standard FSP and cement**

| Case | *w* [%] | Amount of cement added [%] | Standard FSP amount [%] |
|---|---|---|---|
| *w* 100 - C5 - FSP_0 | 100 | 5 | 0 |
| *w* 100 - C5 - FSP_5 | | | 5 |
| *w* 100 - C5 - FSP_10 | | | 1 0 |
| *w* 100 - C8 - FSP_0 | | 8 | 0 |
| *w* 100 - C8 - FSP_2 | | | 2 |
| *w* 100 - C8 - FSP_ 5 | | | 5 |
| *w* 100 - C8 - FSP_10 | | | 1 0 |
| *w* 100 - C10 - FSP_0 | | 1 0 | 0 |
| *w* 100 - C10 - FSP_ 5 | | | 5 |
| *w* 100 - C10 - FSP_10 | | | 1 0 |
| *w* 2 00 - C20 - FSP_0 | 2 00 | 2 0 | 0 |
| *w* 2 00 - C20 - FSP_10 | | | 1 0 |
| *w* 2 00 - C20 - FSP_20 | | | 2 0 |

In addition, to examine the properties of muds with extremely higher water content, cases with a water content of 200 %, standard FSP additions of 0 %, 10 %, and 20 %, and cement addition of 20 % were also conducted. The following methods were used to prepare the specimens:

(1) Add the prescribed amounts of standard FSP and cement to dry clay and mix well.

(2) After adding distilled and degassed water, prepare a homogeneous slurry using a vibrator.

(3) Pour the slurry into a uniaxial compression test mold (diameter of 50 mm and height of 100 mm) and cover the surface with plastic film to prevent drying.

(4) Wet cure the slurry in a container lined with paper and soaked in water in a thermostatic chamber at a temperature of 20°C for 7 days to allow it to solidify (**Figure 4. 7**).

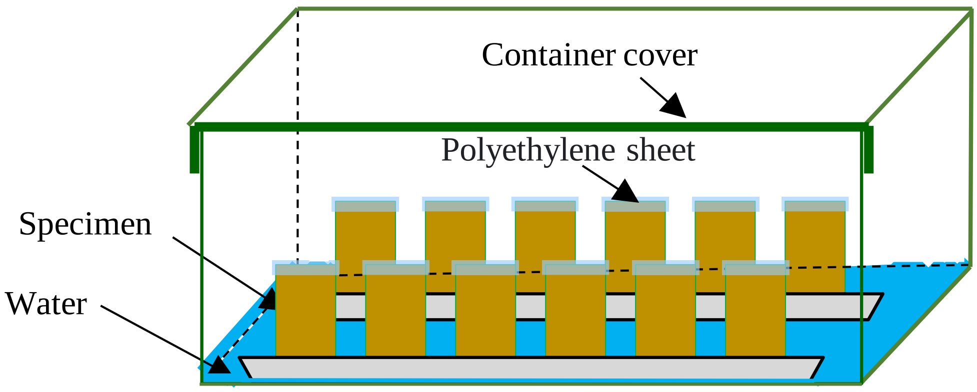


**Figure 4. 7: Wet curing process**

### 4.3.3 Cone index tests

The cone index test is used to classify the quality of treated construction sludge when it is used as soil material in the "Technical Standard for Utilization of Treated Construction Sludge “, which is established by MLIT, Japan, for the proper recycling of construction sludge. In this study, cone index tests were conducted using an automatic penetration device in accordance with JIS A 1228 to investigate the mechanical properties of mud with standard FSP. A schematic diagram of the apparatus is shown in **Figure 4.8**. The cone index, which is the index obtained in the cone index test, is defined by the following equation (4.1).

$$q_c = \left[\frac{Q_c}{A}\right] \times 10^3 \qquad \text{Eq. (4.1)}$$

Where, $q_c$: Cone index [kN/m$^2$].

$Qc$: Mean penetration resistance [N].

$A$: Base area of cone tip [mm$^2$].

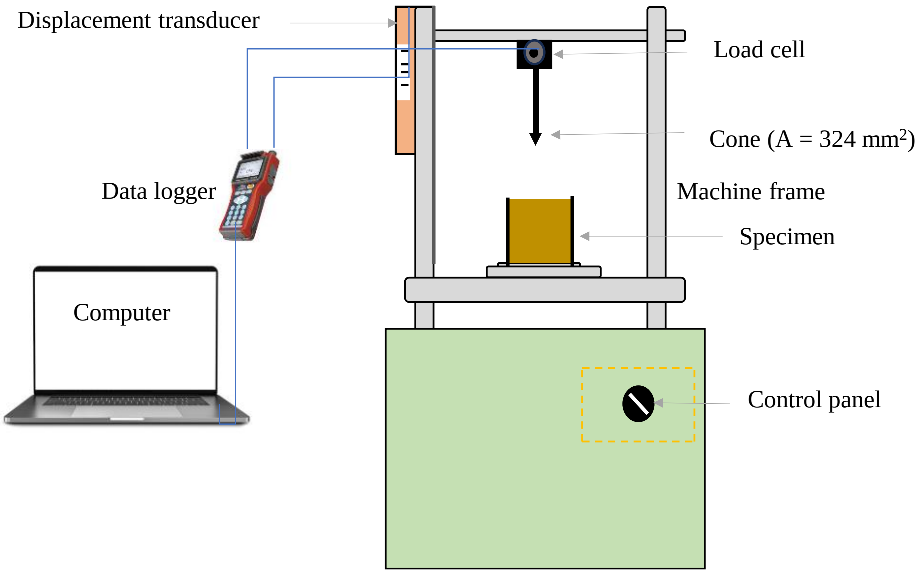


**Figure 4. 8: Cone index test machine for setup**

The average penetration resistance $Q_c$ [N] is the average penetration resistance for penetrations of 50 mm, 75 mm, and 100 mm. The basal area of cone tip $A$ [$mm^2$] is 324 $mm^2$. The experimental procedure is described below.

(1) Place the mold on the test apparatus so that the cone tip is aligned with the center of the specimen.

(2) Penetrate the tip cone by the automatic penetration device at a rate of 10 mm/s and place the tip cone on the specimen at a depth of 50 mm, 75 mm, or 75 mm from the top of the specimen. Calculate the cone index by determining the penetration resistance when the cone has penetrated 50 mm, 75 mm, and 100 mm from the top surface of the specimen.

(3) After the test, take samples from the upper, middle, and lower layers of the specimen, and measure the water content.

### 4.3.4 Uniaxial compressive strength tests

In this study, uniaxial compression tests were conducted in accordance with JIS A 1216:2009 to investigate the compressive strength properties of treated soil with standard FSP. The tests were conducted using a load capacity of up to 2.5 kN. MTS loading equipment with a load capacity of up to 2.5 kN was used in the tests.

The compressive stress obtained in the uniaxial compression test is calculated by the following equations.

$$\sigma = \frac{P}{A_o} \times \left(1 - \frac{\varepsilon}{100}\right) \times 10^6 \qquad \text{Eq. (4.2)}$$

$$A_o = \frac{\pi D_o^2}{4} \qquad \text{Eq. (4.3)}$$

$$\varepsilon = \frac{\Delta H}{H_o} \times 100 \qquad \text{Eq. (4.4)}$$

Where,

$\sigma$: compressive stress [kN/m$^2$].

$P$: compressive force applied to the specimen when the compressive strain is $\varepsilon$ [N].

$A_0$: cross-sectional area of the specimen before compression [mm$^2$].

$D_0$: Diameter of the specimen before compression [mm].

$\varepsilon$: Compressive strain of the specimen.

$\Delta H$: Amount of compression [mm].

$H_0$: height of the specimen before compression [mm].

The compression rate is 1% of the initial height of the specimen per minute. The maximum compressive stress until the compressive strain reaches 15% is determined from the stress-strain curve as the uniaxial compressive strength $q_u$ [kN/m$^2$] and the strain at that point is the failure strain $\varepsilon_f$ [%].

The experimental procedure for this experiment is described below.

(1) Measure the weight, diameter, and height of the specimen.

(2) Compress the specimen at a compression rate of 1%/min.

(3) After the test, take samples from the upper, middle, and lower layers of the specimen, and measure the water content ratio of each part.

To investigate the stiffness of the mud with FSP, the variation of the deformation constant $E_{50}$ with the amount of standard FSP added in the uniaxial compression test is investigated in this study. This deformation coefficient $E_{50}$ is expressed as the slope of a line connecting a point at half the uniaxial compressive stress and the origin. The method for calculating the deformation coefficient $E_{50}$ is shown in the following equation (4.5).

$$E_{50} = \frac{\frac{q_u}{2}}{\varepsilon_{50}} \times \frac{1}{100} \qquad \text{Eq. (4.5)}$$

Where,

$E_{50}$: Coefficient of deformation [MPa]

$q_u$: Uniaxial compressive strength [kN/m$^2$]

$\varepsilon_{50}$: Compressive strain at compressive stress $\sigma = q_u/2$ [%].

### 4.4 Results and Discussions

#### 4.4.1 Clay treated with FSP

##### 4.4.1.1 Cone index tests

**Figure 4.9a** shows the relationship between the amount of penetration and penetration resistance at an initial water content of 60% (*w*60), and **Figure 4.9b** shows that at an initial water content of 100% (*w*100). At least three tests were conducted for each amount of addition of standard FSP. It can be seen from these figures that the penetration resistance increases as the amount of standard FSP increases. **Figure 4.9a** shows that for *w*60, the maximum penetration resistance is 334.4 *N* at 30% addition of standard FSP and 626.1 *N* at 50% addition of standard FSP. On the other hand, Fig. 9b shows that for w 100, the maximum penetration resistance increases to 213.9 *N* only when 50% standard FSP is added. **Figure 4.10** shows the relationship between the addition rate of standard FSP and the cone index $q_c$. *w*60 and *w*100 have a cone index $q_c$ of about 100 kPa up to 10% and 30% of the standard FSP addition rate, respectively, but for *w*60 the strength increases rapidly when 20% and more FSP is added. The treated clay with larger amount of FSP is significantly aggregated due to much amount of water absorption, and the compressive resistance is enhanced compared to the treated clay in a muddy state. Another possible reason is that some fibers fully absorb water up to their limitation, but the others may absorb water incompletely so that they are partially wet condition. The partially wet FSP probably shows stronger interlocking among fibers caused by an interparticle bonding due to higher capillarity than the fully wet FSP, resulting in higher resistance of the treated clay.

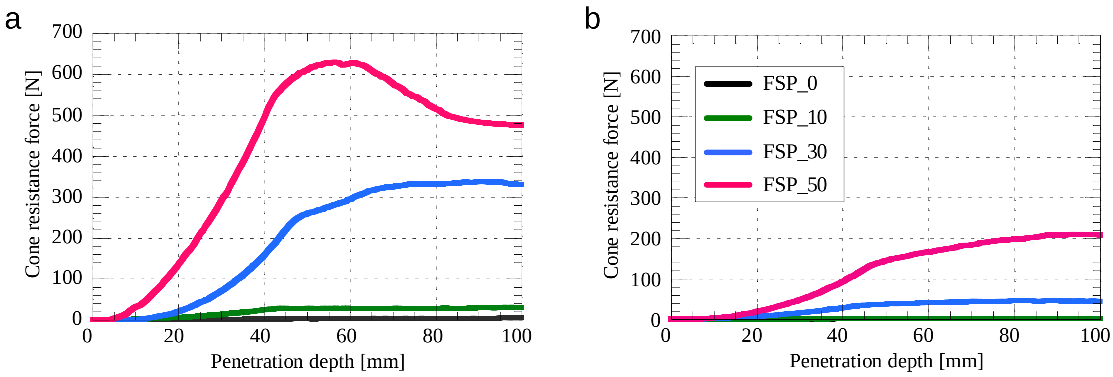


**Figure 4. 9: Penetration resistance at each penetration depth. (a) *w*60 (b) *w*100**

**Figure 4.11** shows the relationship between the water content after the FSP addition and the standard FSP addition rate in the experimental cases of the cone index tests. In this figure, the relationship between the standard FSP addition rate and the liquid limit obtained from the consistency tests is also shown, as well as the water content after the addition of standard FSP for each case. In cases where the water content is higher than the liquid limit, the maximum amount of standard FSP is added in the mix, namely, 10% for the mixing water content of 100% and less for the mixing water content of 60%, respectively. Similarly, in cases where the water content after the addition of standard FSP is lower than the liquid limit, which is below the approximate line between the standard FSP addition amount and the liquid limit, as shown on the **Figure 4.11**, the standard FSP utilized for mixing at a higher water content is higher than 10%. This is probably due to the increase in suction inside the pores due to the transition of the specimen from a liquid state to a plastic state. As the amount of standard FSP added to the mixture was increased, more free water was absorbed which caused the specimen to change to unsaturated condition. This result indicates that the higher amount of added standard FSP makes the specimen stiffer and improves the specimen strength, as shown in **Figure 4.10**, despite the utilization of a high-water content for mixing.

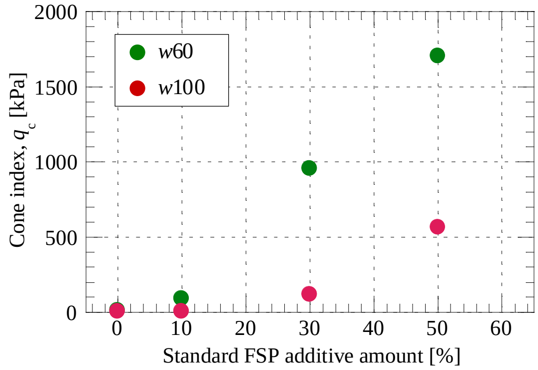


**Figure 4. 10: Relationship between standard FSP amount and cone index**

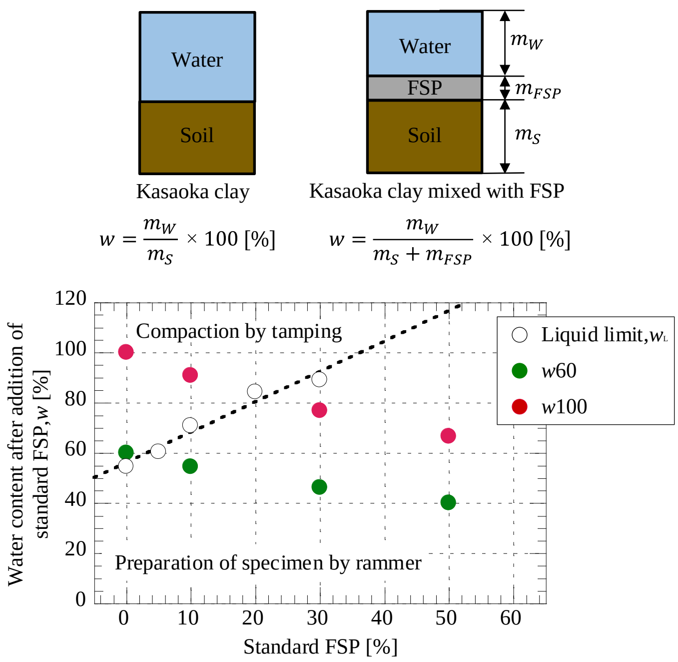


**Figure 4. 11: FSP addition rate and moisture content after FSP addition of cone index test.**

#### 4.4.1.2 Uniaxial compressive strength tests

**Figure 4.12** shows the stress-strain relationship for different amounts of FSP, namely, 0%, 10%, 30%, and 50%. For the *w*40 cases, the stress curve tends to rise for the clay without FSP, as shown in **Figure 4.12a**, while the peak stress in the stress curve becomes more distinct with an increase in the FSP addition.

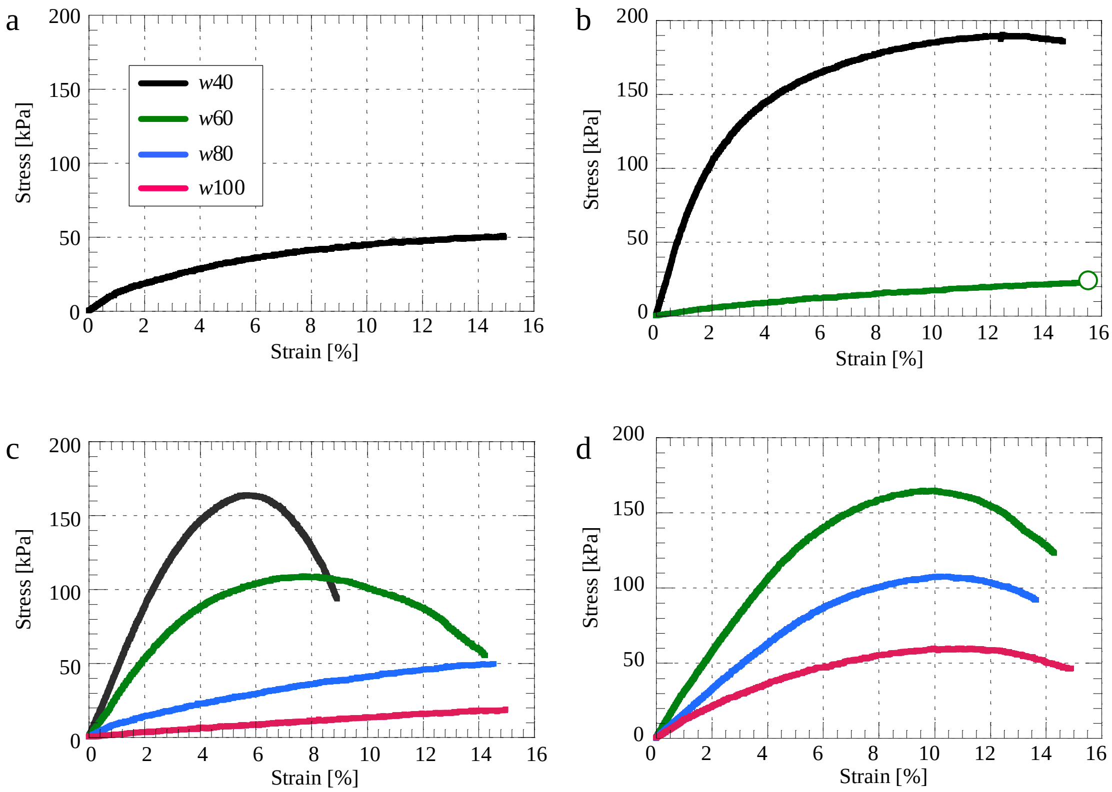


**Figure 4.12: Standard FSP addition amount and failure strain. FSP amount (a) 0%, (b) 10%, (c) 30% and (d) 50%**

The same tendency is observed for the other amounts of water content. **Figure 4.13** shows the relationship between the standard FSP addition rate and the uniaxial compressive strength, while **Figure 4.14** shows the relationship between the standard FSP addition rate and deformation coefficient $E_{50}$. It can be seen from **Figure 4.13** and **4.14** that larger amounts of FSP tend to provide higher levels of compressive strength and $E_{50}$. However, in the case of *w*40, the compressive strength and $E_{50}$ are lower for *w*40 – FSP_30 than for *w*40 – FSP_10.

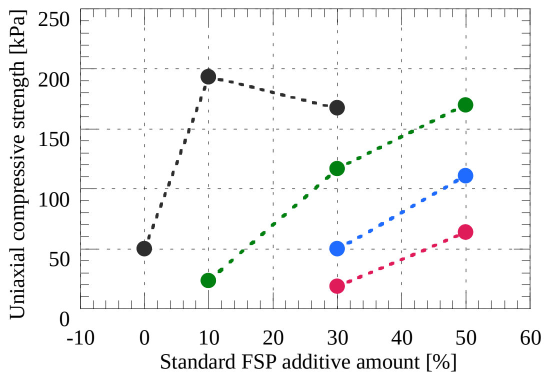


**Figure 4.13: Effect of standard FSP amount on UCS.**

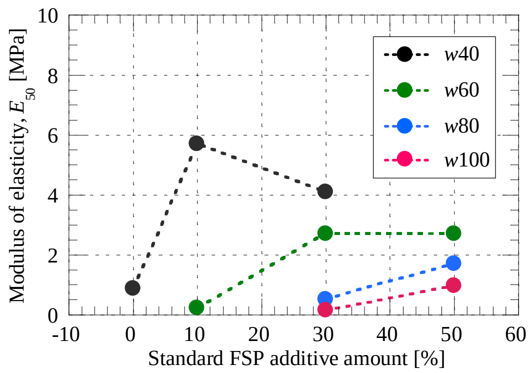


**Figure 4.14: Effect of standard FSP amount on modulus of elasticity E50.**

**Figure 4.15** shows the states of the specimen before and after uniaxial compression. The figure confirms ductile failure for *w*40 - FSP_10, exhibiting the barrel-shaped deformation of the specimen, and brittle failure for *w*40 - FSP_30, exhibiting longitudinal cracking. In cases where the addition of FPS is excessive, compared to the initial water content of the clay, the amount of water absorption for the FSP is not enough to produce strong interlocking among the wet fibers. Some parts of the FSP fibers probably remain dry and in a soft condition and are weak against compression. These results indicate that the balance between the amount of FSP addition and the water content of clays should be carefully considered when anticipating the improvement in the strength of clay with relatively lower water contents, and that further studies are needed to determine such an optimum balance. It is found from a comparison of the results of the FSP additions at 30% and 50%, in **Figure 4.13** and **4.14**, that the strength and $E_{50}$ of the treated clay are lower when the initial water content of the clay is high, while these values linearly increase with an increase in the FSP addition, even for *w*100. These findings indicate that improvements in strength and stiffness can be expected even for clay soil with high water contents, similar to almost two times the liquid limit (liquid limit of 54.6% for Kasaoka clay). **Figure 4.16** shows the relationship between the addition of standard FSP and failure strain $\varepsilon_f$. It can be seen that the failure strain decreases as the standard FSP addition increases, and that the same tendency is observed for all levels of water content.

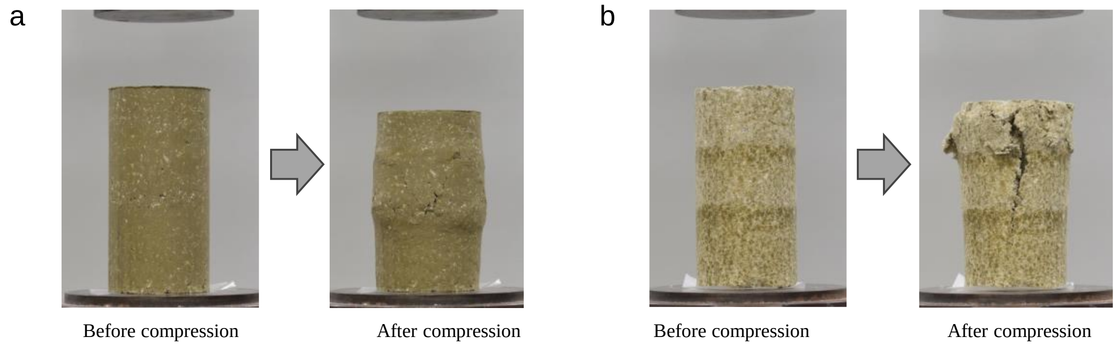


**Figure 4.15: Specimen before and after compression test (a) *w*40 - FSP_10 and (b) *w*40 - FSP_30.**

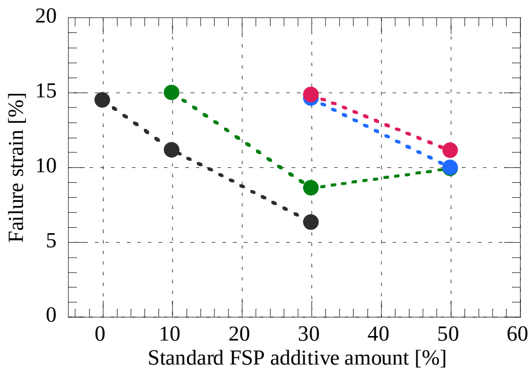


**Figure 4.16: Failure strain at different amount of standard FSP**

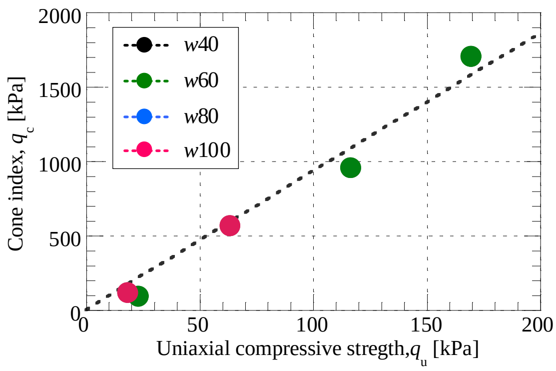


**Figure 4.17: Unconfined compressive strength and cone index relationship**

### 4.4.1.3 Relationship between uniaxial compressive strength and cone index value

**Figure 4. 17** shows the relationship between uniaxial compressive strength $q_u$ and cone index $q_c$. There is a strong correlation between uniaxial compressive strength and cone index values of the specimen.

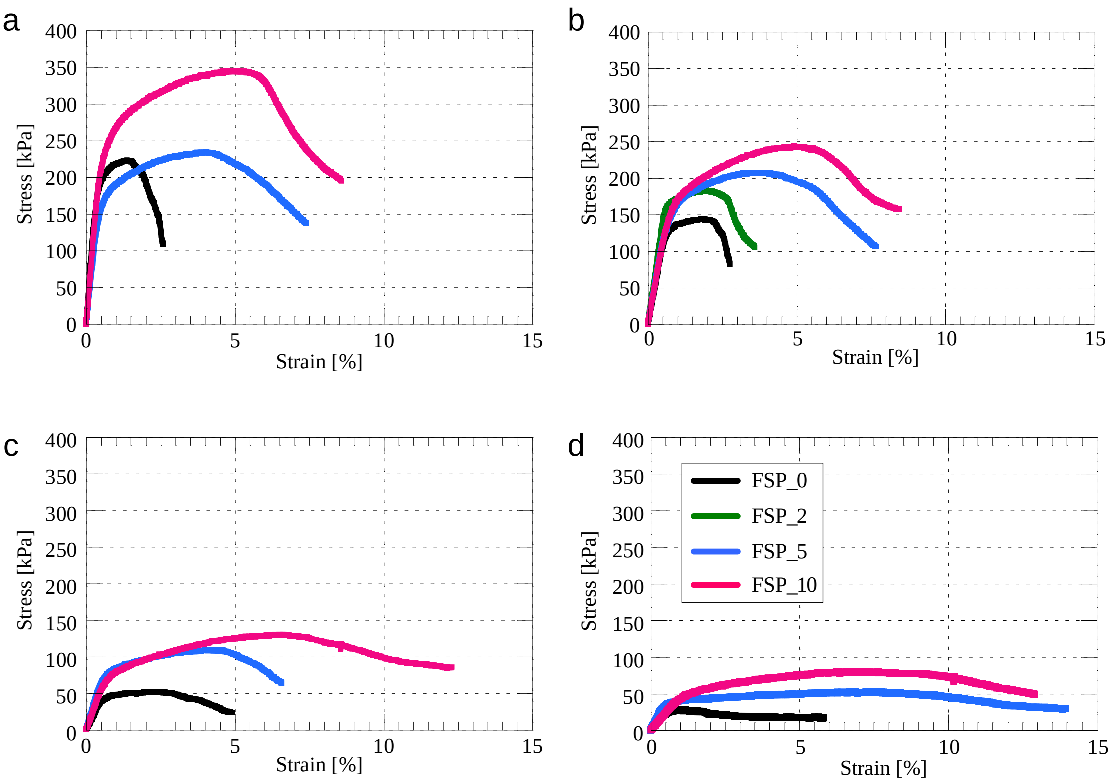


**Figure 4.18: Stress-strain relationship: (a) *w*100 - C10, (b) *w*100 - C8, (c) *w*100 - C5 and (d) *w*200 - C20.**

According to Public Works Research Institute, (2008) the cone index $q_c$ is an index used to classify the quality of treated construction sludge when it is used as a soil material. If the cone Index $q_c$ is greater than 200 kPa, the soil is classified as Type 4 construction generated soil that can be used for embankment with appropriate soil improvement. If it is greater than 400 kPa, it is classified as Type 3 construction generated soil that can be used for road embankment. It is found from **Figure 4.17** and the above classification criteria that a uniaxial compressive strength of $q_u$ greater than 21.5 kPa is applicable to Class 4 construction waste soil, while a value greater than 43.1 kPa is applicable to Class 3 construction waste soil. From **Figure 4.13**, when the water content of the clay is small, as in *w*40 and *w*60, it can be classified as Class 4 construction waste soil or higher at a 10% addition amount. In the case of *w*100 where the water content of the clay is high, although 50% amount of FSP is added to the clay, cone index is 114.8 kPa which is apart from the Class 4 construction soil. Extremely much amount of FSP must be required for satisfying the reuse condition, so that using only FSP is unrealistic for reusing muddy soils with water content over 100% at actual sites.

### 4.4.2 Uniaxial compressive strength of clay treated with FSP and cement

**Figure 4.18** shows the relationship between uniaxial compressive stress and strain. Most cases show a peak stress followed by softening behavior. It is found from **Figure 4.18** that there is a correlation between the addition rate of standard FSP and uniaxial compressive strength. Compared at the same amount of FSP, the peak stress tends to be more distinct as the amount of cement is increased.

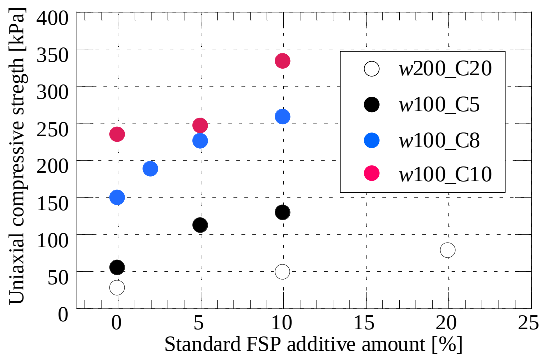


**Figure 4.19: Effect of standard FSP amount on UCS value**

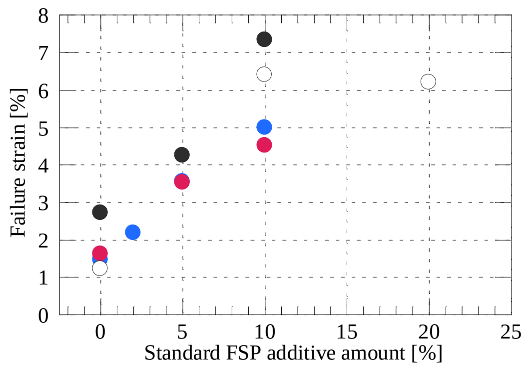


**Figure 4.20: Relationship between standard FSP amount and failure strain**

**Figure 4.19** shows the relationship between standard FSP addition rate and uniaxial compressive strength. At a given FSP addition, the compressive strength is increased as the amount of the cement is increased. Specifically, 10% cement addition provides an increase of compressive strength of around 150 to 200 kPa. On the other hand, at a given cement amount an incremental compressive strength is around 100 kPa from 0% to 10% of FSP addition. It is observed on **Figure 4.19** that the effect of standard FSP addition with cement on the uniaxial compressive strength. This figure illustrates that the utilization of FSP with cement increases the strength of treated soil compared to the clay treated by cement alone. The result suggests that the combination of FSP and cement can be an effective method for improving the strength of high-water content clay soil.

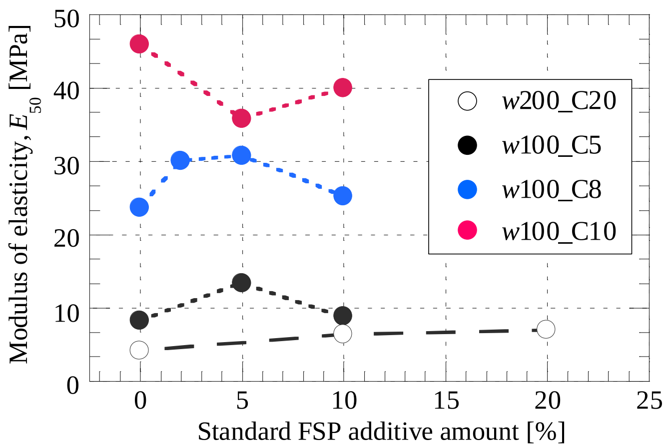


**Figure 4. 21: Effect of standard FSP amount on modulus of Elasticity $E_{50}$**

**Figure 4.20** shows the relationship between the addition rate of standard FSP and failure strain $\varepsilon_f$. At any amounts of cement addition, failure strain increases as the addition of standard FSP increases. The result suggests that the combination of FSP with cement makes the treated clay more persistent compared to the treated clay by only cement. **Figure 4.21** shows the relationship between the addition rate of standard FSP and the deformation coefficient $E_{50}$. It is observed that the stiffness increases with the cement addition rate. The relationship between standard FSP and stiffness is not unique, as there are cases where stiffness increases and decreases with increasing standard FSP addition rate. This indicates the optimum amount of FSP utilized in the mix should be monitored to achieve the highest strength of improved soil.

Considering the low environmental impact of ground improvement, the amount of cement addition should be reduced as much as possible. Even if the amount of cement addition is reduced, it would be useful if the strength of the treated clay can satisfy reusability criteria by adding FSP. In other words, it is necessary to investigate the mixing conditions of FSP with cement to ensure that the treated clay exhibits equivalent strength to the clay improved by only cement. For example, in **Figure 4.19**, the compressive strength for 8% cement and 5% FSP is similar to that for 10% cement and 0% FSP, and higher strength is observed for 8% cement and 5% FSP. Namely, 2% cement can be replaced with larger than 2% FSP because the compressive strength becomes larger compared to the clay treated by only cement. When 10% FSP fiber is used with cement the strength of treated soil increases by 10%. It is also certain that, from the approximate straight line of $w100$ - C8, 6.9% of standard FSP is determined as a sufficient value to show an equivalent strength to the treated soil by only cement. Although it is difficult to suggest the optimum mixing conditions of FSP and cement for ground improvement due to insufficient data so far, further experimental investigations of strength characteristics of treated clays with cement and FSP will make it possible to determine the optimum amount of FSP for ground improvement with reducing cement.

### 4.4.3 Energy analysis: energy principles and energy change analysis

Work is done on a point during deformation of sample due to uniaxial external force. Solid materials possess the capability to do work due to elastic deformation, indicating the storage of strain energy. However, once the deformation exceeds the elastic limit, a certain amount of the energy is dissipated through plastic deformation. This raises the question of whether the strain energy can be totally changed into useful work. If we disregard kinetic energy and some other forms of energy, it becomes evident from the fundamental principle that the total strain energy (w) generated is completely absorbed.

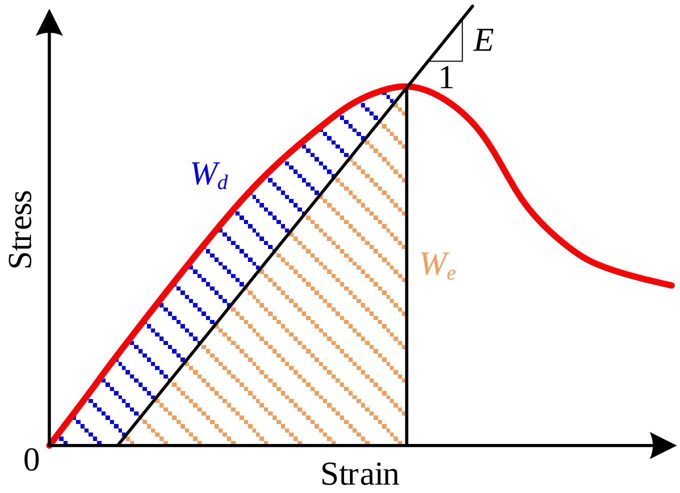


**Figure 4. 22: Energy distribution during UCS test of treated soil (Jiang et al., 2022)**

The work carried out by the testing machine on the treated UCS soil specimen can categorized into two parts: the elastic strain energy ($w_e$) stored within the UCS specimen, and the dissipation of energy ($w_d$) attributed to the formation of inner specimen cracks and the deformation distribution (Jiang et al., 2022).

The stress-strain curve energy analysis from the UCS test is used to calculate how much strain energy is stored within the material relative to the volume it occupies. The strain energy absorbed by the UCS specimen during loading corresponds to the area of stress stain curve up to peak stress as shown in **Figure 4.22** (Jiang et al., 2022). This characteristic is essential for understanding the material's structural behavior and its ability to withstand external forces.

The tendency and distribution of total strain energy density, elastic strain energy density and dissipative strain energy density are shown in **Figures 4.23** and **4.24**, which are calculated at various amounts of FSP and cement additive by equations from (4.6) to (4.9). It is better to analyze the proportion of the dissipated energy ($T$) which shows the improvement mechanism of FSP fiber and cement additive effect on clayey soil.

$$w = w_e + w_d \qquad \text{Eq. (4.6)}$$

$$w_e = \frac{(\varepsilon_f - 0.02 \times \varepsilon_f) \times \sigma_f}{2} \qquad \text{Eq. (4.7)}$$

$$w_d = 0.5 \times \frac{{\sigma_1}^2}{E} \qquad \text{Eq. (4.8)}$$

$$T = \frac{w_d}{w} \qquad \text{Eq. (4.9)}$$

Where,

w: Total strain energy [MPa]

$w_e$: Elastic strain energy [MPa]

$w_d$: The dissipation of energy [MPa]

$\varepsilon_f$: Failure strain [%]

$\sigma_f$: Failure stress [kPa]

$\sigma_1$: The principal stress value [kPa]

T: Proportion of dissipated energy

E: Youngs modulus [kPa], which is the slope of the straight-line section of the stress–strain curve of UCS test

It is observed from **Figure 4. 23** that the elastic, dissipative and total strain energy density increases as standard FSP increases from 10% to 50% for specimen prepared at 60%, 80% and 100% water content. Compared at similar FSP amounts, the strain energy density decreases as the moisture content increases, due to lower FSP fiber inter particle property. However, the specimen, prepared at 40% initial water content, has a different tendency. It shows that both elastic and total strain energy increases up to 10% FSP additive, while they decrease when higher amount of FSP utilized in the mix. For this case the dissipated strain energy increases with increasing FSP additive, which means that the plastic deformation such as crack propagation tends to be more significant, and the same tendency is observed as the water content is decreased.

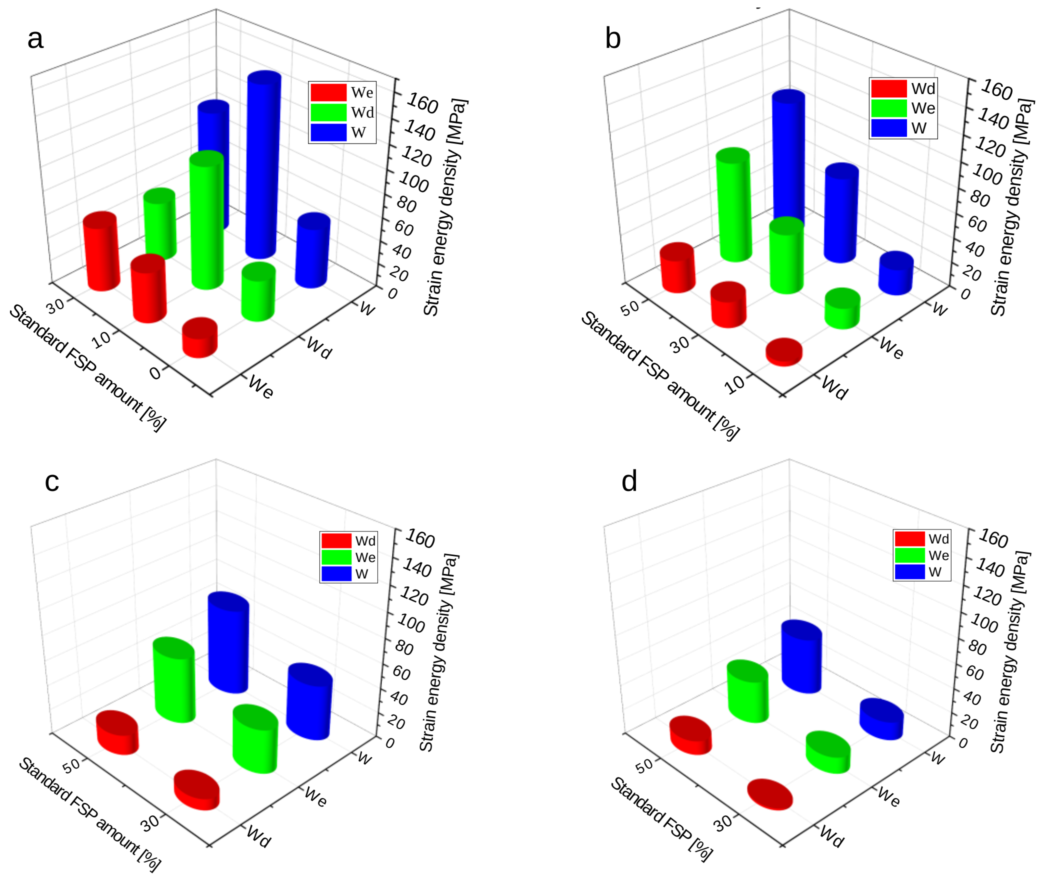


**Figure 4.23: Strain energy density concentration of standard FSP treated soil at initial water content of (a) 40%, (b) 60%, (c) 80% and (d) 100%.**

From **Figure 4.24** it can be observed that the addition of standard FSP enhances the dissipative, elastic, and total strain energy density of specimen made at 100% initial water content and different amount of cement. But the specimen without FSP additive at lower cement content have similar dissipative energy density. It might be due to the loading process effect on the inter particle rearrangement of UCS specimen from initial deformation to failure point. This characteristic leads to similar cracks, deformation distribution and energy loss tendency.

Upon careful examination and analysis, it becomes evident that incorporating an appropriate quantity of standard FSP fibers into cement can significantly boost the capacity to absorb energy, including both total and elastic strain density parameters. In the case of specimens created by mixing cement with clay, the treated soil exhibits pronounced brittleness, leading to the rapid development of internal cracks and a reduced ability to absorb energy.

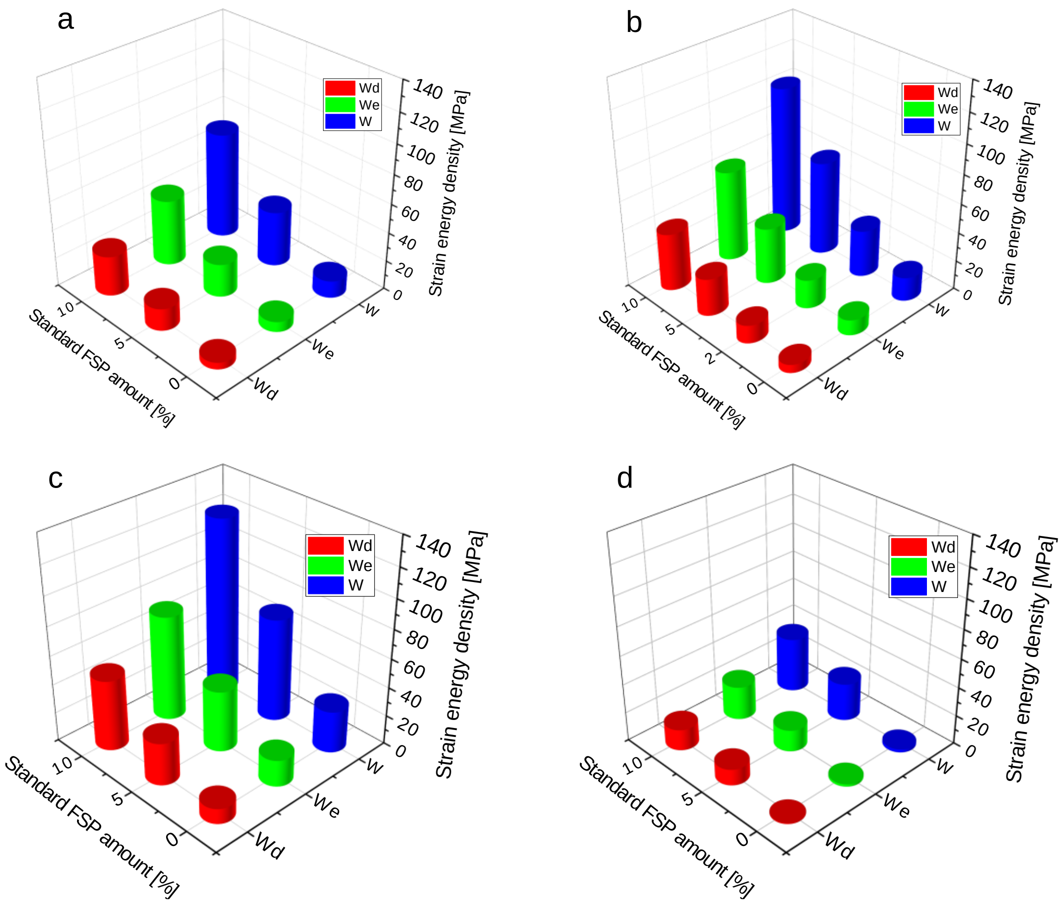


**Figure 4.24: Strain energy density concentration of soil treated with cement and standard FSP (a) *w*100_C5, (b) *w*100_C8, (c) *w*100_C10 and (d) *w*200_C20.**

When the amount of FSP fibers is increased, reaching the optimal content threshold (i.e., 10%), it fosters strong adhesion among the FSP fibers, cement, and clay soil. Under this condition, the FSP fiber addition gives the soil higher tensile strength, resulting in a noticeable enhancement in energy absorption, particularly in the specimens containing a water content of 40%. However, surpassing the optimum amount threshold of fibers results in an excessive distribution of FSP fibers in the specimen, leading to weak interparticle interaction among the fibers, cement, and soil that causes a certain portion of the specimens to exhibit weakened interfaces. When a certain external uniaxial load is applied, this weakened interface easily fails, due to the uneven concentration of stress, leading to the peeling and extraction of some fibers before the improved soil can withstand enough stress, and which indicates a reduction in absorbed energy.

From **Figure 4.25 (a)**, it is observed that the proportion of dissipative strain energy first decreases and then increases for the initial water content of 40% and vice versa for that of 60% in the sample preparation. When the amount of water used for the sample preparation is increased, the dissipative energy proportion is lower for similar amounts of FSP additive.

For the initial water content of 60% to 100%, the absorbed energy and deformation propagation increase due to higher plasticity up to 50% and more FSP fibers. This shows that the addition of FSP fibers improves the internal deformation and stress distribution of treated soil and, when energy is added, the plastic deformation becomes minimal, while the material tends to become more elastic when the reinforcing characteristics of the fibers are utilized sufficiently at the initial water content of 40%. However, a greater addition of FSP fibers (i.e., 30%) will lead to excessive fiber distribution and desaturation, as well as an uneven distribution of stress, which will decrease the effect of the improvement.

**Figure 4.25 (b)** shows that in the UCS test, the dissipative energy proportion of treated soil generally shows the tendency of first increasing and then decreasing, and the dissipative energy proportion is the lowest when the FSP fiber content is 0%, which are 0.35, 0.36, and 0.26 respectively for *w*100 C8_FSP, *w*100 C10_FSP and *w*200 C10_FSP test cases. In the other way the dissipative energy is lower at 10% FSP fiber of C5_FSP which have relatively lower pozzolanic properties.

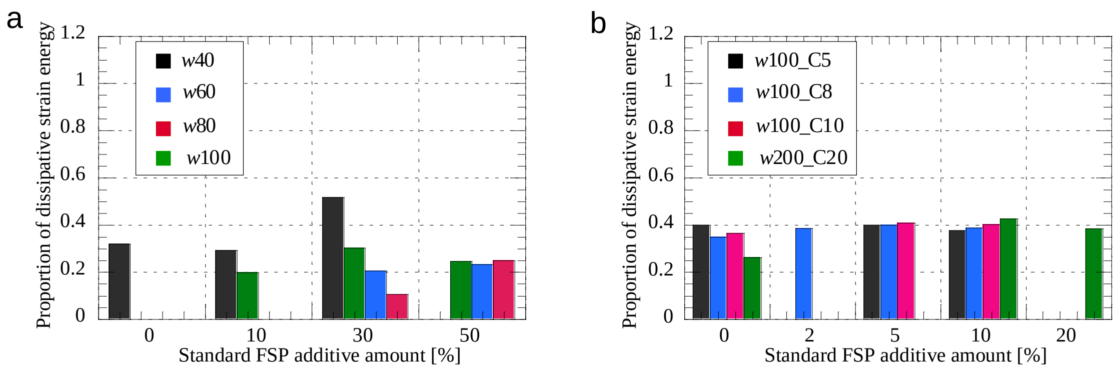


**Figure 4. 25: Proportion of dissipative strain energy: (a) standard FSP in the treated soil and (b) standard FSP and cement in the treated soil.**

When FSP fiber of 5% for 100% initial water content and 10% for 200% water content was added in the mix, the dissipated energy in the UCS test accounted for the largest proportion. which indicates that the internal cracks and damage propagation in the treated sample, as well as the phenomenon of stress concentration, were significant, and higher energy consumption at this stage. When a certain amount of FSP fiber is added, the proportion of dissipated energy gradually increases and decreases when the FSP fiber amount is reached at 10% and 20% for 100% and 200% initial water content of mix respectively. This shows that the addition of fiber improves the internal crack, deformation distribution and stress density of treated soil. The FSP fiber can adequately absorb the applied load energy and fully utilize its potential reinforcing characteristics. However, the subsequent addition of fibers will lead to excessive fiber distribution, agglomeration, uneven stress distribution and contact between fibers, which will reduce the treatment effect.

### 4.4.4 Mechanism of FSP and cement treated clay soil

While the standard FSP serves as a crucial reinforcement agent in this stabilization process, the interlocking network of the FSP fibers imparts tensile strength to the soil, effectively mitigating the problems of soil cracking and fissuring during drying and shrinking. This physical interaction not only reinforces the soil, but also contributes to its cohesion, preventing excessive water-induced erosion and instability observed in the test results of the specimens made at water contents of 40% to 200%. Cement, on the other hand, plays a pivotal role in binding the components of the mixture together as the cement particles coming into contact with the water, present in the clay soil and the mixture, a process called cement hydration, is initiated. This chemical reaction leads to the formation of cementitious compounds that act as a binder, connecting the soil particles and paper fibers, as shown in **Figure 4.26**. As the cement hydrates and solidifies, it creates a robust matrix within the soil, significantly enhancing its shear strength. Moreover, the hydration process itself serves to control the water content within the mixture, helping to regulate the moisture levels and minimize undesirable swelling and shrinking behaviors in the soil matrix.

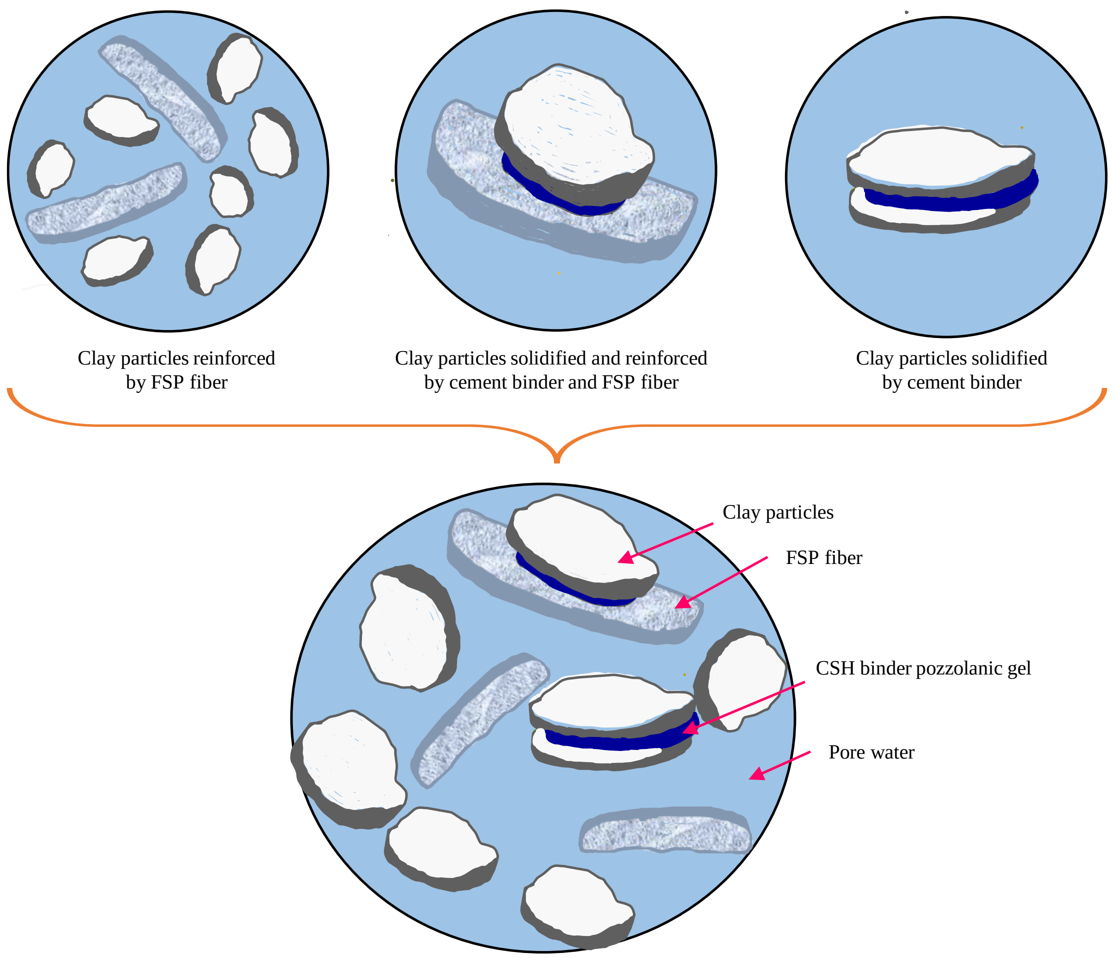


**Figure 4.26: Mechanism of cement and standard FSP treated soil with high water content.**

When standard FSP, that has a smaller particle size than the soil particle size, is utilized, the surface area is reduced. However, even if the surface area is reduced, the ratio of the surface area to volume is increased when standard FSP with a smaller particle size is used. This helps provide proper hydration and increases the solidification process which conveniently consumes the free water in between the particles over time. This combination not only helps with the dissociation and agglomerate formation of the clay particles and FSP fibers, but also decreases the brittleness of the mixture forming the non-plastic treated soil with proper moisture and resistance to uniaxial and tensile stress.

## 4.5 Conclusions

The purpose of this study was to investigate the additive effect of the original FSP, the standard FSP, and the combination of cement and the standard FSP on the mechanical properties of treated high-water-content clay soil. The following is a summary of the findings of this study.

(1) Standard FSP, which has a particle size of 178 μm, has the largest water absorption. Similarly, the water absorption of standard FSP with a particle size sieve of 90.5 μm, has the second largest water absorption. In both cases, the entangled structure of the fibers is large, which was observed from the SEM image, indicating that the entangled porous structure of the fibers contributed to higher water absorption.

(2) FSP can enhance the strength of treated clay at any level of water content. This is because of the aggregation of the soil and the interlocking effect of the fibers. However, with a very low water content, the strength and stiffness decrease due to insufficient water absorption by the FSP, such that some of the FSP remains in a dry and soft condition and its resistance is weak.

(3) When higher shear strength is the target for structures with heavier weights and impervious barriers, such as landfill liners, the utilization of the combined additive of standard FSP and cement is recommended. The addition of FSP alone is not enough to improve the strength, especially when the water content is very high, namely, over 100%. In such cases, the combination of FSP and cement is beneficial, because both additives will enhance the compressive strength to the desired level.

(4) Reducing the amount of cement and adding FSP is a good way to improve the ground with a low impact on the environment. This reduction in the cement content, by the inclusion of natural fibers, can lead to a lower carbon footprint that is associated with cement production. Cement production is known to be energy-intensive and releases a significant amount of carbon dioxide which has an immensely negative effect on the environment.

(5) The mechanisms for improving muddy clay soil are different between FSP and cement. FSP plays a reinforcing role that enhances the tensile strength and reduces cracking by absorbing excessive moisture between soil particles and creating a network of interconnected fibers within the soil matrix, while cement acts as a binder through hydration reactions, forming chemical bonds with the soil particles, leading to the creation of a more solid and cohesive matrix and increasing the compressive strength. The standard FSP and combination of FSP and cement represent a new treatment process. This process occurs when the mixing water dissociates calcium oxide which forms binding gel. This binding gel generates chemical reactions with clay alumina and clay silica through a hydration process that binds the soil particles together as well as binds the soil particles with the standard FSP fibers. This combination not only helps the dissociation and agglomerate formation with clay particles and FSP fibers, but also decreases the brittleness of the mixture by absorbing and reducing the apparent free water from the muddy clay soil that makes non-plastic improved soil which can resist uniaxial and tensile stress.

## References for Chapter 4


Abedi, M., Hassanshahi, O., Rashiddel, A., Ashtari, H., Seddik Meddah, M., Dias, D., Arjomand, M. A., & Keong Choong, K. (2023). A sustainable cementitious composite reinforced with natural fibers: An experimental and numerical study. *Construction and Building Materials*, *378*. https://doi.org/10.1016/j.conbuildmat.2023.131093

Abo El-Naga, I., Elsiragy, M. N., & Ragab, M. (2020). Utilization of synthetic reinforcement for enhancement of oil-contaminated subgrade soil in highway pavement. *Innovative Infrastructure Solutions*, *5*(2). https://doi.org/10.1007/s41062-020-00289-9

ACI Committee 230, S. Cement., & American Concrete Institute. (2009). *Report on soil cement (ACI 230.1R-09)*. American Concrete Institute.

Ahmad, F., Bateni, F., & Azmi, M. (2010). Performance evaluation of silty sand reinforced with fibres. *Geotextiles and Geomembranes*, *28*(1), 93–99. https://doi.org/10.1016/j.geotexmem.2009.09.017

Akbari, H. R., Sharafi, H., & Goodarzi, A. R. (2021). Effect of polypropylene fiber and nano-zeolite on stabilized soft soil under wet-dry cycles. *Geotextiles and Geomembranes*, *49*(6), 1470–1482. https://doi.org/10.1016/j.geotexmem.2021.06.001

Amar, M., Benzerzour, M., Kleib, J., & Abriak, N. E. (2021). From dredged sediment to supplementary cementitious material: characterization, treatment, and reuse. In *International Journal of Sediment Research* (Vol. 36, Issue 1, pp. 92–109). Elsevier B.V. https://doi.org/10.1016/j.ijsrc.2020.06.002

Arifin, Y. F. (2022). Tensile Strength and Durability of Oil Palm Empty Fruit Bunch Fiber in Soft Soil. *International Journal of Geomate*. https://doi.org/10.21660/2022.99.3610

Asai, Y., Ryunosuke, K., Sawamura, Y., & Makoto, K. (2021). Mechanical properties of clayey soil with fine shredded paper by the addition of cement. *Environmental Geotechnical Engineering Symposium*, *14*(September), 415–422.

Asim, M., Jawaid, M., Abdan, K., Ishak, M. R., & Alothman, O. Y. (2018). Effect of Hybridization on the Mechanical Properties of Pineapple Leaf Fiber/Kenaf Phenolic Hybrid Composites. *Journal of Renewable Materials*, *6*(1), 38–46. https://doi.org/10.7569/JRM.2017.634148

Babu, G. L. S., Srivastava, A., & Sivapulliah, P. V. (2011). Reliability analysis of strength of cement treated soils. *Georisk: Assessment and Management of Risk for Engineered Systems and Geohazards*, *5*(3–4), 157–162. https://doi.org/10.1080/17499518.2010.490116

Bo, M. W., Arulrajah, A., & Nikraz, H. (2007). Preloading and prefabricated vertical drains design for foreshore land reclamation projects: a case study. *Ground Improvement*, *11*, 67–76. https://api.semanticscholar.org/CorpusID:55080359

Cao, Z., Ma, Q., & Wang, H. (2019). Effect of Basalt Fiber Addition on Static-Dynamic Mechanical Behaviors and Microstructure of Stabilized Soil Compositing Cement and Fly Ash. *Advances in Civil Engineering*. https://doi.org/10.1155/2019/8214534

Çevikbilen, G., Merve Başar, H., Karadoğan, Ü., Teymur, B., Dağlı, S., & Tolun, L. (2020). *Assessment of the use of marine dredged materials in the sanitary landfills: A case study from the Marmara Sea Assessment of the use of dredged marine materials in sanitary landfills: a 1 case study from the Marmara Sea 2*.

Chaiyaput, S., Arwaedo, N., Kingnoi, N., Nghia-Nguyen, T., & Ayawanna, J. (2022). Effect of curing conditions on the strength of soil cement. *Case Studies in Construction Materials*, *16*. https://doi.org/10.1016/j.cscm.2022.e01082

Chan, C. M., & Abdul Jalil, A. N. (2014). Some insights to the reuse of dredged marine soils by admixing with activated steel slag. *Advances in Civil Engineering*, *2014*. https://doi.org/10.1155/2014/345134

Chian, S. C., & Bi, J. (2021). Influence of grain size gradation of sand impurities on strength behaviour of cement-treated clay. *Acta Geotechnica*, *16*(4), 1127–1145. https://doi.org/10.1007/s11440-020-01090-9

Chian, S. C., Chim, Y. Q., & Wong, J. W. (2017). Influence of sand impurities in cement-treated clays. *Geotechnique*, *67*(1), 31–41. https://doi.org/10.1680/jgeot.15.P.179

Chu, S. H., & Yao, J. J. (2020). A strength model for concrete made with marine dredged sediment. *Journal of Cleaner Production*, *274*. https://doi.org/10.1016/j.jclepro.2020.122673

Consoli, N. C., Vendruscolo, M. A., Fonini, A., & Rosa, F. D. (2009). Fiber Reinforcement Effects on Sand Considering a Wide Cementation Range. *Geotextiles and Geomembranes*. https://doi.org/10.1016/j.geotexmem.2008.11.005

Duong, N. T., Satomi, T., & Takahashi, H. (2021). Potential of corn husk fiber for reinforcing cemented soil with high water content. *Construction and Building Materials*, *271*. https://doi.org/10.1016/j.conbuildmat.2020.121848

Duong, T. N., Satomi, T., & Takahashi, H. (2019). *Mechanical Behavior Comparison of Cemented Sludge Reinforced by Waste Material and Several Crop Residues*.

Estabragh, A. R., Namdar, P., & Javadi, A. A. (2012). Behavior of Cement-Stabilized Clay Reinforced with Nylon Fiber. *Geosynthetics International*. https://doi.org/10.1680/gein.2012.19.1.85

Fard, H. S., König, D., & Goudarzy, M. (2022). SOIL-WATER CHARACTERISTICS CURVE OF FIBER REINFORCED SOILS. *Journal of Geo Engineering*, *17*(3), 153–163. https://doi.org/10.6310/jog.202209_17(3).4

Feng, D., Liang, B., He, X., Yi, F., Xue, J., Wan, Y., & Xue, Q. (2023). Mechanical properties of dredged soil reinforced by xanthan gum and fibers. *Journal of Rock Mechanics and Geotechnical Engineering*, *15*(8), 2147–2157. https://doi.org/10.1016/j.jrmge.2023.02.010

Flatt, R. J., Roussel, N., & Cheeseman, C. R. (2012). Concrete: An eco material that needs to be improved. *Journal of the European Ceramic Society*, *32*(11), 2787–2798. https://doi.org/10.1016/j.jeurceramsoc.2011.11.012

Fukushima, S., Kitajima, A., Ishiguro, K., Ikeda, Y., Sakamaki, K., & Tani, S. (2000). Applicability of cement-stabilized pond-mud soil as embankment material for irrigation pond dam repairment. *Journal of Japan Society of Civil Engineers* , *666*(in Japanese), 99–116.

Gao, Z., & Zhao, J. (2013). Evaluation on Failure of Fiber-Reinforced Sand. *Journal of Geotechnical and Geoenvironmental Engineering*. https://doi.org/10.1061/(asce)gt.1943-5606.0000737

García, G., José, R., Jiménez, A., Iván, V., Manteca, A., Encarnación, M., & Moreno, M. (2022). *RESOLUTION OF GEOTECHNICAL ENGINEERING PROBLEMS WITH PLAXIS 2D*.

Ghadir, P., & Ranjbar, N. (2018). Clayey Soil Stabilization Using Geopolymer and Portland Cement. *Construction and Building Materials*. https://doi.org/10.1016/j.conbuildmat.2018.07.207

Ghosh, S. K., Bhattacharyya, R., & Mondal, M. M. (2017). Potential Applications of Open Weave Jute Geotextile (Soil Saver) in Meeting Geotechnical Difficulties. *Procedia Engineering*, *200*, 200–205. https://doi.org/10.1016/j.proeng.2017.07.029

Gowthaman, S., Nakashima, K., & Kawasaki, S. (2018). A state-of-the-art review on soil reinforcement technology using natural plant fiber materials: Past findings, present trends and future directions. In *Materials* (Vol. 11, Issue 4). MDPI AG. https://doi.org/10.3390/ma11040553

Guo, Q., Zhan, L., Shen, Y., Wu, L., & Chen, Y. (2022). Classification and quantification of excavated soil and construction sludge: A case study in Wenzhou, China. *Frontiers of Structural and Civil Engineering*, *16*(2), 202–213. https://doi.org/10.1007/s11709-021-0795-8

Gupta, A., & Kumar, M. (2021). Clayey soil stabilization using flyash and jute fibre. *Materials Today: Proceedings*, *48*, 1205–1210. https://doi.org/10.1016/j.matpr.2021.08.246

Haakeel, M. S. S., Ramzi, M. Z. M., & Nasvi, M. C. M. (2019). Compressibility Behaviour of Peat Reinforced with Single and Multiple Deep Soil Mixing (DSM) Columns. *Engineer: Journal of the Institution of Engineers, Sri Lanka*, *52*(3), 1. https://doi.org/10.4038/engineer.v52i3.7360

Hassan, H. J. A., Rasul, J., & Samin, M. (2021). Effects of Plastic Waste Materials on Geotechnical Properties of Clayey Soil. *Transportation Infrastructure Geotechnology*, *8*(3), 390–413. https://doi.org/10.1007/s40515-020-00145-4

He, J., Shi, X. kang, Li, Z. xiang, Zhang, L., Feng, X. ying, & Zhou, L. rong. (2020). Strength properties of dredged soil at high water content treated with soda residue, carbide slag, and ground granulated blast furnace slag. *Construction and Building Materials*, *242*. https://doi.org/10.1016/j.conbuildmat.2020.118126

Hejazi, S. M., Sheikhzadeh, M., Abtahi, S. M., & Zadhoush, A. (2012). A simple review of soil reinforcement by using natural and synthetic fibers. In *Construction and Building Materials* (Vol. 30, pp. 100–116). https://doi.org/10.1016/j.conbuildmat.2011.11.045

Ho, L. S., Nakarai, K., Eguchi, K., & Ogawa, Y. (2020). Difference in strength development between cement-treated sand and mortar with various cement types and curing temperatures. *Materials*, *13*(21), 1–15. https://doi.org/10.3390/ma13214999

Hoang, N. H., Ishigaki, T., Kubota, R., Tong, T. K., Nguyen, T. T., Nguyen, H. G., Yamada, M., & Kawamoto, K. (2020). Waste generation, composition, and handling in building-related construction and demolition in Hanoi, Vietnam. *Waste Management*, *117*, 32–41. https://doi.org/10.1016/j.wasman.2020.08.006

Hossen, Md. F., Hamdan, S., Rahman, Md. R., Rahman, Md. M., Liew, F. K., & Lai, J. C. (2015). Effect of fiber treatment and nanoclay on the tensile properties of jute fiber reinforced polyethylene/clay nanocomposites. *Fibers and Polymers*, *16*(2), 479–485. https://doi.org/10.1007/s12221-015-0479-x

Hu, Q. M., Huang, Y. X., Zhang, W. Y., Shao, G. T., Xu, Y., Zhang, Y. H., Pan, Y., & Mi, J. X. (2023). Industrial-scale extraction of high value-added kaolin from excavation waste: Demonstration from Xiamen, China. *Waste Management*, *163*, 144–153. https://doi.org/10.1016/j.wasman.2023.03.028

Huayang, L., Yinggang, X., Xin, L., Mingjing, J., & Liangzhi, L. (2019). Effect of Polyacrylamide on Improvement of Dredger Fill with Vacuum Preloading Method. *Journal of Materials in Civil Engineering*, *31*(9), 04019193. https://doi.org/10.1061/(ASCE)MT.1943-5533.0002860

Ibrahim, I. D., Jamiru, T., Sadiku, E. R., Kupolati, W. K., & Agwuncha, S. C. (2016). Impact of Surface Modification and Nanoparticle on Sisal Fiber Reinforced Polypropylene Nanocomposites. *Journal of Nanotechnology*, *2016*. https://doi.org/10.1155/2016/4235975

Jan, O. Q., & Mir, B. A. (2018). Strength Behaviour of Cement Stabilised Dredged Soil. *International Journal of Geosynthetics and Ground Engineering*, *4*(2). https://doi.org/10.1007/s40891-018-0133-y

Javadian, A. A., Wielopolski, M. B., Smith, I. F. C., Hebel, D. E., Javadian, A., Wielopolski, M., Smith, I. F. C., & Hebel, D. E. (2016). *Bond-behavior study of newly developed bamboo-composite 4 reinforcement in concrete*.

Jiang, P., Chen, L., Li, N., Qian, J., & Wang, W. (2022). Study on the mechanical properties of fiber-modified iron tailings stabilized by lime and fly ash based on energy analysis. *Case Studies in Construction Materials*, *17*. https://doi.org/10.1016/j.cscm.2022.e01638

Jing, P., Song, X., Zhang, J., & Nowamooz, H. (2022). A review of hydro-mechanical coupling behaviour of cement-treated materials. In *Construction and Building Materials* (Vol. 322). Elsevier Ltd. https://doi.org/10.1016/j.conbuildmat.2022.126446

John, E., & Lothenbach, B. (2023). Cement hydration mechanisms through time – a review. In *Journal of Materials Science* (Vol. 58, Issue 24, pp. 9805–9833). Springer. https://doi.org/10.1007/s10853-023-08651-9

Kamaruddin, F. A., Nahazanan, H., Huat, B. K., & Anggraini, V. (2020). Improvement of marine clay soil using lime and alkaline activation stabilized with inclusion of treated coir fibre. *Applied Sciences (Switzerland)*, *10*(6). https://doi.org/10.3390/app10062129

Kampala, A., Jitsangiam, P., Pimraksa, K., & Chindaprasirt, P. (2021). An investigation of sulfate effects on compaction characteristics and strength development of cement-treated sulfate bearing clay subgrade. *Road Materials and Pavement Design*, *22*(10), 2396–2409. https://doi.org/10.1080/14680629.2020.1753564

Kanayama, M., & Kawamura, S. (2019). Effect of Waste Bamboo Fiber Addition on Mechanical Properties of Soil. *Open Journal of Civil Engineering*, *09*(03), 173–184. https://doi.org/10.4236/ojce.2019.93012

Kasama, K., Zen, K., & Kiyoharu, I. (2007). High-strengthening of cement -treated clay by mechanical dehydration. In *SOILS AND FOUNDATIONS* (Vol. 47, Issue 2).

Khodabandeh, M. A., Nagy, G., & Török, Á. (2023). Stabilization of collapsible soils with nanomaterials, fibers, polymers, industrial waste, and microbes: Current trends. In *Construction and Building Materials* (Vol. 368). Elsevier Ltd. https://doi.org/10.1016/j.conbuildmat.2023.130463

Kida, S., Sawamura, Y., Yano, T., & Kimura, M. (2018). *Changes in strength and transportability of high water content mud treated by fine powder made from waste paper*.

Kitazume, M. , & T. M. (2013). The Deep Mixing Method (1st ed.). In *The Deep Mixing Method (1st ed.)*. CRC Press.

Kodicherla, S. P. K., & Nandyala, D. K. (2019). Influence of randomly mixed coir fibres and fly ash on stabilization of clayey subgrade. *International Journal of Geo-Engineering*, *10*(1). https://doi.org/10.1186/s40703-019-0099-1

Koga, C., Kenichi, S., & Fujikawa, T. (2016). Examination of the Utilization of the Bamboo in the Soft Ground Improvement. *Journal of the Society of Materials Science*, *65*(1), 16–21.

Koike, K., Nakazaki, K., Miyoshi, M., Nishijima, T., Matsumoto, K., Yamaguchi, F., & Todoroki, K. (2004). In-situ test of vacuum consolidation method for the densification of fine-grained dredging material (Vol.1). *Proceedings of 58th Japan National Conference on Geotechnical Engineering*, *478*(In Japanese), 955–956.

Kumar, A., Walia, B. S., & Mohan, J. (2006). Compressive strength of fiber reinforced highly compressible clay. *Construction and Building Materials*, *20*(10), 1063–1068. https://doi.org/10.1016/j.conbuildmat.2005.02.027

Kutter, B. L. (1992). *Dynamic Centrifuge Modeling of Geotechnical Structures*.

Lang, L., Chen, B., & Chen, B. (2021). Strength evolutions of varying water content-dredged sludge stabilized with alkali-activated ground granulated blast-furnace slag. *Construction and Building Materials*, *275*. https://doi.org/10.1016/j.conbuildmat.2020.122111

Lang, L., Chen, B., & Duan, H. (2021). Modification of nanoparticles for the strength enhancing of cement-stabilized dredged sludge. *Journal of Rock Mechanics and Geotechnical Engineering*, *13*(3), 694–704. https://doi.org/10.1016/j.jrmge.2021.01.006

Lee, J. Y., An, J., & Chua, C. K. (2017). Fundamentals and applications of 3D printing for novel materials. In *Applied Materials Today* (Vol. 7, pp. 120–133). Elsevier Ltd. https://doi.org/10.1016/j.apmt.2017.02.004

Li, J. S., Chen, X., Lang, L., He, X. X., & Xue, Q. (2023a). Evaluation of natural and artificial fiber reinforcements on the mechanical properties of cement-stabilized dredged sediment. *Soils and Foundations*, *63*(3). https://doi.org/10.1016/j.sandf.2023.101319

Li, J. S., Chen, X., Lang, L., He, X. X., & Xue, Q. (2023b). Evaluation of natural and artificial fiber reinforcements on the mechanical properties of cement-stabilized dredged sediment. *Soils and Foundations*, *63*(3). https://doi.org/10.1016/j.sandf.2023.101319

Li, J., Tang, C., Wang, D., Pei, X., & Shi, B. (2014). Effect of discrete fibre reinforcement on soil tensile strength. *Journal of Rock Mechanics and Geotechnical Engineering*, *6*(2), 133–137. https://doi.org/10.1016/j.jrmge.2014.01.003

Lirer, S., Liguori, B., Capasso, I., Flora, A., & Caputo, D. (2017). Mechanical and chemical properties of composite materials made of dredged sediments in a fly-ash based geopolymer. *Journal of Environmental Management*, *191*, 1–7. https://doi.org/10.1016/j.jenvman.2017.01.001

Liu, H., Lin, P., & Wang, J. (2023). Machine Learning Approaches to Estimation of the Compressibility of Soft Soils. *Frontiers in Earth Science*. https://doi.org/10.3389/feart.2023.1147825

Liu, L., Zhou, A., Deng, Y., Cui, Y., Yu, Z., & Yu, C. (2019). Strength performance of cement/slag-based stabilized soft clays. *Construction and Building Materials*, *211*, 909–918. https://doi.org/10.1016/j.conbuildmat.2019.03.256

Liu, Y., He, L. Q., Jiang, Y. J., Sun, M. M., Chen, E. J., & Lee, F. H. (2019). Effect of in situ water content variation on the spatial variation of strength of deep cement-mixed clay. *Geotechnique*, *69*(5), 391–405. https://doi.org/10.1680/jgeot.17.P.149

Liu, Y., Lu, H., Liu, M., Cai, L., Wei, N., & Liu, Y. (2022). Microanalytical characterizations, mechanical strength and water resistance performance of solidified dredged sludge with industrial solid waste and architecture residue soil. *Case Studies in Construction Materials*, *17*. https://doi.org/10.1016/j.cscm.2022.e01492

Ma, C., Chen, B., & Chen, L. (2018). Experimental feasibility research on a high-efficiency cement-based clay stabilizer. *KSCE Journal of Civil Engineering*, *22*(1), 62–72. https://doi.org/10.1007/s12205-017-0782-8

Medvey, B., & Dobszay, G. (2020). Durability of Stabilized Earthen Constructions: A Review. In *Geotechnical and Geological Engineering* (Vol. 38, Issue 3, pp. 2403–2425). Springer. https://doi.org/10.1007/s10706-020-01208-6

Ministry of Land, I. T. and T. [MLIT]. (2017). *Part I National Land and Transportation Administration for Dramatically Changing Lifestyles: Aiming for a Society where Everyone Can Shine*.

Miyazaki, Y., Tang, Y. X., Ochiai, H., Yasufuku, N., Omine, K., & Tsuchida, T. (2003). Utilization of cement treated dredged soil with working ship. *Journal of Japan Society of Civil Engineers* , *750*(in Japanese), 193–204.

MLIT. (2020, January). Results of the survey on Construction By-Products in FY 2018 (in Japanese) Ministry of Land, Infrastructure, Transport and Tourism (2020) Results of the Survey On Construction By-Products in FY2018 (in Japanese). *MLIT*. https://www.mlit.go.jp/report/press/sogo03_hh_000233.html

Mu, C., Shen, S., Arulrajah, A., Wu, H.-N., & Hou, D. (2015). Laboratory Evaluation on the Effectiveness of Polypropylene Fibers on the Strength of Fiber-Reinforced and Cement-Stabilized Shanghai Soft Clay. *Geotextiles and Geomembranes*. https://doi.org/10.1016/j.geotexmem.2015.05.004

Nadeem, M., Ullah, S., Chen, S., Alkahtani, M. Q., Khan, M. A., Salih, R., Jian, L., Mursaleen, M., Islam, S., & Ahmad, J. (2023). Evaluation of engineering properties of clayey sand bio-mediated with terrazyme enzyme. *Frontiers in Materials*, *10*. https://doi.org/10.3389/fmats.2023.1195310

Nazir, M. H., Al-Marzouqi, A. H., Ahmed, W., & Zaneldin, E. (2023). The potential of adopting natural fibers reinforcements for fused deposition modeling: Characterization and implications. In *Heliyon* (Vol. 9, Issue 4). Elsevier Ltd. https://doi.org/10.1016/j.heliyon.2023.e15023

Nguyen, B. T. T., Takeyama, T., & Kitazume, M. (2015). Numerical analyses on the failure of deep mixing columns reinforced by a shallow mixing layer. *15th Asian Regional Conference on Soil Mechanics and Geotechnical Engineering, ARC 2015: New Innovations and Sustainability*, 2144–2148. https://doi.org/10.3208/jgssp.VNM-01

Onyekwena, C. C., Xue, Q., Li, Q., Umeobi, H. I., Ghaffar, A., & Fasihnikoutalab, M. H. (2023). Advances in the carbonation of MgO-based binder and CO2 utilization in the construction industry. In *Clean Technologies and Environmental Policy* (Vol. 25, Issue 6, pp. 1763–1782). Springer Science and Business Media Deutschland GmbH.

https://doi.org/10.1007/s10098-023-02482-7

Paula Furlan, A., Razakamanantsoa, A., Ranaivomanana, H., Levacher, D., & Katsumi, T. (2018). Shear strength performance of marine sediments stabilized using cement, lime and fly ash. *Construction and Building Materials*, *184*, 454–463. https://doi.org/10.1016/j.conbuildmat.2018.06.231ï

Phan Thanh, C., Tomoaki, S., & Hiroshi TAKAHASHI. (2018). Study on Strength Characteristics of Rice Straw Fiber-Cement-Reinforced Sludge. *Int. J. Soc. Mater. Eng. Resource*, *23*(2), 147–151.

Phan Thanh Chien, B. (2019). *Study on Mechanical Properties of Rice by-Products-Cement-Reinforced Sludge as Banking Materials.*

*PLAXIS 3D Tutorial Manual*. (2016).

Public Works Research Institute. (2008). *Construction Sludge Recycling Manual.*

Puspita, N., & Capri, A. (2020). The effectiveness of vacuum consolidation to soft soil settlement. *International Journal on Advanced Science, Engineering and Information Technology*, *10*(4), 1610–1616. https://doi.org/10.18517/ijaseit.10.4.3943

Rachman, R. M., Ngii, E., & Sriyani, R. (2021). Effect of using Portland cement and tras soil to stabilize and solidify mercury-contaminated tailings in small-scale gold mining. *IOP Conference Series: Earth and Environmental Science*, *871*(1). https://doi.org/10.1088/1755-1315/871/1/012026

Sarasini, F., Luzi, F., Dominici, F., Maffei, G., Iannone, A., Zuorro, A., Lavecchia, R., Torre, L., Carbonell-Verdu, A., Balart, R., & Puglia, D. (2018). Effect of different compatibilizers on sustainable composites based on a PHBV/PBAT matrix filled with coffee silverskin. *Polymers*, *10*(11). https://doi.org/10.3390/polym10111256

Sawamura, Y., Yano, T., & Kimura, M. (2017). Property variation of high moisture sludge by fine powder mainly composed of Cellulose. *Environmental Geotechnical Engineering Symposium*, *12*(September), 505–510.

Sena Da Fonseca, B., Vilão, A., Galhano, C., & Simão, J. A. R. (2014). Reusing coffee waste in manufacture of ceramics for construction. *Advances in Applied Ceramics*, *113*(3), 159–166. https://doi.org/10.1179/1743676113Y.0000000131

Shi, W., Chen, Q., Nimbalkar, S., & Liu, W. (2017). A new mixing technique for solidifier and dredged fill in coastal area. *Marine Georesources & Geotechnology*, *35*(1), 52–61. https://doi.org/10.1080/1064119X.2015.1102183

Shinsha, H., & Kumagai, T. (2018). Material properties of solidified soil grains produced from dredged marine clay. *Soils and Foundations*, *58*(3), 678–688. https://doi.org/10.1016/j.sandf.2018.03.003

Sugimura, Y., Okada, T., Kuwae, T., Mito, Y., Naito, R., & Nakagawa, Y. (2022). New possibilities for climate change countermeasures in ports: Organic carbon containment and creation of blue carbon ecosystems through beneficial utilization of dredged soil. *Marine Policy*, *141*. https://doi.org/10.1016/j.marpol.2022.105072

Takahashi, H., Mori, M., Shibata, S., & Sasaki, K. (2006). Urgent countermeasure construction for imogawa river channel blockage by fiber-cement-stabilized method. Proceedings of 3rd symposium on sediment disasters. *Proceedings of 3rd Symposium on Sediment Disasters*, *in Japanese*, 1–6.

Takeyama, K., Hamatani, S., Kashima, F., Wakuri, N., Yamauchi, H., Iwamoto, H., & Ukai, A. (2017). Environmental improvement technology utilizing modified soil using paper sludge ash and dredged soil. *Journal of Japan Society of Civil Engineers, Ser. B3 (Ocean Engineering)*, *73 (2)*(in Japanese), 947–952.

Tang, C., Shi, B., & Zhao, L. (2010). Interfacial Shear Strength of Fiber Reinforced Soil. *Geotextiles and Geomembranes*. https://doi.org/10.1016/j.geotexmem.2009.10.001

Tiwari, N., Satyam, N., & Patva, J. (2020). Engineering Characteristics and Performance of Polypropylene Fibre and Silica Fume Treated Expansive Soil Subgrade. *International Journal of Geosynthetics and Ground Engineering*, *6*(2). https://doi.org/10.1007/s40891-020-00199-x

Vidal, H. (1969). *The principle of reinforced earth*.

Vinoth, G., Moon, S. W., Moon, J., & Ku, T. (2018). Early strength development in cement-treated sand using low-carbon rapid-hardening cements. *Soils and Foundations*, *58*(5), 1200–1211. https://doi.org/10.1016/j.sandf.2018.07.001

Vu, N. B., Do, M. N., Thi, N. N., & Ho, L. S. (2022). Effects of additives on the results of improving peat soil: A case study at Mekong delta in Vietnam. *Journal of Applied Science and Engineering (Taiwan)*, *25*(5), 799–807. https://doi.org/10.6180/jase.202210_25(5).0011

Vu, T. B., Dang, V. Q., Ngo, Q. A., & Ho, L. S. (2023). Influence of some factors on the mechanical properties of cement-treated clay for shallow mixing in Vietnam: A comparative study. *Results in Engineering*, *17*. https://doi.org/10.1016/j.rineng.2023.101011

Wang, D., Xiao, J., & Gao, X. (2019). Strength gain and microstructure of carbonated reactive MgO-fly ash solidified sludge from East Lake, China. *Engineering Geology*, *251*, 37–47. https://doi.org/10.1016/j.enggeo.2019.02.012

Wang, J., Cai, Y., Fu, H., Hu, X., Cai, Y., Lin, H., & Zheng, W. (2018). Experimental study on a dredged fill ground improved by a two-stage vacuum preloading method. *Soils and Foundations*, *58*(3), 766–775. https://doi.org/10.1016/j.sandf.2018.02.028

Wang, R., Tang, C. S., Pan, X. H., Wang, D. L., Dong, Z. H., & Shi, B. (2023). Stabilization of dredged sludge using bio-carbonation of reactive magnesia cement method. *Acta Geotechnica*, *18*(3), 1529–1541. https://doi.org/10.1007/s11440-022-01683-6

Wang, X., Cheng, D., Huang, X., Song, L., Gu, W., Liang, X., Li, Y., & Xu, B. (2020). Effect of high-temperature saturated steam treatment on the physical, chemical, and mechanical properties of moso bamboo. *Journal of Wood Science*, *66*(1). https://doi.org/10.1186/s10086-020-01899-8

Wassermann, A., Abdallah, A., & Cuisinier, O. (2022). Impact of wetting and drying cycles on the mechanical behaviour of a cement-treated soil. *Transportation Geotechnics*, *36*. https://doi.org/10.1016/j.trgeo.2022.100804

Wu, J., Liu, L., Deng, Y., Zhang, G., Zhou, A., & Xiao, H. (2022). Use of recycled gypsum in the cement-based stabilization of very soft clays and its micro-mechanism. *Journal of Rock Mechanics and Geotechnical Engineering*, *14*(3), 909–921. https://doi.org/10.1016/j.jrmge.2021.10.002

Wu, Y., Li, Y., & Niu, B. (2014). Assessment of the mechanical properties of sisal fiber-reinforced silty clay using triaxial shear tests. *The Scientific World Journal*, *2014*. https://doi.org/10.1155/2014/436231

Xiaoyuan, W., Pengju, H., Xiaohong, B., & Xiangyu, L. (2019). Influences of slag on properties of lightweight cement-treated soils subjected to sulfate corrosion. *Construction and Building Materials*,*205*, 511–518. https://doi.org/10.1016/j.conbuildmat.2019.02.043

Xu, G., Han, Q., Geng, W., Yin, J., & Liu, L. (2023). Evaluation of fiber reinforcement on the strength behaviors of dredging slurry cemented at high water content. *Soils and Foundations*, *63*(1). https://doi.org/10.1016/j.sandf.2022.101264

Yamashita, E., Aristo Cikmit, A., Tsuchida, T., & Hashimoto, R. (2020). Strength estimation of cement-treated marine clay with wide ranges of sand and initial water contents. *Soils and Foundations*, *60*(5), 1065–1083. https://doi.org/10.1016/j.sandf.2020.05.002

Yang, Q., & Du, C. (2021). Experimental Study on the Effect of Plant Ash on Soft Clay Stabilized with Cement-Based Composites. *Geotechnical and Geological Engineering*, *39*(1), 105–117. https://doi.org/10.1007/s10706-020-01476-2

Yin, J., Han, W., Xu, G., Hu, M., & Miao, Y. (2019). Effect of Salinity on Strength Behavior of Cement-treated Dredged Clay at High Initial Water Contents. *KSCE Journal of Civil Engineering*, *23*(10), 4288–4296. https://doi.org/10.1007/s12205-019-0695-9

Yohanna, P., Johnson, P., Victor, B. P., Badamasi, A., Mije, F. G., Ako, T., & Bassey Bassey, A. (2022). Evaluation of Geotechnical Properties of Black Cotton Soil Reinforced with Sisal Fibre for Waste Containment Application. *Engineering Science & Technology*, 151–168. https://doi.org/10.37256/est.3220221354

Zaini, M. S. I., Hasan, M., Yie, L. S., Masri, K. A., Jaya, R. P., Hyodo, M., & Winter, M. J. (2021). The Effect of Utilizing Silica Fume and Eggshell Ash on the Geotechnical Properties of Soft Kaolin Clay. *Journal Technology*. https://doi.org/10.11113/jurnalteknologi.v84.17115

Zeng, L. L., Bian, X., Zhao, L., Wang, Y. J., & Hong, Z. S. (2021). Effect of phosphogypsum on physiochemical and mechanical behavior of cement stabilized dredged soil from Fuzhou, China. *Geomechanics for Energy and the Environment*, *25*. https://doi.org/10.1016/j.gete.2020.100195

Zhang, J., Deng, A., & Jaksa, M. (2021). Enhancing mechanical behavior of micaceous soil with jute fibers and lime additives. *Journal of Rock Mechanics and Geotechnical Engineering*, *13*(5), 1093–1100. https://doi.org/10.1016/j.jrmge.2021.04.008

Zhang, M., Na, M., Yang, Z., Shi, Y., Guerrieri, M., & Pan, Z. (2022). Study on mechanical properties and solidification mechanism of stabilized dredged materials with recycled GFRP fibre reinforced geopolymer. *Case Studies in Construction Materials*, *17*. https://doi.org/10.1016/j.cscm.2022.e01187

Zhang, Y., Ong, Y. J., & Yi, Y. (2022). Comparison between CaO- and MgO-activated ground granulated blast-furnace slag (GGBS) for stabilization/solidification of Zn-contaminated clay slurry. Chemosphere, 286. https://doi.org/10.1016/j.chemosphere.2021.131860

Zhu, W., Chiu, C. F., Zhang, C. L., & Zeng, K. L. (2009). Effect of humic acid on the behaviour of solidified dredged material. *Canadian Geotechnical Journal*, *46*(9), 1093–1099. https://doi.org/10.1139/T09-045

## Chapter 5

## Numerical analysis on the road performance constructed on soft soil treated with finely shredded paper and cement.

### 5.1 Introduction

Nowadays the need for various kinds of infrastructure like roads and railways is increasing. However, the shortage of strong and suitable ground is the main challenge for such kind projects in different parts of the world. To counterbalance this problem, embankments are constructed on top of soft ground to provide better ground supports for roads and railways infrastructures. The use of soft ground as foundation layer below the embankment and other surface structure has various problems due to its low bearing capacity, insufficient shear strength and higher deformation characteristics. In addition, the unavailability of the required embankment fill materials in the vicinity of the project site. Therefore, it's crucial to employ appropriate ground improvement methods to guarantee the stability of embankments and surface structures by enhancing the engineering properties of soft soils throughout both the construction phase and their long-term usage. This method can solve the shortage of selected fill materials near the construction site.

Various methods have been developed and studied to address the challenges associated with soft soil ground formation. One of method is the use of preloading and prefabricated vertical drains (PVDs) which has been found to be highly effective in improving soft clay ground under land reclamation projects (Bo et al., 2007; Griffin & O'Kelly, 2014; Hambirao & Rakaraddi, 2014; Indraratna et al., 2013; Liu et al., 2008; Pham et al., 2022). To achieve uniform settlement of the soft ground by accelerating the consolidation process of soft, saturated soils, vacuum consolidation has been found effective which is crucial for avoiding construction failures and rising maintenance expenses (Puspita & Capri, 2020) . Replacing the existing soft ground with high shear strength and bearing capacity selected soil after the in-situ soil up to required extent, construction of embankment in stages with proper consolidation time and improving soft ground underneath embankment by chemical treatment (Nguyen et al., 2015). Where deep soil mixing (DSM) is a widely used chemical stabilization method for ground improvement in soft clay soil which increases the strength and reduces the compressibility of in situ foundation soil (Haakeel et al., 2019).

There are several additives commonly used for the treatment of soft soils. The most common one is cement additives which are used for improvement of soft soils. The cement can be mixed with soft soils which creates a hardened matrix to increase strength, reduce plasticity and enhance durability that improves the soft soil by altering its chemical properties. Cement stabilization techniques have also been studied extensively and found to be dependent on factors such as mineralogy, environmental conditions, curing period, and initial clay water content (Babu et al., 2011). In spite of stiffer soil matrix and higher strength, cement treated soil will increase brittleness, reduce sorption capacity and at some point, ductility of construction during static and cyclic loading (Ma et al., 2018; Wassermann et al., 2022).

To mitigate this adverse effect, different fibers were introduced for reinforcement in combination with cement (Duan & Zhang, 2019; Estabragh et al., 2012; Li et al., 2019; L. Mei et al., 2022; Wang et al., 2020; Yang et al., 2022). The incorporation of waste fibers, such as cornsilk fibers, into cement treated soil has been studied for enhancing the mechanical behavior of the soil (Tran et al., 2018). Similarly, the addition of sewage sludge ash, geopolymer, fly ash into cement has treated soil been investigated for the treatment of soft subgrade soil, leading to improved cohesion and shear strength of the treated soil (Chen & Lin, 2009; Ghadir & Ranjbar, 2018; Radwan et al., 2021).

The reinforcement of cemented soil with fibers, such as polyvinyl alcohol fiber, has been found to effectively improve compressive and splitting strength, contributing to the overall stiffer mechanical properties of the treated soil (Zhao & You, 2020) However, the natural fibers were preferable for the economical, sustainable, and ecofriendly treatment process that reduce environmental burdens (Duong et al., 2021).

The natural fibers (i.e., coconut fiber, sisal fiber, palm fiber, jute fiber, coir fiber, bamboo fiber, etc.). The corn husk fiber used to reinforce by Duong et al. (2021) cemented soil with high water content that the fiber inclusion improves compressive strength and tensile strength of cemented soil, and the higher amount of fiber content leads to higher the increase in energy absorption. The study shows that with 100% water content, at the same strain, stiffness increases with increasing fiber content for a given strain value.

Once the change in the mechanical properties of soil is known during laboratory work, researchers evaluate its performance as subgrade soil. Singh et al., (2021) investigated the incorporation of municipal solid waste incineration ash and marble dust in clayey soil for subgrade construction, demonstrating the potential for alternative materials in subgrade improvement. Such kind of treated soil materials usage effectiveness is reported by (Shalabi et al., 2019). Moreover, the effects of ground granulated blast-furnace slag (GGBS) and fly ash in binders on soil treatment for road construction, highlighting the potential of alternative binders in soil improvement process (Lindh & Lemenkova, 2022). These studies collectively support the use of cement and alternative materials for subgrade treatment, providing valuable insights into the effectiveness and sustainability of such approaches in road construction.

In this study the improved soil by utilization of finely shredded paper (here in after called FSP) fibers incorporated into mixture of clay soil and cement at high water content where the treatment method is economical and ecofriendly is used for analysis. For the performance evaluation of treated soil used for construction of road is performed using Plaxis 3D FEM program.

**5.2 Finite element modelling**

Finite Element Modeling (FEM) is a powerful computational technique that has revolutionized the method engineers and scientists analyze and solve complex problems in various fields of engineering, physics, mathematics, and others. It is a numerical method used to approximate and simulate physical phenomena by dividing complex geometries of model region into smaller, simpler elements with each element analyzed separately using matrices. These elements are interconnected to form a mesh, and mathematical equations are applied to each element to describe its properties effectively. Nevertheless, the computation procedure involved in the finite element method is complex and not feasible for manual calculations. However, most of the finite element software's have sophisticated codes and a robust computational framework to address this type of challenge.

FEM enables us to understand the behavior of structures, materials, and systems under different conditions, making it an indispensable tool for designing and optimizing everything from roads, bridges, buildings to dams and others. This approach provides valuable insights into real-world problems, allowing engineers and scientists to make precise decisions and innovations in various industries. Look at appendix A to read some of the advantages of FEM.

Plaxis is a finite element program that has gained significant recognition and utilization in the field of geotechnical engineering that was specifically designed for the numerical analysis of geotechnical problems. It incorporates constitutive models that simulate the behavior of soils under various loading conditions (García et al., 2022).

In the late 1980s, Plaxis was initiated as a 2D finite element program for analyzing river embankments in collaboration with the Dutch Ministry of Infrastructure and Water Management at Delft University of Technology in the Netherlands (Lin et al., 2020). The software has been upgraded to include advanced geometric tools for creating arbitrary 3D geometries and incorporates advanced computation and iterative tools, making it widely used in the field (Simões et al., 2017).

Plaxis 3D has been extensively applied in various geotechnical analyses, including stability studies on geological formatio(Zhao & You, 2020)oal batters (Zhao & You, 2020) and open pit slopes (Zhao & You, 2018). Furthermore, recent advancements have focused on digital-based approaches to automate and optimize geotechnical design processes, reflecting the continuous development and integration of new technologies in geotechnical engineering (Lam et al., 2022). Additionally, Plaxis 3D has been employed in the investigation of the behavior of single under-reamed piles under compression load in clay (Nasr et al., 2022). Furthermore, the software has been instrumental in the study of the effect of geogrid reinforcement of embankments over soft foundations (Mohammed et al., 2022), as well as in the geotechnical modeling and subsurface analysis of complex underground structures (Hemeda, 2019a). Its application extends to the behavior of disconnected and connected piled raft foundations (Tarenia & Patra, 2019). load (Tarenia & Patra, 2019). These broader applications demonstrate the versatility and significance of Plaxis 3D in addressing various complex geotechnical and structural problems.

### 5.3. Soil Models in Plaxis

In Plaxis software, soil models are essential components used to represent the behavior of soils under various scenarios. There are several soil models used in Plaxis 3D to simulate the target ground conditions which is written in appendix B. In this study it mainly proposed four different types of soil across the proposed road cross section. So based on each property we utilized soft soil models (for soft clay subgrade) and Mohr Coulomb model (for embankment fill, treated soil section and silty sand sub surface layer). We will describe in detail about this two-soil model behavior as follows:

### 5.4.1 Mohr-Coulomb Model

The Mohr-Coulomb model is a simple and well-known linear elastic perfectly plastic model as shown in **Figure 5.1**, which can be used to model and effectively represent soil behaviors. For its failure criteria formulation Hooks laws were used. The basic principle of elasto-plasticity is that strains and strain rates are decomposed into two parts as an elastic part and a plastic part as shown in **Figure 5.1**.

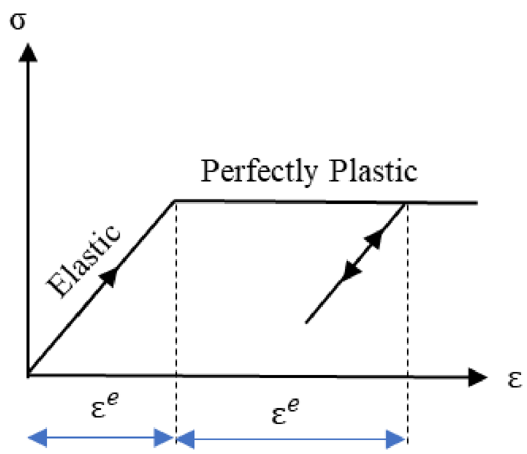


**Figure 5. 1: Basic principle of an elastic perfectly plastic model**

The behavior of materials which is modeled with Mohr-Coulomb model has certain features:

1. It shows isotropic shear strength, with both peak and residual values, featuring a cohesive-frictional nature that linearly increases with stress or confinement levels.
2. Tensile strength using a tension cutoff yield function.
3. It accounts for either dilation, due to increased volume, or critical state behavior with constant volume at failure.
4. It takes into consideration the dependency of shear strength on Lode's angle, an observation common for most geomaterials.

This model is particularly suitable for assessing the stability of geotechnical and mining problems within a limited range of stress and confinement conditions. In certain cases, it can provide more accurate predictions of failure modes and safety factors. For instance, it is effective in simulating load-displacement behaviors of subgrade geomaterials like gravel, sand, and rocks. When the Coulomb criterion is combined with the Mohr circle representation of stress states and admissible conditions, the Mohr-Coulomb failure criterion in terms of principal stresses can be defined in equation (5.1) as follows:

$$F_s = \frac{1}{2}(\sigma_1 - \sigma_3) + \frac{1}{2}(\sigma_1 + \sigma_3)\sin\phi - c\cos\phi = 0 \tag{5.1}$$

The yield functions have two familiar plastic model parameters: the widely recognized friction angle $\varphi$ and the cohesion $c$. When all the yield functions, each denoted by $f_i$, satisfy the condition $f_i = 0$, collectively, it shows a stable hexagonal cone within the principal stress space, as illustrated in **Figure 5.2**.

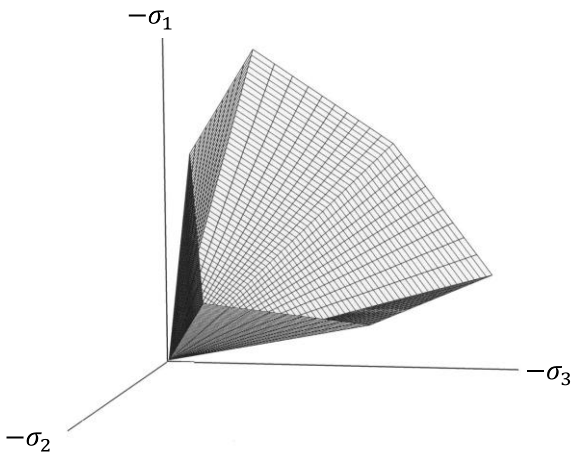


**Figure 5.2: Hexagonal yield surface for Mohr-Coulomb model in principal stress space (Brinkgreve et al., 2013)**

The Mohr-Coulomb model with linear elastic perfectly plastic behavior necessitates five parameters in total where two for stiffness and three for strength as shown in **Table 5.1**. These parameters are commonly well-known among professional geotechnical engineers and can be obtained from basic soil sample tests.

**Table 5.1: Parameters used for Mohr-Coulomb model**

| **Stiffness parameters** | | |
|---|---|---|
| **Parameters** | **Demotion** | **Unit** |
| Young's modulus | $E_{ref}$ | [kN/m$^2$] |
| Poisson's ratio | $v$ | - |
| **Strength parameters** | | |
| Cohesion | $c$ | [kN/m$^2$] |
| Friction angle | $\varphi$ | [°] |
| Dilatancy angle | $\psi$ | [°] |

Youngs modulus (E): Young's modulus serves as the fundamental stiffness modulus in both the elastic model and the Mohr-Coulomb model, although there are also alternative stiffness moduli to consider. Careful attention must be given to the selection of stiffness parameters in calculations, particularly because many geological materials exhibit non-linear behavior right from the onset of loading. As shown in **Figure 5.3**, the triaxial testing of soil samples, the initial slope of the stress-strain curve, indicated as the tangent modulus $E_0$, is typically referenced, and the secant modulus at 50% strength is denoted as $E_{50}$.

For materials with a substantial linear elastic range, $E_0$ is a reasonable and practical choice, but when dealing with soil loading, $E_{50}$, becomes the preferred option. When addressing unloading conditions, such as those encountered in tunneling and excavations, one typically requires an unload-reload modulus $E_{ur}$ instead of $E_{50}$.

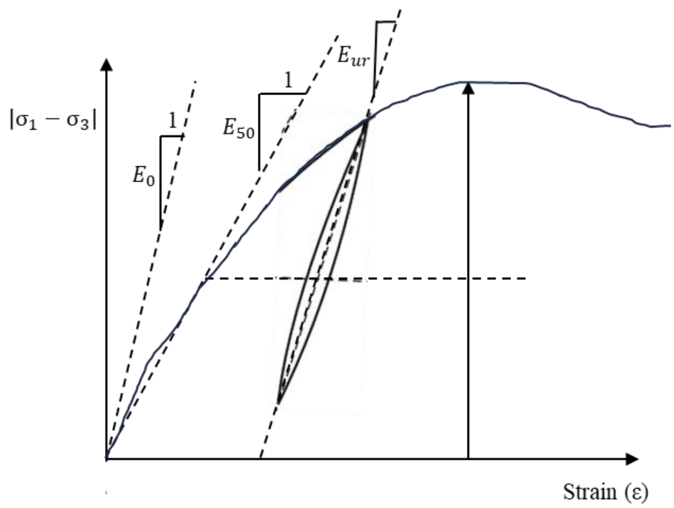


**Figure 5.3: Definition of $E_0$, $E_{50}$ and $E_{ur}$ for drained triaxial test (Brinkgreve et al., 2013)**

From Hooks law the shear modulus ($G$) Oedometer modulus ($E_{oed}$) can be calculated using the young's modulus and poisons ratio relationship as shown in equation (5.2) and (5.3) respectively results (Plaxis 3D user manual, 2013)

$$G = \frac{E}{2(1+v)} \tag{5.2}$$

$$E_{oed} = \frac{(1-v)E}{(1-2v)(1+v)} \tag{5.3}$$

### 5.4.2. Soft soil model

A soft soil model (Brinkgreve, 2002) is utilized for soil having high degree of compressibility like, normally consolidated clays, clayey silt and peat which is demonstrated with odometer test data. From modified compression index ($\lambda$*) value which is slope of elastic compression line as shown in **Figure 5.4**, the oedometer modulus can be computed from the relationship:

$$E_{oed}^{ref} = \frac{p^{ref}}{\lambda^*} \tag{5.4}$$

Where, $E_{oed}^{ref}$, Tangent stiffness for primary oedometer loading
$\lambda*$, modified compression index

A hardening soft soil model is quite suitable for soft soil modelling in most cases unless we consider very soft soils with high compressibility. So, for such kind of soils soft soil models are used. Soft soil model has certain features like: -

- Stress dependent stiffness (logarithmic compression behavior),
- Distinction between primary loading and unloading reloading,
- Memory for pre-consolidation stress,
- Failure behavior according to the Mohr-Coulomb criterion.

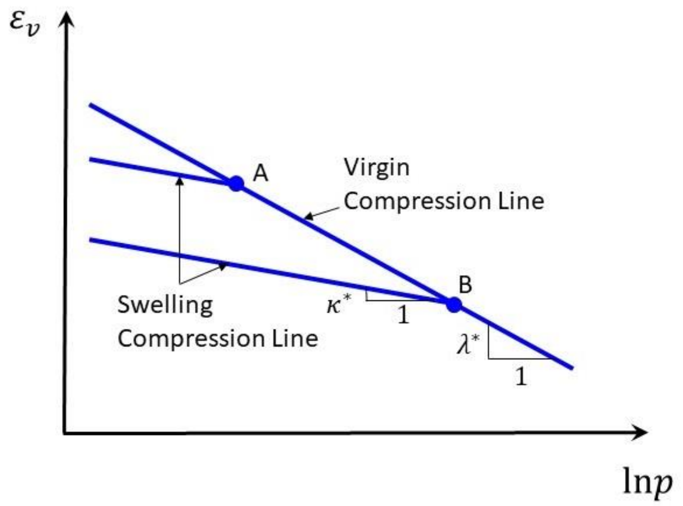


**Figure 5.4: Logarithmic relation between volumetric strain and mean stress (Xue et al., 2022)**

Among changes in volumetric strain, $\varepsilon_V$, and changes in mean effective stress, $p'$in soft soil model logarithmic relationship is assumed ich can be formulated as:

$$\varepsilon_v - \varepsilon_v^0 = -\lambda^* \ln\left(\frac{p'}{p^0}\right) \quad \text{....Virgin compression.......} \quad (5.5)$$

During isotropic unloading and reloading a different path (line) is followed, which can be formulated as:

$$\varepsilon_v^e - \varepsilon_v^{e0} = -k^* \ln\left(\frac{p'}{p^0}\right) \quad \text{.... Unloading reloading .......} \quad (5.6)$$

The Hooks law in equation 3 describes the elastic properties and the bulk modulus calculated according to equation 3. In the bulk modulus calculation, the minimum value of “p” and for the elastic Hooks law constant poisons ratio is considered.

$$K = \left(\frac{p}{k^*}\right) = \frac{E}{3(1-2v)} \quad \text{....Unloading reloading .......} \quad (5.7)$$

It is noted that the material parameters $\lambda^*$ and $\kappa^*$ (using the superscript asterisk to denote “modified”) are based on the increment of volumetric strains (**Figure** 5.4); they are different from the material parameters $\lambda$ and $\kappa$ used in the modified Cam-Clay model which are based on the increment of void ratios. Modified compression index, or slope of elastic compression line, $\lambda^* = \frac{\lambda}{1+e}$ where λ is the compression index in the Cam-Clay model, and $e$ can be approximately the initial or average void ratio during a compression path. Modified swelling index, $\kappa^*$, or slope of elastic swelling line, $k^* = \frac{k}{1+e}$, where κ is the swelling index in the Cam-Clay model, and $e$ can be approximately the initial or average void ratio during a swelling path.

The parameter modified compression index ( $\lambda^*$), which determines the compressibility of the material in primary loading and $k^*$is the modified swelling index, which determines the compressibility of the material in unloading and subsequent reloading.

The relationship between the modified compression and swelling indexes are given below that obtained from one dimensional compression as:

$$\lambda^* = \frac{\lambda}{1+e} = \frac{C_c}{2.3\,(1+e)} \tag{5.8}$$

$$k^* = \frac{k}{1+e} = \frac{2C_r}{2.3\,(1+e)} \tag{5.9}$$

The compressibility of the materials in a given volume is represented in an elliptical cap which has close similarity to the modified cam clay model as shown in **Figure 5. 5**. Where the Yield surface of this elastic cap with its apex on the critical state line defined as:

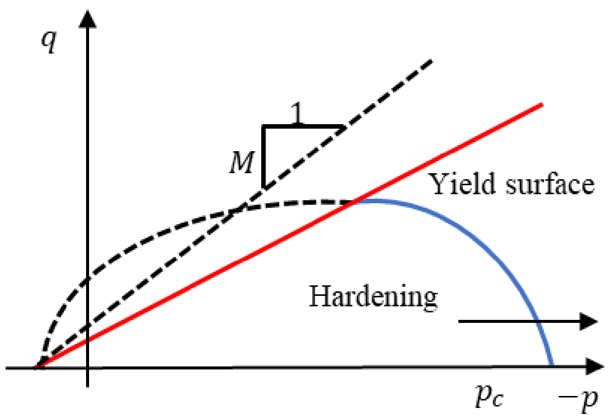


**Figure 5.5: The yield surfaces of the Soft Soil model; Mohr Coulomb yield surface (red) and elliptical cap (blue) (Brinkgreve et al., 2013)**

$$F_C = \frac{q^2}{M^2(p + c\cot(\varphi))} + p - p_c = 0 \tag{5.10}$$

Where,

= $p_c$ is the location of the intersection of this yield surface with the $p$ axis, and

=$M$ is the slope of critical state line where this line is different in triaxial compression and extension    configurations like Mohr Coulomb model.

The hardening for these yield surfaces is considered for $p_c$ and it is attributed to volumetric plastic strain generated only by the cap yield surface.

$$p_c = p_0 \exp\left(\frac{-\varepsilon_v^p}{\lambda^* - \kappa^*}\right) \tag{5.11}$$

The slope of the critical state line, $M$, is obtained largely from the coefficient of lateral earth pressure $K_0^{nc}$ evaluated from an oedometer test.

$$M = 3\sqrt{\frac{(1-K_0^{nc})^2}{(1+2K_0^{nc})^2} + \frac{(1-K_0^{nc})\,(1-2v)(\frac{\lambda^*}{\kappa^*}-1)}{\frac{\lambda^*}{\kappa^*}(1+2K_0^{nc})(1-2v)-(1-K_0^{nc})(1+v)}} \tag{5.12}$$

For general states of stress *(p, q)*, the plastic behavior of the Soft Soil model is defined by the combination of the cap yield function and the Mohr-Coloumb yield functions. In **Figure 5.6** the total yield contour in principal stress space is clearly indicated.

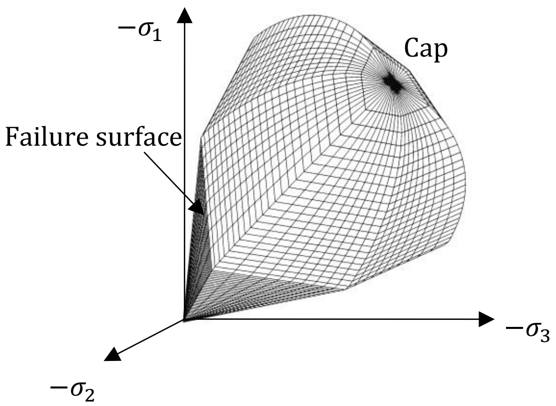


**Figure 5.6: Representation of total yield contour of Soft Soil model in principal stress space (Brinkgreve et al., 2013)**

## 5.5. Meshing condition in the model

Mesh sensitivity in Plaxis 3D models is a critical aspect which influences the accuracy of overall simulations. The selection of a suitable mesh size and shape is paramount in ensuring reliable results (Bomers et al., 2019). It is shown that the model output is more sensitive to mesh properties, such as grid shape and size, than to other factors like friction spatial distribution. For mesh sizes below a certain limit, the accuracy of results diminishes (Hellander et al., 2015).

Adaptive mesh refinement plays an essential role in enhancing the precision of simulations by allowing for the adjustment of mesh density based on the requirements of the model (Lambe & Czekanski, 2017) .This approach has been successfully implemented to optimize the boundary of structures and improve the overall quality of computational solutions (Paulino et al., 2010).

Furthermore, the use of adaptive mesh refinement has been shown to be more computationally efficient compared to uniformly refining the entire mesh (Shu-min et al., 2021). In the context of Plaxis 3D modeling, the implementation of adaptive mesh refinement can lead to more detailed and accurate representations of complex structures and geotechnical problems (Hemeda, 2019). This refinement method enables the generation of more intricate mesh patterns that closely mimic field conditions, thereby enhancing the overall simulation quality (Mansur et al., 2022). Moreover, compared to other modeling approaches, Plaxis-3D modeling has been described as more elegant, representative, and accurate (Sanjei & Silva, 2016).

After creating the model geometry material properties are assigned to each soil layer, which is generated from meshing mode. Plaxis 3D stands out with its unique mesh structure comprised of 10-node tetrahedral elements as shown in **Figure 5.7**, unlike that of 2D finite element software that allows for triangular and square mesh elements. Users have the flexibility to adjust element sizes within the mesh settings to tailor them to specific problem requirements.

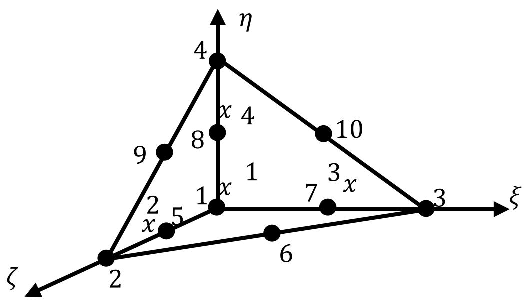


**Figure 5.7: Tetrahedral mesh elements in Plaxis 3D (Brinkgreve et al., 2013)**

The quality of the mesh depends on two major parameters, target element size ($I_e$) and relative element size ($r_e$). The element size ($I_e$) depends on the overall dimensions of the model boundaries (XYZ plane) and can be calculated using the equation (5.13) (Brinkgreve et al., 2013).

$$I_e = \frac{r_e}{20}\sqrt{(x_{max} - x_{min})^2 + (y_{max} - y_{min})^2 + (z_{max} - z_{min})^2} \qquad 5.13$$

The relative element size, $r_e$, is assigned with five different values based on global mesh levels: very coarse ($r_e$ = 1.5), coarse ($r_e$ = 1), medium ($r_e$ = 0.7), and very fine ($r_e$ = 0.5). Once the user selects the appropriate $r_e$ value, the targeted element size, $I_e$ is automatically calculated, and the mesh is generated accordingly. In our case the very fine ($r_e$ = 0.5) is selected for the better accuracy even if it takes relatively larger time for simulations.

## 5.5. Geometry of the model

As shown in **Figure 5.8** the embankment was constructed on soft soil subsurface profile. The embankment has a total height of 1.50m from the existing ground surface which has a side slope with a ratio of 4:1. This embankment is underlined by soft clay soil which extends up to 5.0m below natural ground surface, where silty sand soil covers the lower layer of the sub surface soil that extends to 12.0m below the ground surface. This sub soil stratum is obtained from drilling bore hole logs at outskirt of Addis Ababa city, Ethiopia. This typical soil model is selected based on ERA design manual for low volume road (ERA, 2011). It states the allowable slope and embankment height of road built on soft ground soil. The assumed roadway consisted of a 2-lane rural road with 10m total width. Where point **O** (0,0,0) is origin, point **A** (0.5, 0, -0.5m) and Point **B** (0.5,0, -4.5m) of x, y and z axis respectively is taken for evaluation of the performance of additive across the model.

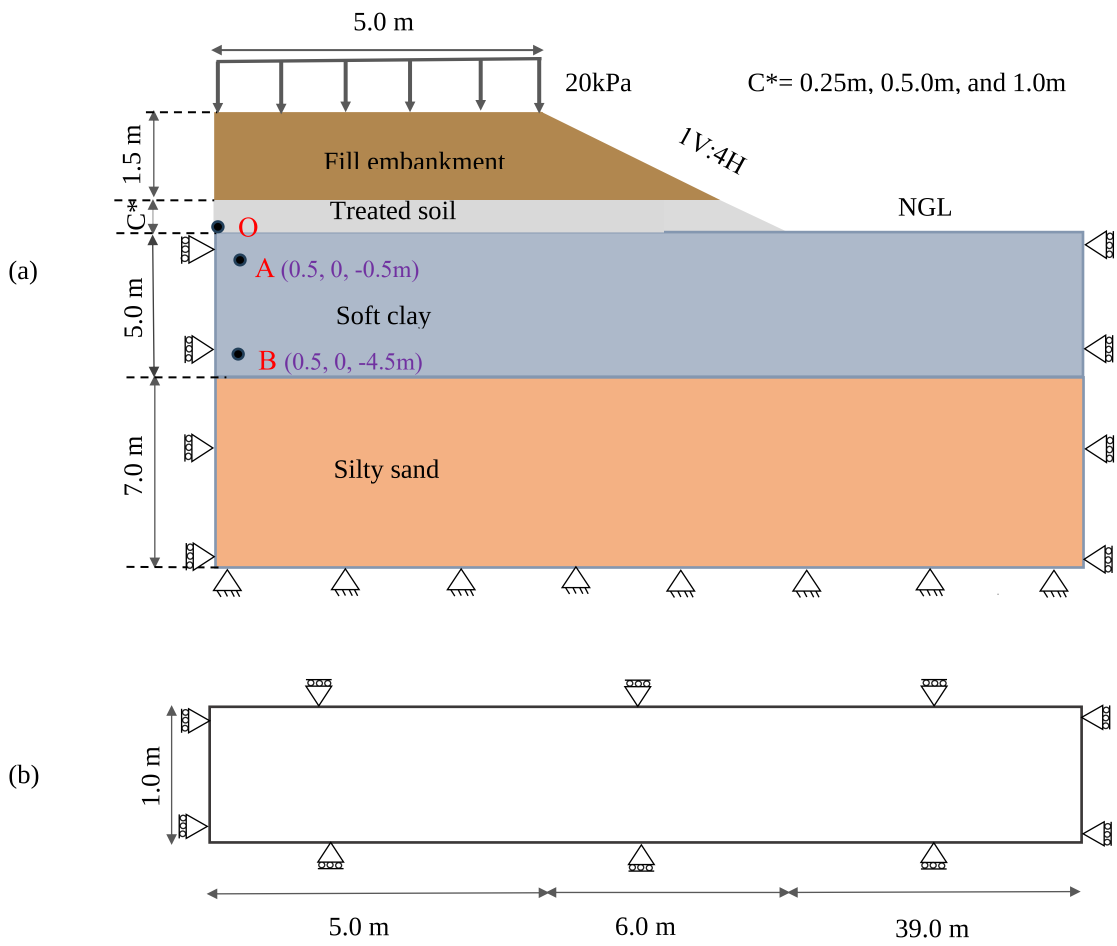


**Figure 5.8: Geometry and boundary condition of the soil model used for simulation.**

### 5.5.1. Boundary condition

In Plaxis, during the consolidation and deformation analysis of an embankment on soft soil, the displacement boundary and the consolidation boundary are established. The origin coordinate point is situated at the base of the embankment's centerline. It is set with the rightward direction as the positive x-axis, the direction towards the page (longitudinal direction of the road) as positive y -axis, and the upward direction as the positive z-axis. To ensure accurate calculation results and minimize the effect of boundary conditions, both wide and narrow embankment models with dimensions of 50 meters are employed in the positive x-direction.

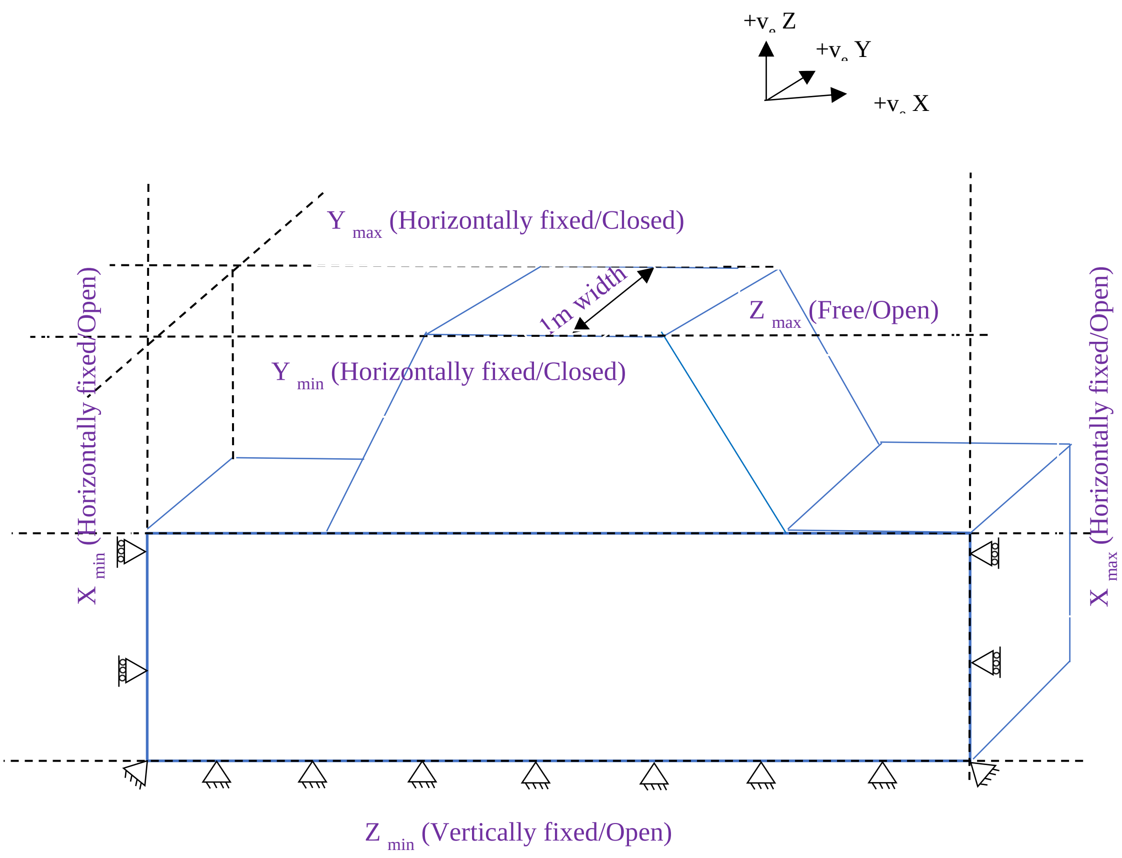


**Figure 5.9: Boundary condition of the model**

**Table 5.2: Material properties used for the analysis**

| | Unit | Embankment fill | Soft soil | Silty sand | Soil treated with cement and FSP |
|---|---|---|---|---|---|
| Model type | | Mohr coulomb | Soft soil | Mohr coulomb | Mohr coulomb |
| Unsaturated unit weight, γ | $kN/m^3$ | 16 | 15 | 17 | 14 |
| Young's modulus, E | kPa | 8000 | - | 20000 | 12000 |
| Poisson's ratio, υ | - | 0.3 | 0.3 | 0.3 | 0.3 |
| Cohesion, c' | kPa | 1 | 25 | 4 | 120 |
| Friction angle, φ' | deg. | 35 | 5 | 33 | 54 |
| Permeability, k | m/day | 1.0 | 7.305E-05 | 0.25 | 4.228E-04 |
| Modified swelling index, κ* | - | - | 0.01818 | - | - |
| Modified compression index, λ* | - | - | 0.091 | - | - |

## 5.6. Loading of the model

The scope of the numerical model was broadened to encompass the intricacies of simulating the road surface, enabling a comprehensive analysis of how it interacts and responds to the repetitive stresses imposed by traffic flow over time. Top of Form The current approach to road cross section modeling assumes that the material is homogeneous, linearly elastic, and isotropic, and it undergoes static loading to evaluate strain (Pooni et al., 2022).

The inclusion of static traffic loading in road embankment simulations holds significant importance for various reasons. Firstly, it enables the assessment of long-term stability and deformation characteristics by(Chaiyaput et al., 2022; Chai & Miura, 2002). This is particularly crucial for evaluating embankments on soft subsoils, where permanent deformation induced by traffic loads needs careful consideration. Moreover, analyzing traffic-induced permanent deformation is essential for ensuring the safety and performance of road embankments, especially in areas with diverse soil properties.

Mei et al., (2019) reported that the primary source of rutting damage on pavement emphasizes to the repetitive application of loads over the course of their lifespan, which emphasizing the need to consider the effects of dynamic loading on pavement deterioration. However, in this research it is considered that the long-term effect of the road embankment deformation without pavement where the static loading condition is utilized for the simulations. For this simulation, the traffic survey conducted by AACRA (Addis Ababa City Road Authority) for project area analyzed and forecasted for the proposed road construction is approximately taken as 20 kPa. This estimate serves as a critical input for modeling and assessing the structural integrity and performance of the road infrastructure under anticipated traffic loads.

### 5.7. Validation of numerical model

Constructing a reliable soil model beneath the analyzed embankment is crucial, with the model accurately simulating real-world conditions. Therefore, comprehending the variations in soil characteristics across different sub soil profiles is vital for conducting thorough investigations into how they respond to the earth fill load.

The study conducted by Puppala et al., (2011) utilize Plaxis 2D for simulation of the embankment to understand the settlement behavior of embankments by measuring the vertical and horizontal displacement for over 800 days. The general overview of this soil model is discussed in the following paragraphs as it is used for the calibration of our model.

A cross-section and subsurface profile of the lightweight fill embankment constructed with a side slope of 2H:1V. The embankment is constructed on a soft clay layer with a thickness of 5 m and underlain by a 3.0m sand layer. on the top of the embankment model, it covered with highway pavement. For this numerical analysis, a soft soil model is used to simulate the soft clay material while a Mohr-Coulomb model is used to simulate the lightweight embankment and sandy soil layer.

The consolidation-based simulation was carried out to study the settlement behavior for a long-term duration by applying static loading until the excess pore water pressure dissipated. Due to symmetry, the model displacement of the boundary at x=0, y=0 was restricted in all directions to the right side of the center line.

To validate the untreated and treated soil parameters used in this model, the results obtained from the given soil model analysis were used to compare with the data recorded from field experiments of Puppala et al., (2011) . From the field experimental results, the elevation survey at the surface of the embankment was used to compare the vertical displacements of the road embankment structure. From **Figure 5.10** it’s observed that the vertical deformation values with the given time of both experimental and numerical simulation is showing a similar tendency.

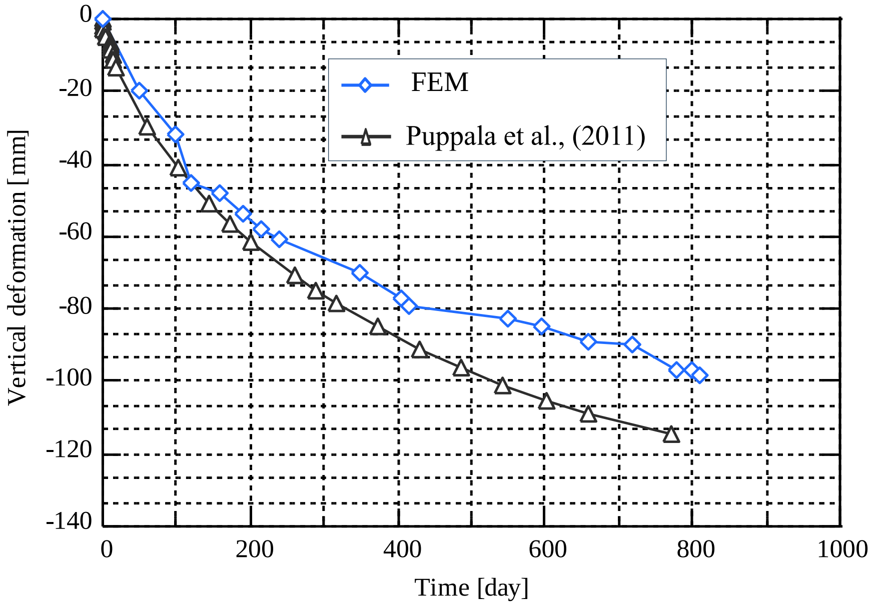


**Figure 5.10: Comparison of the Vertical deformation in the Test Section of field test and Numerical Analysis.**

## 5.8. Settlement analysis

The traffic load was assumed to be 20kN/$m^2$ where due to symmetry of the embankment only half of the embankment with all the cross section and loading as displayed in this figure, in this model simulation, a soft soil model is used to simulate the soft clay material below the embankment while a Mohr-Coulomb model is used to simulate the embankment, treated soil layer and silty sand soil. The input parameters used in this analysis were derived from the laboratory experiment results which are shown in previous Chapters 3 and 4. In addition some of the input parameters are derived from those laboratory tests and customized into suitable form. Those materials properties, drainage condition and soil model type are summarized in **Table 5.2**.

The analysis of Plaxis 3D has input, calculation, and analysis phases from defining the material property, geometry, soil models, meshing and stage construction. For the soft soil layer undrained condition is set in the analysis due to soil properties, but for the other soil layer drained condition is considered which also prevents generation of pore water pressure. After the proper discretization is made and refined shown in **Figure 5.11** and **Figure 5.12** for treated and untreated road section, the calculation phase starts from the initial stresses. In Plaxis, four different types of calculation are allowed, which are consolidation analysis, deformation analysis, a plastic calculation, dynamic calculation, and phi-c reduction for safety analysis. The elastic-plastic consolidation analysis was selected as the appropriate method for simulating the road embankment, evaluating on how excess pore pressure dissipates in a saturated clay layer over time.

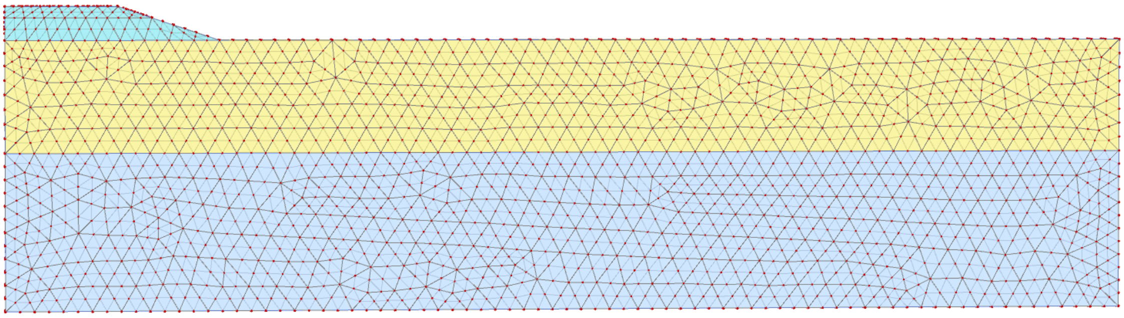

**Figure 5.11: Finite element mesh with nodes in the model of untreated cross section.**

In the calculation process the embankment is analyzed in three layers each with 0.5m height. In the initial stage, the subgrade soil weight was used for the analysis. The construction step started by constructing the 0.50m thick fill embankment for 1 day and allow to consolidate for 8 days to assist the excess pressure dissipation, the construction at second stage and the rest stage was simulated in that way until the whole embankment construction was completed. The simulation was conducted to accurately replicate the compaction process as it occurs in practical, real-world applications. After the end of embankment construction, the traffic load of 20kPa was applied for the period of 1800 days. The loaded section of the road deforms to a certain amount, for instance in **Figure 5.14** the vertical deformation of the embankment and soft ground subsurface soil reduced due to utilization of improved soil layer.

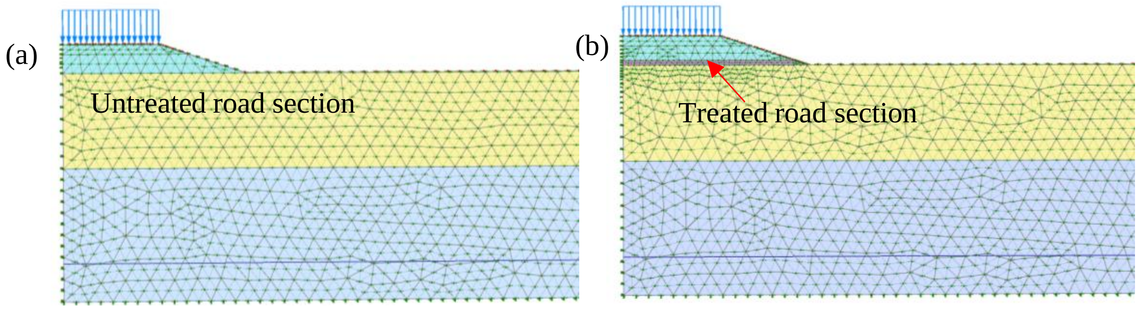


**Figure 5.12: Finite element mesh with traffic loading (a) untreated soil (b) 0.50m treated soil.**

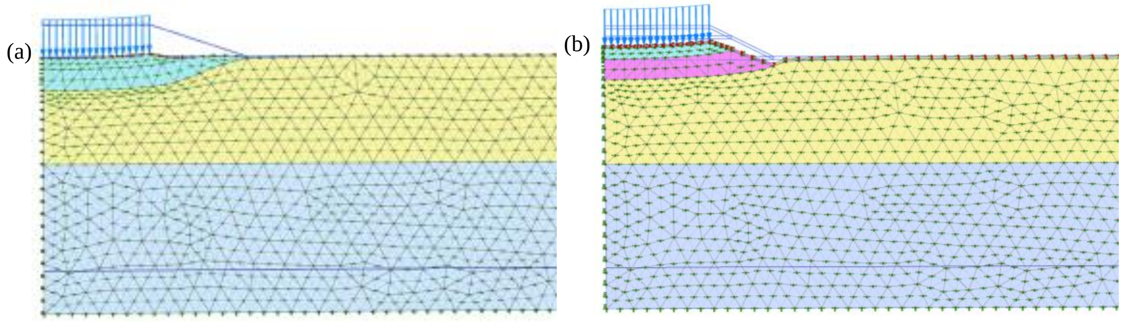


**Figure 5.13: Deformation mesh of (a) untreated soil (b) 1.0m treated road cross section.**

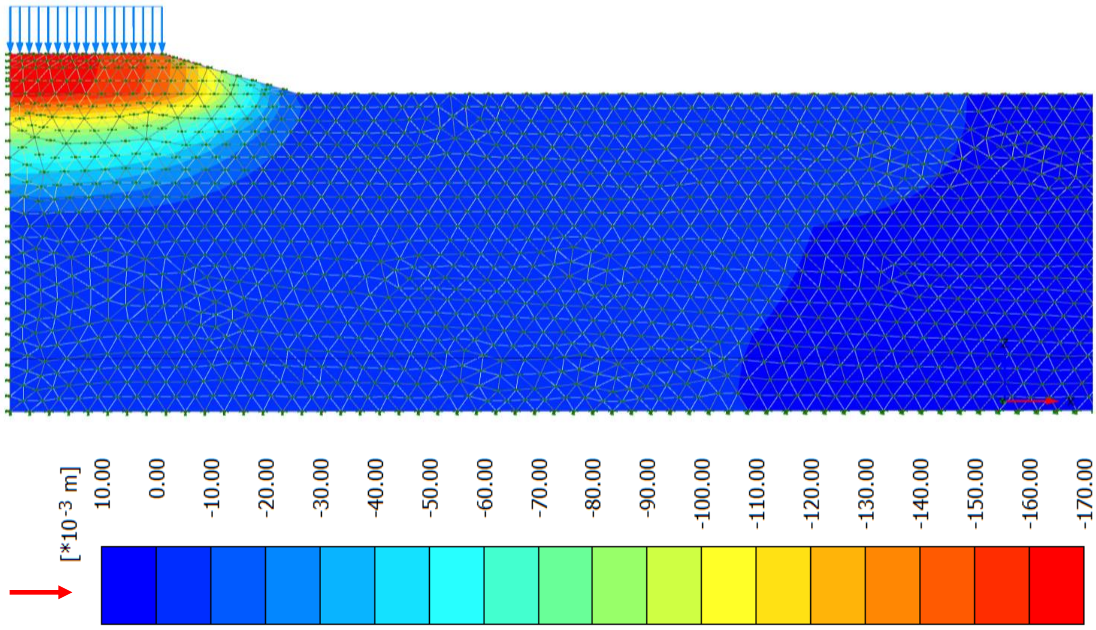


**Figure 5.14: Vertical deformation distribution untreated soft soil layer after 20kPa traffic load is applied for 1800days.**

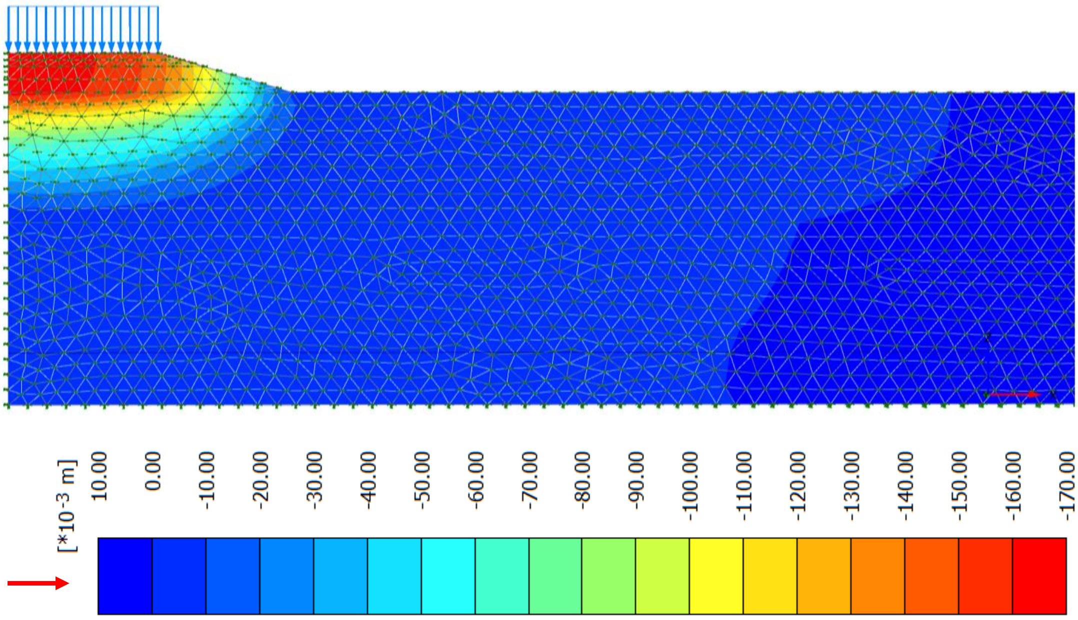


**Figure 5.15: Vertical deformation distribution of 0.50m thick treated soft soil layer after 20kPa traffic load is applied for 1800days.**

**Figure 5.16** illustrates the variation of vertical settlement with time for untreated and treated soft soil with different thicknesses of FSP cement treatment (ranging from 0.25 m to 1.0 m) at the surface and 0.50m below the base of the embankment. It is found from the figure that, in general the value of vertical deformation tends to be reduced by increasing the thickness of the treated soil section of the road at both points. In the case of untreated soft soil, the vertical deformation reached 167 mm and 137 mm after 1818 days is reached at the surface and 0.50 m below the base of the embankment. On the other hand, in the case of treated soil with a 1.0 m thickness, the vertical displacement is reduced to 142 mm and 110 mm of maximum vertical deformation after 1818 days of consolidation process, at surface and 0.5m below the base of the embankment. This result is obtained by the utilization of cement and 2% FSP fiber in combination as shown in **Figure 5.16** below. This indicate also indicates deformation amount at the embankment top section and soft ground top section that reduced by 18% and 23% respectively for the untreated and 1.0m thickness treated soil. Which is shown in **Figure 5.14** that the tendency of the vertical deformation value for the specified time is higher in the embankment section than the soft soil section. It should be noted that the decrease in vertical movement (settlement) is linked to improvements in soil strength characteristics and lower time required for more pervious soil specimen.

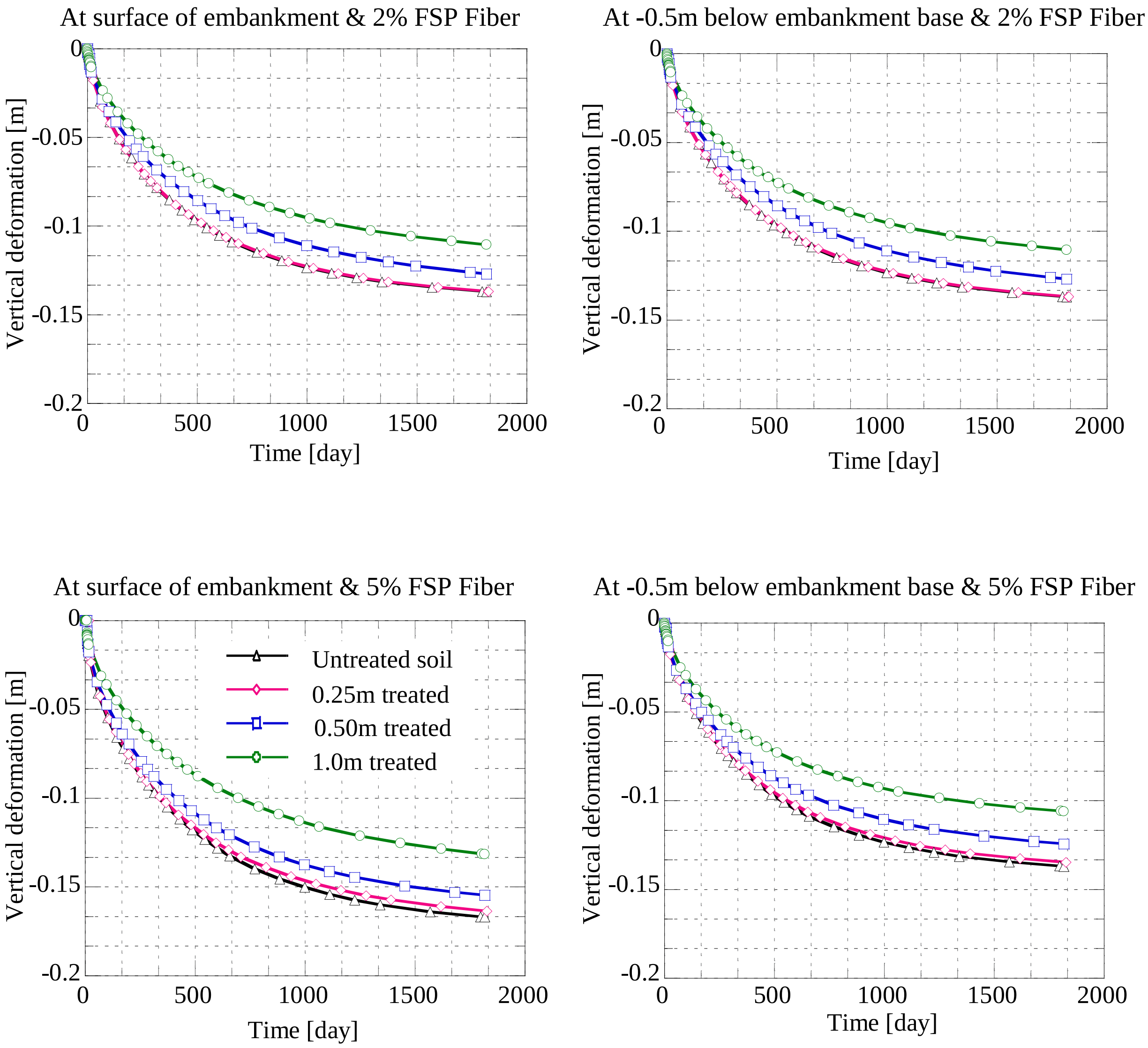


**Figure 5.16: Vertical deformation of untreated and cement -FSP treated soil with different thickness and FSP fiber amount.**

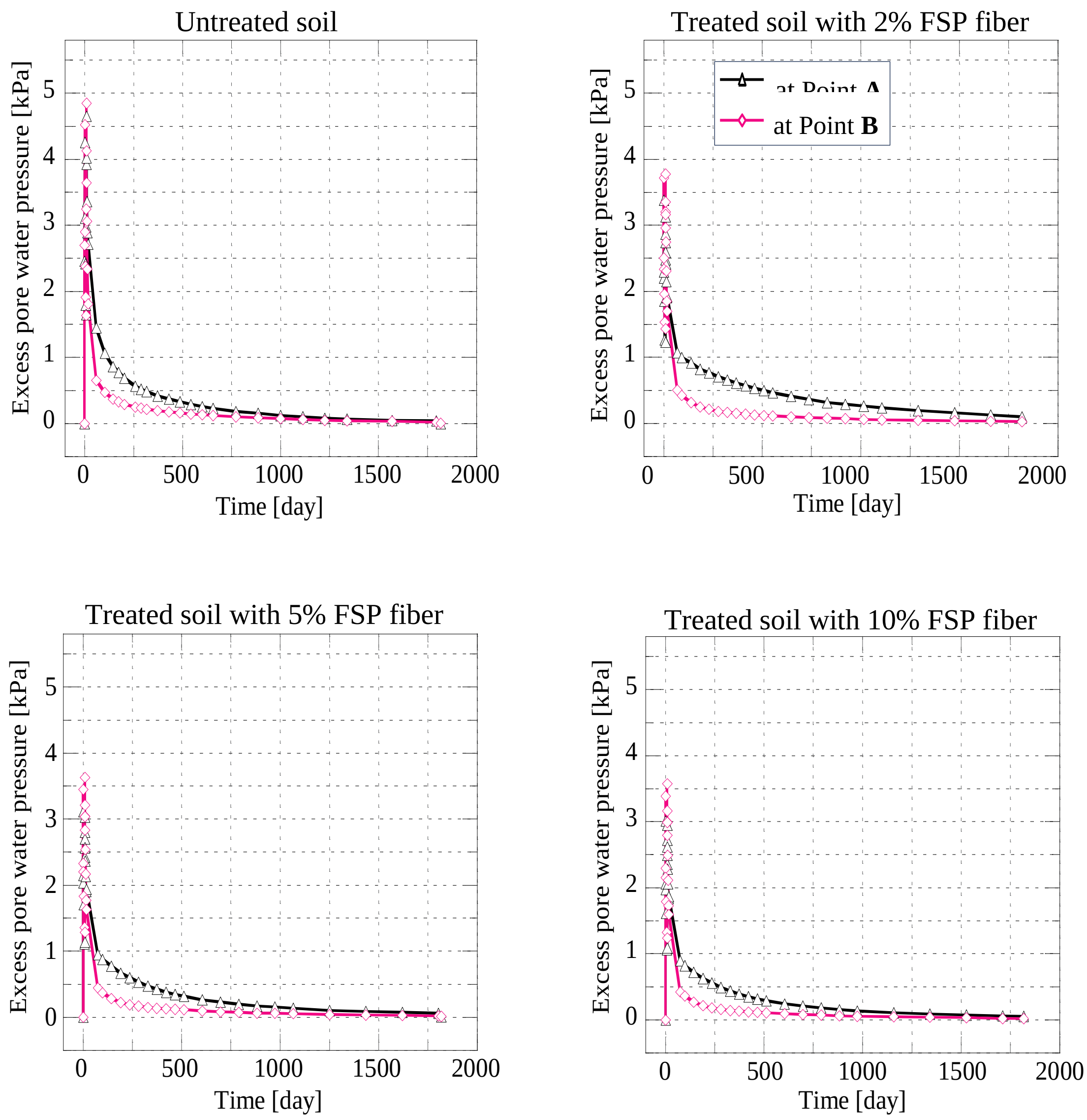


**Figure 5.17: Excess pore water pressure of untreated and cement -FSP treated soil at different depths (at point A and B) and FSP fiber amount.**

**Figure 5.17** illustrates the generation and dissipation of excess pore water pressure in the soft soil section at 1.0m thick reinforced embankment. The reason the excess pore water pressure value investigation is focused is that in all the other soil sections in the model (i.e., embankment, treated soil and silty sand soil layers) use drained simulation condition. Two points were selected in the soft soil layer at the center line of the road for every treatment scenario: one is at 0.5m below the embankment base and the other is at 4.5m below the embankment base where the behavior of excess pore water pressure is evaluated. It is observed from **Figure 5.17** that, during the initial phases of each construction stage, the dissipation of the excess pore water pressure immediately increases due to an increase in the embankment loading, and each sudden increase is followed by a gradual reduction in pressure. The excess water pressure shows peak values of 4.84 kPa and 3.78 kPa at 4.5 m below the embankment base due to the embankment construction and then dissipated at different rates to nearly zero after 1800 days for the untreated and 1.0m depth treated soil road cross sections, respectively when 2% FSP fiber is used. Similarly, for the point at 0.50m below the embankment depth, the maximum value of dissipated excess pore water pressure is 4.65 kPa and 3.37 kPa for untreated and 1.0m treated road section respectively.

For the 5% FSP fiber addition, the excess water pressure shows peak values of 3.62 kPa and 3.17 kPa at 4.5 m below the embankment base when 5% and 10% FSP fiber is used, respectively. For the point at 0.50m below the embankment depth, the maximum value of excess pore water pressure is 3.11 kPa and 2.95 kPa for 5% and 10% FSP fiber inclusion respectively at 1.0m treatment thickness. In addition, it is observed that the rate of dissipation between two points (i, e., 0.5m and 4.5m below the ground surface) increases as depth increases. It means that the excess water pressure at point 4.5m below the embankment base is rapidly reduced due to the higher amount of vertical stress application and shorter distance to permeable silty sand soil.

### 5.9. Conclusions

In this study, Plaxis 3D simulations of road cross section was conducted to evaluate the performance of stabilized soft soil. From the analysis results, we can conclude:

1) Vertical settlement was significantly reduced by increasing the thickness of treated soil sections, indicating an association between reduced settlement and improved soil strength and permeability due to treatment process.
2) These findings give valuable insights into the performance of soft soil ground under various treatment thickness and material behavior, which can inform engineering decisions for road construction and stability.
3) The excess pore water pressure value shows peak values of 4.84 kPa at (untreated) case and 3.78 kPa for (treated with 1.0m thickness case using 2% FSP fiber) at 4.5 m below the base of the embankment.
4) Peak excess pore water pressure development during the initial embankment construction stage is reduced when the FSP fiber addition amount increases improved soil is utilized.

## References for Chapter 5


Babu, G. L. S., Srivastava, A., & Sivapulliah, P. V. (2011). Reliability analysis of strength of cement treated soils. Georisk: Assessment and Management of Risk for Engineered Systems and Geohazards, 5(3–4), 157–162 https://doi.org/10.1080/17499518.2010.490116.

Bo, M. W., Arulrajah, A., & Nikraz, H. (2007). Preloading and prefabricated vertical drains design for foreshore land reclamation projects: a case study. *Ground Improvement*, 11, 67–76. https://api.semanticscholar.org/CorpusID:55080359.

Bomers, A., Schielen, R. M. J., & Hulscher, S. J. (2019). The Influence of Grid Shape and Grid Size on Hydraulic River Modelling Performance. *Environmental Fluid Mechanics*. https://doi.org/10.1007/s10652-019-09670-4

Brinkgreve, R. B. J. (2002). *PLAXIS Finite Element Code for Soil and Rock Analyses, 2D-Version 8*. *Balkema* (Rotterdam).

Brinkgreve, R., Engin, E., & Swolfs, W. M. (2013). Plaxis 3D 2013 user manual. *Plaxis by, Delft*, *Plaxis bv, Delft.*

Chaiyaput, S., Arwaedo, N., Kingnoi, N., Nghia-Nguyen, T., & Ayawanna, J. (2022). Effect of curing conditions on the strength of soil cement. *Case Studies in Construction Materials*, *16*. https://doi.org/10.1016/j.cscm.2022.e01082

Chen, L., & Lin, D.-F. (2009). Stabilization Treatment of Soft Subgrade Soil by Sewage Sludge Ash and Cement. *Journal of Hazardous Materials*. https://doi.org/10.1016/j.jhazmat.2008.05.060

Duan, X.-L., & Zhang, J. (2019). Mechanical Properties, Failure Mode, and Microstructure of Soil-Cement Modified with Fly Ash and Polypropylene Fiber. *Advances in Materials Science and Engineering*. https://doi.org/10.1155/2019/9561794

Duong, N. T., Satomi, T., & Takahashi, H. (2021). Potential of corn husk fiber for reinforcing cemented soil with high water content. *Construction and Building Materials*, *271*. https://doi.org/10.1016/j.conbuildmat.2020.121848

ERA. (2011). *Federal Democratic Republic of Ethiopian Roads Authority Design Manual for low volume roads road maintenance booklet-part g*.

Estabragh, A. R., Namdar, P., & Javadi, A. A. (2012). Behavior of Cement-Stabilized Clay Reinforced with Nylon Fiber. *Geosynthetics International*. https://doi.org/10.1680/gein.2012.19.1.85

García, G., José, R., Jiménez, A., Iván, V., Manteca, A., Encarnación, M., & Moreno, M. (2022). *Resolution of Geotechnical Engineering problems with Plaxis 2D*.

Haakeel, M. S. S., Ramzi, M. Z. M., & Nasvi, M. C. M. (2019). Compressibility Behavior of Peat Reinforced with Single and Multiple Deep Soil Mixing (DSM) Columns. *Engineer: Journal of the Institution of Engineers, Sri Lanka*, *52*(3), 1. https://doi.org/10.4038/engineer.v52i3.7360

Hellander, S., Hellander, A., & Petzold, L. R. (2015). Reaction Rates for Mesoscopic Reaction-Diffusion Kinetics. *Physical Review E*. https://doi.org/10.1103/physreve.91.023312

Hemeda, S. (2019a). 3D Finite Element Coupled Analysis Model for Geotechnical and Complex Structural Problems of Historic Masonry Structures: Conservation of Abu Serga Church, Cairo, Egypt. *Heritage Science*. https://doi.org/10.1186/s40494-019-0248-z

Hemeda, S. (2019b). 3D Finite Element Coupled Analysis Model for Geotechnical and Complex Structural Problems of Historic Masonry Structures: Conservation of Abu Serga Church, Cairo, Egypt. *Heritage Science*. https://doi.org/10.1186/s40494-019-0248-z

Kasama, K., Zen, K., & Kiyoharu, I. (2007). High-strengthening of cement -treated clay by mechanical dehydration. In *Soils and Foundations* (Vol. 47, Issue 2).

Lam, A. K. M., Wong, A. T. F., & Chan, K. P. (2022). *A New Digital-Based Approach to Automate and Optimize Geotechnical Design*. https://doi.org/10.21467/proceedings.133.7

Lambe, A. B., & Czekanski, A. (2017). Topology Optimization Using a Continuous Density Field and Adaptive Mesh Refinement. *International Journal for Numerical Methods in Engineering*. https://doi.org/10.1002/nme.5617

Li, Y.-F., Yang, T.-H., Kuo, C.-Y., & Tsai, Y.-K. (2019). A Study on Improving the Mechanical Performance of Carbon-Fiber-Reinforced Cement. *Materials*. https://doi.org/10.3390/ma12172715

Lin, D.-G., Chang, K.-P., Ku, C.-Y., & Chou, J.-C. (2020). Three-Dimensional Numerical Investigation on the Efficiency of Subsurface Drainage for Large-Scale Landslides. *Applied Sciences*. https://doi.org/10.3390/app10103346

Lindh, P., & Lemenkova, P. (2022). Effects of GGBS and Fly Ash in Binders on Soil Stabilization for Road Construction. *Romanian Journal of Transport Infrastructure*. https://doi.org/10.2478/rjti-2022-0010

Ma, C., Chen, B., & Chen, L. (2018). Experimental feasibility research on a high-efficiency cement-based clay stabilizer. *KSCE Journal of Civil Engineering*, *22*(1), 62–72. https://doi.org/10.1007/s12205-017-0782-8

Mansur, A., Roesyanto, & Iskandar, R. (2022). Deterioration Analysis and Consolidation Time Using Terzaghi 1-D Method and 3D Plaxis Modeling: A Case Study of the Tebing Tinggi Toll Road Development Project - Indrapura STA. 103 + 200. International Journal of Research and Review. https://doi.org/10.52403/ijrr.20220224

Medvey, B., & Dobszay, G. (2020). Durability of Stabilized Earthen Constructions: A Review. In *Geotechnical and Geological Engineering* (Vol. 38, Issue 3, pp. 2403–2425). Springer. https://doi.org/10.1007/s10706-020-01208-6

Mei, H., Leng, W., Nie, R., Tu, R., Li, Y., & Dong, J. (2019). Experimental Research on the

Dynamic Response Characteristics of the Transition Subgrade Induced by Heavy-Haul Train Passage. Proceedings of the Institution of Mechanical Engineers Part F Journal of Rail and Rapid Transit. https://doi.org/10.1177/0954409718822924

Mei, L., Dong, X., & Yang, S. (2022). Experimental Study on Mechanical Properties of Cement-Solidified Remolded Soil Reinforces by Polyvinyl Alcohol Fiber. *Advances in Materials Science and Engineering*. https://doi.org/10.1155/2022/5169404

Mohammed, S. A., Naimi, S., & Abdulkareem, A. H. (2022). The Effect of Geogrid Reinforcement of Embankment Over Soft Foundation. *Periodicals of Engineering and Natural Sciences (Pen)*. https://doi.org/10.21533/pen.v10i6.3345

Nasr, A., Azzam, W., & Harran, I. (2022). The Behavior of Single Under-Reamed Piles Under Compression Load in Clay - Numerical Study. *Journal of Engineering Research*. https://doi.org/10.21608/erjeng.2022.146929.1076

Nguyen, B. T. T., Takeyama, T., & Kitazume, M. (2015). Numerical analyses on the failure of deep mixing columns reinforced by a shallow mixing layer. *15th Asian Regional Conference on Soil Mechanics and Geotechnical Engineering, ARC 2015: New Innovations and Sustainability*, 2144–2148. https://doi.org/10.3208/jgssp.VNM-01

Paulino, G. H., Park, K., Celes, W., & Espinha, R. (2010). Adaptive Dynamic Cohesive Fracture Simulation Using Nodal Perturbation and Edge-swap Operators. *International Journal for Numerical Methods in Engineering*. https://doi.org/10.1002/nme.2943

Pooni, J., Robert, D., Giustozzi, F., Setunge, S., & Venkatesan, S. (2022). Stabilization of expansive soils subjected to moisture fluctuations in unsealed road pavements. *International Journal of Pavement Engineering*, *23*(3), 558–570. https://doi.org/10.1080/10298436.2020.1762083

Puppala, A. J., Archeewa, E., Saride, S., Nazarian, S., & Hoyos, L. (2011). Recommendations for design, construction, and maintenance of bridge approach slabs project 0-6022 13 *in cooperation with the Texas Department of Transportation and the Federal Highway Administration.*. http://www.ntis.gov

Puspita, N., & Capri, A. (2020). The effectiveness of vacuum consolidation to soft soil settlement. *International Journal on Advanced Science, Engineering, and Information Technology*, *10*(4), 1610–1616. https://doi.org/10.18517/ijaseit.10.4.3943

Sanjei, C., & Silva, L. I. N. De. (2016). *Numerical Modelling of the Behavior of Model Shallow Foundations on Geocell Reinforced Sand*. https://doi.org/10.1109/mercon.2016.7480142

Shalabi, F. I., Mazher, J., Khan, K., Alsuliman, M., Almustafa, I., Mahmoud, W., & Alomran, N. (2019). Cement-Stabilized Waste Sand as Sustainable Construction Materials for Foundations and Highway Roads. *Materials*. https://doi.org/10.3390/ma12040600

Shu-min, S., Braun, M., Wiegard, B., Herrnring, H., & Ehlers, S. (2021). Combining H-Adaptivity With the Element Splitting Method for Crack Simulation in Large

Structures. *Materials*. https://doi.org/10.3390/ma15010240

Simões, S., Oh, R. Y., Wang, M. F. Z., Fernández-González, R., & Tepaß, U. (2017). Myosin II Promotes the Anisotropic Loss of the Apical Domain During <i>Drosophila</I> Neuroblast Ingression. *The Journal of Cell Biology*. https://doi.org/10.1083/jcb.201608038

Singh, P., Boora, A., & Gupta, A. K. (2021). Sub-Grade Characteristics of Clayey Soil Incorporating Municipal Solid Waste Incineration Ash and Marble Dust. *Journal of Engineering Design and Technology*. https://doi.org/10.1108/jedt-08-2020-0347

Tarenia, K., & Patra, N. R. (2019). *Behavior of Disconnected and Connected Piled Raft Foundations Subjected to Compressive Load*. https://doi.org/10.11159/icgre19.180

Tran, K. Q., Satomi, T., & Takahashi, H. (2018). Improvement of Mechanical Behavior of Cemented Soil Reinforced with Waste Cornsilk Fibers. *Construction and Building Materials*. https://doi.org/10.1016/j.conbuildmat.2018.05.104

Wang, S., Chen, F., Xue, Q., & Zhang, P. (2020). Splitting Tensile Strength of Cement Soil Reinforced with Basalt Fibers. *Materials*. https://doi.org/10.3390/ma13143110

Wassermann, A., Abdallah, A., & Cuisinier, O. (2022). Impact of wetting and drying cycles on the mechanical behavior of a cement-treated soil. *Transportation Geotechnics*, *36*. https://doi.org/10.1016/j.trgeo.2022.100804

Xue, Y., Miao, F., Wu, Y., & Dias, D. (2022). Dynamic stability assessment of reservoir colluvial landslide using a hypoplastic clay constitutive model considering the effects of drying-wetting cycles on the hydro-fluctuation belt. *Engineering Geology*, *307*. https://doi.org/10.1016/j.enggeo.2022.106791

Yang, X., Hou, Z., Dong, F., Xiao, Y., & Zhou, S. (2022). Experimental Study on Strength of Polypropylene Fiber Reinforced Cemented Silt Soil. *Applied Sciences*. https://doi.org/10.3390/app12168318

Zhao, L., & You, G. (2018). Stability Study on the Northern Batter of MBC Open Pit Using Plaxis 3D. *Arabian Journal of Geosciences*. https://doi.org/10.1007/s12517-018-3454-1

Zhao, L., & You, G. (2020). Rainfall Affected Stability Analysis of Maddingley Brown Coal Eastern Batter Using Plaxis 3D. *Arabian Journal of Geosciences*.

# Chapter 6

## Conclusions and Recommendations

### 6.1 Conclusions

In summary, the utilization of combined natural fiber and cement for high water content clay soil improvement represents an innovative advancement in sustainable construction practices. The environmental, mechanical strength and economic advantages highlight the transformative potential of this approach. By addressing the challenges associated with unstable soft clay soils in a comprehensive and eco-friendly manner, this innovative technique not only strengthens the foundation of constructed structures but also contributes to a more resilient, sustainable, and economically viable future for the construction industry.

The utilization of a combined natural fiber and cement approach for high water content clay soil improvement presents numerous advantages, revolutionizing traditional soil stabilization practices and offering a holistic solution to prevalent the adverse effect. The main purpose of the study focuses on a profound environmental benefit derived from the integration of natural fibers. Unlike traditional stabilizers that may rely on non-renewable resources, natural fibers provide a sustainable alternative, tapping into the inherent regenerative capacity of organic materials. This not only reduces the ecological footprint associated with construction but also aligns with global efforts towards more environmentally friendly practices.

Mechanically, the synergistic effect of natural fibers and cement within the soil matrix results in a remarkable enhancement of structural integrity. The combination forms a stiffer and resilient composite material that effectively addresses the inherent weaknesses of high-water content clay soils. This newfound strength translates into improved load-bearing capacity, making the improved soil suitable foundation material for a diverse range of construction projects. The robustness of improved soil by the composite additive material extends beyond mere strength that introduces a level of durability that is particularly crucial in areas prone to environmental stressors such as heavy rainfall, erosion, or ground movement. The resulting stability mitigates deformation risks, ensuring the longevity and reliability of constructed structures over this soil.

Its application spans can be various domains of construction, offering solutions to challenges in road construction, embankment stabilization, and slope protection. In road construction, the improved soil provides a stable and durable base, reducing the maintenance demands of the infrastructure over time. Embankment stabilization benefits from the reinforced soil structure, preventing erosion, excessive settlement, and potential collapses. The method can be adopted for slope protection, providing an effective means to counteract the erosive forces that often threaten hillsides and embankment slopes. This adaptability makes the combined natural fiber and cement treatment a comprehensive solution applicable across a spectrum of construction and infrastructure projects.

The utilization of natural fibers and cement can contribute to cost-effectiveness in construction projects. Natural fibers are generally cost-efficient, and their integration into the soil stabilization process can lead to optimized project budgets. Moreover, the enhanced durability of the improved soil reduces the need for frequent maintenance and repairs, resulting in long-term cost savings for infrastructure development.

## 6.2 Recommendations for Future studies

To improve the Geotechnical properties of high-water content clay by developing sustainable and ecofriendly stabilization techniques, the following recommendations are made for further investigations:

- At current stage the study addresses the behavior of the clay soil improvement at the laboratory scale. After addressing the capability of finely shredded paper for soil improvement, it’s essential to evaluate the performance of the additive at field condition by incorporating practical scenarios.
- The field test model that includes the actual traffic loading and different environmental conditions which proper monitoring measuring will give more substantial result. This approach will not only give actual performance of the road built on soft ground but also the proper on-site mixing design method can be developed.
- The resilient modulus characterization of improved high water content clay soil using FSP is essential input for analytical pavement design procedures. It can be performed in different wet and dry seasons.
- The numerical simulation that includes the performance of the stabilized soil layer under different embankment slope, height and weather conditions might give better understanding

## Appendix

### A: The basic principle and advantage of utilization of FEM

Currently the finite element method becomes the most efficient and versatile technique for conducting nonlinear boundary value problems like:

- ❖ Versatility: FEM can handle a wide range of complex geotechnical problems, including soil-structure interaction, consolidation, seepage, ground deformations, and stability analysis.
- ❖ Accurate Representation: It gives us a highly accurate representation of the properties of soil and structures under various loading, sub soil profile and environmental conditions.
- ❖ Mesh Flexibility: FEM allows for adaptability in mesh refinement which easily achieved different degrees of fineness, enabling engineers to focus computational resources where they are needed most, for precise results.
- ❖ Nonlinear Analysis: Nonlinear material behavior and contact interactions can be more efficiently simulated, which are often encountered in geotechnical problems.
- ❖ Boundary Conditions: It can incorporate different and complex boundary conditions and constraints, reflecting in situ behaviors across the model.
- ❖ Parametric Studies: FEM facilitates parametric studies to assess the impact of different variables on the geotechnical system's response, like adjacent element with different material properties which encountered during the computation.
- ❖ Visualization: It provides excellent visualization tools for interpreting results, aiding in decision-making, helps to understand loading and failure mechanism and design optimization.
- ❖ Interdisciplinary Applications: FEM can be seamlessly integrated with other engineering fields, such as structural analysis, to solve multidisciplinary problems.
- ❖ Cost-Effective: While it requires computational resources and skills, FEM is often more cost-effective than physical testing for complex geotechnical problems, especially for projects having higher budget constraint.
- ❖ Risk Assessment: It helps in assessing the safety and reliability of geotechnical structures and can aid in risk mitigation.
- ❖ Historical Data: FEM allows for the incorporation of historical data and evaluating the outputs, improving the accuracy of predictions. It helps in computing the safety and reliability of geotechnical structures which are used in risk mitigation.
- ❖ Innovation: It supports the development of innovative geotechnical solutions by allowing engineers to explore different design alternatives, utilization of different

combination of loading and in situ conditions representation.

**Appendix B**

Utilization of this program have various advantages like:-

- Realistic 3D Modeling: Plaxis 3D provides engineers to create accurate 3D models of road structures and the surrounding soil, which better represents the complex interactions and behavior of in situ materials in three dimensions.
- Improved Accuracy: By considering 3D effects, such as vertical and lateral soil movements in x, y and z direction, the simulation provides a more accurate representation of the road's response to various loads and environmental conditions.
- Complex Geometries: Plaxis 3D can handle complex geometric configurations, including intersections, bridges, embankments, and tunnels, making it suitable for modeling real-world road networks.
- Variability and Heterogeneity: It accommodates soil heterogeneity and variability by allowing users to define different soil layers and properties when soil stratification exists in the sub soil profile.
- Advanced Material Models: The software supports the use of advanced material models for soil and pavement structure layers, enabling the simulation of various soil types, pavement materials, and their nonlinear behavior. This enables us to use different soil models for each soil layer.
- Load and Boundary Conditions: Plaxis 3D enables engineers to apply realistic loading and boundary conditions, including surfacing materials, traffic loads, temperature effects, rainfall precipitation and settlement-induced stresses.
- Safety Assessment: It can be used to assess the safety and stability of road structures under different scenarios, helping to identify potential failure modes and risks and also the portion of the road section failure during analysis easily monitored.
- Optimization: Engineers can use Plaxis 3D to optimize road design by evaluating different configurations and materials to achieve cost-effective and durable solutions which is the result of precise analyses of nonlinear ground modeling.
- Visualization: The software provides powerful visualization tools, including 3D animations, load distribution and contour plots, deformed structure shape, making it easier to interpret results and communicate findings to stakeholders.
- Risk Mitigation: Plaxis 3D analysis helps in identifying potential issues early in the design stage, allowing for proactive risk mitigation measures and reducing the likelihood of economical loss or maintenance problems.
- Compliance with Standards: It enables engineers to analyze road structures against relevant design codes and given standards, ensuring that projects meet regulatory requirements. It can also be used to study the environmental impact of road

construction and assess potential effects on surrounding environment and groundwater.

Several PLAXIS soil models are summarized in the table below:

**Table A.1: Plaxis soil model**

| Soil model | Description |
|---|---|
| Linear Elastic model | This model relies on Hooke's isotropic elasticity law, incorporating two fundamental elastic properties: Young's modulus (E) and Poisson's ratio (ν). While the Linear Elastic model may not be appropriate for representing soil behavior, it can effectively simulate the characteristics of rigid elements within the soil, such as concrete walls or intact rock formations. |
| Mohr-Coulomb model | This model includes five input parameters: E and ν for soil elasticity, φ and c for soil plasticity, and ψ as the angle of dilatancy. It serves as a 'first-order' approximation for simulating soil or rock properties. Utilizing this model is advised for the initial analysis of the given problem. For each layer, a constant average stiffness or a stiffness that progressively increases with depth is estimated. The use of constant stiffness enables relatively fast computations, providing an initial estimation of deformations. |
| Hoek-Brown model | It is a model for weathered rock that combines isotropic elasticity with perfect plasticity, and it is grounded in the 2002 version of the Hoek-Brown failure criterion. This criterion, which is non-linear and stress-dependent, characterizes shear and tensile failures through a continuous function and is well-known among geologists and rock engineers. In addition to the elastic parameters (E and ν), the model incorporates key rock properties like the uniaxial compressive strength of intact rock, the Geological Strength Index (GSI), and the disturbance factor (D). |
| Jointed Rock model | This model is designed as an anisotropic elastic-plastic representation, specifically tailored to replicate the characteristics of rock layers that exhibit stratification and distinct fault orientations. Plastic deformation is limited to a maximum of three shear directions or planes, each characterized by its unique strength parameters φ and c. The intact rock is assumed to display fully elastic behavior with constant stiffness properties (E and ν), while adjusted elastic properties can be specified for the stratification direction. |
| Hardening Soil model | This model represents an advanced approach for simulating soil behavior. Similar to the Mohr-Coulomb model, it defines limiting stress states using the friction angle (φ), cohesion (c), and dilatancy angle (ψ). However, it provides a more accurate description of soil stiffness through three distinct input stiffness values: triaxial loading stiffness (E50), triaxial unloading stiffness ($E_{ur}$), and oedometer loading stiffness ($E_{oed}$). Default settings propose average values for different soil types, with $E_{ur}$ approximately equal to $3E_{50}$ |

| | |
|---|---|
| | and $E_{oed}$ approximately equal to E50. Nevertheless, for very soft or very stiff soils, users can input alternative $E_{oed}/E_{50}$ ratios. Unlike the Mohr-Coulomb model, the Hardening Soil model incorporates the stress-dependency of stiffness moduli, indicating that all stiffness values increase with pressure. These three input stiffness values are referenced to a standard stress, typically set at 100 kPa (1 bar). In addition to the mentioned model parameters, initial soil conditions, including pre-consolidation, play a crucial role in addressing most soil deformation issues, and these conditions can be considered during initial stress generation. |
| Hardening Soil model with small-strain stiffness (HS small) | HS small is a modification of the aforementioned Hardening Soil model, designed to accommodate the enhanced stiffness observed in soils at small strains. At low strain levels, most soils exhibit greater stiffness compared to engineering strain levels, and this stiffness nonlinearly varies with strain. The HS small model captures this behavior by introducing an additional strain-history parameter and two extra material parameters: the small-strain shear modulus and the strain level at which the shear modulus decreases to approximately 70% of the small-strain shear modulus. The distinctive characteristics of the HS small model become particularly evident under working load conditions, providing more dependable displacements than the HS model. In dynamic applications, the Hardening Soil model with small strain stiffness also introduces hysteresis in material damping. |
| Modified Cam-Clay model | This model is widely recognized in the international literature on soil modeling, as illustrated by Muir Wood (1990) on page 248, for example. Its primary application is in the modeling of nearly normally consolidated soils of the clay type. The inclusion of this model in PLAXIS facilitates comparisons with other software codes. |
| Soft Soil Creep model | It is generally applicable to all soil types, but it does not consider viscous effects such as creep and stress relaxation. In reality, all soils undergo some degree of creep, and primary compression is followed by a certain amount of secondary compression. This secondary compression is particularly significant in soft soils, such as normally consolidated clays, silts, and peat. To address this, PLAXIS has incorporated a model known as the Soft Soil Creep model. Primarily developed for settlement issues related to foundations and embankments, this model proves especially useful. However, in unloading scenarios typical of tunneling and other excavation challenges, the Soft Soil Creep model doesn't significantly outperform the simple Mohr-Coulomb model. Similar to the Hardening Soil model, accurate initial soil conditions, including information about pre-consolidation stress, are crucial when employing the Soft Soil Creep model. This consideration extends to the initial creep rate, which is determined by the initial over-consolidation ratio. |
| Sekiguchi-Ohta model | It is a model of the Cam-Clay type, featuring an anisotropic yield contour defined by $Knc_0$. There are two versions of the model: the inviscid model, which is time-independent and shares similarities |

| | |
|---|---|
| | with the Soft Soil model, and the viscid model, which is time-dependent and resembles the Soft Soil Creep model. Both versions originated in Japan and were initially user-defined models but have since been integrated as standard models in PLAXIS. |
| UBC3D-PLM model | It is an advanced model designed to simulate liquefaction behavior in dynamic scenarios. This model utilizes two yield surfaces to ensure a smooth transition near the mobilized friction angle. The UBC3D-PLM model employs the Mohr-Coulomb yield condition with a hardening law similar to the Hardening Soil model. For the secondary state, the UBC3D-PLM model integrates a densification law through a second yield surface with a kinematic hardening rule based on the number of loading cycles. This correlation enhances the accuracy of the evolution of excess pore pressure. Dynamic applications necessitate a thorough and extensive investigation of the soil deposit. |